RESEARCH & DEVELOPMENT

Development of a Testing System for Asphalt Surface Treatments

Y. Richard Kim, Ph.D., P.E., F. ASCE
Edwin Jones, E.I.
Department of Civil, Construction, & Environmental Engineering
North Carolina State University

NCDOT Project 2009-01

FHWA/NC/2009-01

January 2015

Development of a Testing System for Asphalt Surface Treatments

FINAL REPORT
(FHWA/NC/2009-01)

Submitted to the North Carolina Department of Transportation
(Research Project No. HWY-2009-01)

Submitted by

Y. Richard Kim, Ph.D., P.E., F.ASCE
Campus Box 7908
Department of Civil, Construction, & Environmental Engineering
North Carolina State University
Raleigh, NC 27695-7908
Tel: 919-515-7758, Fax: 919-515-7908
E-mail: kim@ncsu.edu

Edwin L. Jones, E.I.
Former Graduate Research Assistant
Campus Box 7908
Department of Civil, Construction, & Environmental Engineering
North Carolina State University
Raleigh, NC 27695-7908
E-mail: eljones@ncsu.edu

Department of Civil, Construction, & Environmental Engineering
North Carolina State University
Raleigh, NC

January 2015

Technical Report Documentation Page

1. Report No. FHWA/NC/2009-01	2. Government Accession No.	3. Recipient's Catalog No.
4. Title and Subtitle Development of a Testing System for Asphalt Surface Treatments		5. Report Date January 2015
		6. Performing Organization Code
7. Author(s) Y. Richard Kim and Edwin L. Jones		8. Performing Organization Report No.
9. Performing Organization Name and Address Campus Box 7908, Dept. of Civil, Construction, & Environmental Engrg. NCSU, Raleigh, NC 27695-7908		10. Work Unit No. (TRAIS)
		11. Contract or Grant No.
12. Sponsoring Agency Name and Address NC Department of Transportation Research and Analysis Group 1 South Wilmington Street Raleigh, NC 27601		13. Type of Report and Period Covered Final Report July 2007 – December 2010
		14. Sponsoring Agency Code 2009-01
15. Supplementary Notes		

16. Abstract

The objective of this research project is to develop a simple asphalt surface treatment (AST) testing system that is based on a review of existing AST test methods, the experience of the North Carolina State University (NCSU) research team gleaned from previous AST projects, and experience of field personnel who construct ASTs. The bitumen bond strength (BBS) test is identified as a promising, inexpensive, and simple test method to determine the adhesive and cohesive properties of emulsions. Also, a modified sweep test and three-dimensional (3-D) laser profiler method are developed from this study. The modified sweep test is based on the sweep test specified in ASTM D7000, but replaces the stiff-bristled brush in the original sweep tester with a free-rolling, free-spinning rubber wheel to simulate the horizontal and vertical forces induced by the front wheels of a vehicle. Also, a height adjustment mechanism and load cell are incorporated in the modified sweep test machine to ensure and maintain constant vertical pressure of the wheel on the chip seal specimen. The 3-D laser profiler is equipped with a point laser and photoelectric sensor to measure the surface profile and to take digital images of the chip seal pavement surface for the evaluation of aggregate embedment and bleeding. A preliminary investigation is undertaken to determine the aggregate embedment depth from the chip seal surface profile measured by the 3-D laser profiler, and the results indicate that the 100% valley average is close to the 50% passing sieve size. This finding can be used to establish the surface profile of chip seal pavements that have different percentages of embedment depth from the aggregate gradation.

17. Key Words Asphalt Surface Treatment, laser profiler, modified sweep tester, bitumen bond strength, aggregate loss, embedment depth	18. Distribution Statement		
19. Security Classif. (of this report) Unclassified	20. Security Classif. (of this page) Unclassified	21. No. of Pages 81	22. Price

Form DOT F 1700.7 (8-72) **Reproduction of completed page authorized**

DISCLAIMER

The contents of this report reflect the views of the authors and are not necessarily the views of North Carolina State University. The authors are responsible for the facts and the accuracy of the data presented herein. The contents do not necessarily reflect the official views or policies of the North Carolina Department of Transportation or the Federal Highway Administration at the time of publication. This report does not constitute a standard, specification, or regulation.

ACKNOWLEDGEMENTS

This research was sponsored by the North Carolina Department of Transportation. The Steering and Implementation Committee was comprised of Dennis Wofford (Chair), Judith Corley-Lay, Ph.D., P.E.; Jack Cowsert, P.E.; Terry McLaurin; Averette Moore; Christopher Peoples, P.E.; James Phillips, P.E.; Vann Price; Jackson Provost, P.E.; Dale Register; Archie Smith, Jr.; David Spainhour, P.E.; David L. Thomas, P.E.; and Todd Whittington, P.E. These advisors have given invaluable direction and support to the research team throughout the project.

Table of Contents

1. INTRODUCTION

1.1 Research Needs and Significance

The North Carolina Department of Transportation (NCDOT) spends millions of dollars annually on road maintenance. Among many different road maintenance techniques, the asphalt surface treatment (AST) is a common treatment in the NCDOT's pavement preservation program. The effectiveness of ASTs in North Carolina is evident in the fact that ASTs cover 56.5% of the total paved miles using only 16.8% of the total pavement construction budget. Not only are ASTs among the most efficient and cost-effective methods utilized by state highway agencies to preserve and rejuvenate existing pavements, they also have been shown to provide structural value to the pavement as well.

The NCDOT has undertaken four research projects in recent years aimed at improving the performance of ASTs. These projects are: HWY-2004-04, *Optimizing Gradations for Surface Treatments*, to evaluate the impact of aggregate gradation on the performance of ASTs; HWY-2006-06, *Quantifying the Benefits of Improved Rolling of Chip Seals*, to improve the performance of ASTs by optimizing rolling patterns; HWY-2007-06, *Performance-Based Analysis of Polymer-Modified Emulsions in Bituminous Surface Treatments*, to evaluate the performance benefits of polymer-modified emulsions; and HWY-2008-04, *Development of a New Chip Seal Mix Design Method*, to develop a performance-based AST mix design method.

The aggregate loss performance of ASTs can be evaluated using various laboratory test methods, including the aggregate retention test (ART) (Tex-216-F), vacuum test, Vialit test, Pennsylvania aggregate retention test (PART), flip-over test (FOT), and the sweep test (ASTM D7000) (Kandhal 1987, Hank and Brown 1949, Benson and Gallaway 1954, Barnat 2001, Yazgan 2004). However, each of these methods applies a different form of mechanical energy to assess the aggregate-binder bond interaction; none of these methods simulates the mechanical force from traffic wheel loading that is imparted on the pavement. To alleviate this shortcoming, a performance-based AST test method was developed and tested for the HWY-2004-04 project. This accelerated test method uses the third-scale model mobile load simulator (MMLS3), which is a scaled-down unidirectional vehicle load simulator that uses a continuous loop for trafficking. The wheels travel at a speed of roughly 5,500 wheel applications per hour, thus allowing an accelerated evaluation of pavement performance under more realistic loading conditions than is possible using other available AST tests. In addition, the MMLS3 was found to reproduce the change of surface texture of ASTs well during the HWY-2008-04 project.

The original goal of this project was to develop a field testing system that mimics the MMLS3 loading. However, a feasibility study of developing such a system that works under a wide range of field conditions concludes that the system is going to be too complex and expensive. One of the major factors in making this conclusion is the test temperature, which is one of the most important factors for the aggregate retention performance of ASTs. As a result, the research team focused on developing test methods that estimate the performance of ASTs and are still simple and inexpensive enough to be implemented by the NCDOT. The performance characteristics of ASTs that are targeted in this project are aggregate loss and bleeding.

1.2 Research Objective

The objective of this research project is to develop a simple AST testing system or systems that are based on a review of existing AST test methods, experience of the NCSU research team gleaned from previous AST projects, and experience of field personnel who construct ASTs.

1.3 Report Organization

This report is composed of ten chapters. Chapter 1 presents the research needs and objectives. Chapter 2 summarizes the literature review of chip seal aggregate distress types, performance test methods and existing laser profilers. Chapter 3 outlines the development of the three-dimensional (3-D) laser profiler and the steps taken to improve its performance in the field. Chapter 4 describes the modifications and improvements made to the sweep tester, and Chapter 5 evaluates the results of the Bitumen Bond Strength (BBS) test using PATTI device. In Chapter 6, preliminary research efforts to predict aggregate embedment depth from the surface profile measured by the 3-D laser profiler are summarized. Conclusions from this research and future research recommendations are given in Chapter 7.

2. LITERATURE REVIEW

2.1 Distresses in ASTs

The most common failure modes associated with ASTs are streaking, the debonding of the existing surface and the new AST, flushing/bleeding, and the loss of cover aggregate.

2.1.1 Streaking

Streaking is caused by the failure to apply asphalt uniformly inch by inch across the road surface, as shown in Figure 1. Streaking is usually caused by the asphalt sprayer's nozzle being clogged or inoperable during the emulsion spraying phase of construction.

2.1.2 Debonding

With regard to debonding failure, a new AST may not have a good bond with an existing roadway surface after construction. This debonding can occur for various reasons, including the presence of high amounts of dust (fine content) on the existing surface, the existing surface being wet or too cold, or the asphalt being too hard. Normally, this failure to establish a good bond with the existing surface causes a problem on a small area of only a few square inches to a few square feet. Occasionally, however, a few square yards or even the entire surface treatment can fail for these reasons (McLeod 1969). A typical debonding failure of an AST is shown in Figure 2.

Figure 1 Example of streaking in an asphalt surface treatment

Figure 2 Typical example of debonding failure

2.1.3 Bleeding

Another major long-term distress that appears in ASTs is bleeding, or flushing, as shown in Figure 3. This failure usually is caused by the application of excessive asphalt in the mix design phase, which causes the excess asphalt to rise out of the cover aggregate onto the road surface. Flushing or bleeding may also result from the loss, or 'whip-off', of the aggregate for any number of reasons, such as a rainfall shortly after construction, asphalt that is too hard and fails to develop adequate adhesion with the cover aggregate, and use of cover stone that is too dirty or too wet to establish good adhesion to the asphalt. The main problem with bleeding is the loss of skid resistance associated with the distress, which decreases the overall safety of the road as well as the effectiveness of the AST (McLeod 1969, Gransberg 2005).

Figure 3 Example of partial bleeding failure

2.1.4 Aggregate Loss

Aggregate loss is one of the most critical AST failure distresses. Generally, most of the aggregate loss occurs during the initial traffic passes after a newly-constructed AST is opened to traffic. Other major causes of aggregate loss include excessive aggregate application, poor traffic control during construction, inadequate embedment of the aggregate particles into the emulsion, poor aggregate gradation qualities, and dusty aggregate (Shuler 1990, Gransberg 2005). Aggregate loss issues due to construction problems usually occur within a few months, and an AST with these types of problems should be repaired rather than resealed, because a reseal alone will not normally last the expected life of the AST (Transit New Zealand 2005). The inherent aggregate properties of the surface treatment, such as gradation, shape, moisture condition, and dust proportion, play a major role in aggregate retention. Also, the McLeod procedure (McLeod 1969) recognizes that some of the cover aggregate will be forced to the side of the roadway by the initial passing vehicles while the newly sprayed seal coat is still in its initial curing phase. The amount of aggregate that is whipped off in this manner is related to the speed and number of vehicles on the new seal coat. To account for this occurrence, a traffic whip-off factor is included in the aggregate design equation. Reasonable values to assume are 5% for low volume residential types of traffic and 10% for higher speed roadways, such as county roads (McHattie 2001).

2.1.5 Loss of Skid Resistance

One of the major roles of surface treatments, in general, is to provide an increase in skid resistance (Gransberg 2005). Loss of skid resistance associated with an existing asphalt surface is one of the common road conditions that trigger the need for a new surface treatment. Existing surface conditions that can indicate the existence of a potential safety hazard include bleeding and rutting, among others.

Skid resistance changes as a function of time. Usually, skid resistance increases in the first two years following construction as the asphalt is worn away by traffic, then decreases over the remaining life of the pavement as the surface aggregate becomes more polished. Skid resistance tends to increase in winter when wet and cold weather conditions roughen the surface, and tends to decrease in the summer. This seasonal variation in skid resistance is significant and should be taken into account when considering skid resistance at particular locations. Additionally, it is believed that the winter recovery in skid resistance is not enough to overcome the summer polishing of the road surface (Jayawickrama and Thomas 1998, Hunter 2000).

2.2 Factors Affecting AST Performance

2.2.1 Aggregate and Emulsion Application Rates

One of the most important components of AST design and construction is the selection of appropriate application rates. In particular, the application of an excessive amount of aggregate can be problematic in AST field construction. If too much aggregate is applied, excess aggregate is whipped off by rapidly moving traffic, which creates a safety hazard and wastes materials. An

incorrect assumption often made regarding the over-application of aggregate is that the excess aggregate will simply be swept off the surface, leaving the correct application quantity in place. Although it is reasonable to assume that some traffic whip-off will occur during the initial traffic loading, lack of care and the application of excessive aggregate can be detrimental, resulting in at least two major forms of distress, pavement distress and vehicular distress. Pavement distress occurs when more than one layer of aggregate is present and the excess aggregate on the surface is forced into the layer below. This action causes the aggregate on the first layer to dislodge, therefore leading to loss of aggregate. This dislodgement, in addition to creating early aggregate loss, can potentially lead to flushing issues as well (Shuler 1990). When large quantities of aggregate are applied, the small stones adhere and the large stones are likely to be brushed off (Benson and Gallaway 1953), which affects the grading of the aggregate layer as well. It has been reported that an excess of aggregate material is often more detrimental than a slight shortage of aggregate, in that with an excess of cover material the amount of fines applied also increases (Kearby 1952).

2.2.2 Aggregate Gradation

Aggregate gradation also plays an important role in the design, construction, and ultimately the performance of ASTs. Ideally, the specified gradation should be such that the texture of the seal is consistent. Tight gradation bands, which ensure a uniformly graded aggregate with minimal fines and dust, are desirable for an effective treatment. The literature and field surveys indicate that single-sized aggregate with less than 2% fine passing the No. 200 sieve is considered ideal (Gransberg 2005). One advantage of using a single-sized aggregate in an AST is that it maximizes the contact area between the tire and the seal surface. This contact increases the frictional area and, in effect, improves the skid resistance as long as the emulsion application rate (EAR) is appropriate (Herrin et al. 1968).

Ideally, the aggregate should be economically reasonable and as close to uniform size as possible so that the surface treatment has a single aggregate layer. If there is a significant difference between the largest and the smallest particles, the asphalt film may completely cover the smaller aggregate and thus prevent the proper embedment of the larger particles. As a general rule, the largest sized aggregate in a surface treatment should be no more than twice the smallest sized aggregate, with a reasonable allowable tolerance for both oversize and undersize to allow for economical surface treatment production (Asphalt Institute 1964). As the magnitude of tolerance is increased (for budgetary reasons), it is believed that overall performance quality decreases. Therefore, depending on the economic conditions, it may be favorable to have higher initial construction costs and obtain close to one size of aggregate that performs well than to have lower initial construction costs with poor performance. Such poor performance will ultimately lead to high annual maintenance expenses (McLeod 1960). Therefore, state agencies must find a balance between the two alternatives.

Additionally, Benson and Gallaway (1959) found that an increase in the fine content from 0% to 30% of the total aggregate causes 10% more aggregate loss. This gradation issue, as discussed earlier, is tied directly to economic considerations, because aggregate costs increase as the gradation requirements for AST construction become more restricted. However, in the case

where two aggregates are otherwise the same in price and quality, the aggregate that has the most uniform gradation is preferred.

Kandhal (1987) also reports a reduction in the aggregate retention capabilities of a surface treatment with the use of graded aggregate. These graded stones contain additional smaller particles that tend to fill the voids between large particles and, thus, may not become embedded effectively into the applied asphalt.

2.2.3 Material Selection

Material selection for AST design and construction generally is based on product availability, aggregate/emulsion quality, and the climate at the potential construction site. Aggregate selection is a function of geological availability and the distance that the aggregate must be transported. The existing pavement's surface, the size of the job, the aggregate gradation, and local climate must be taken into consideration for the asphalt selection process (Gransberg 2005).

The specifications for ASTs in North Carolina call for granite (No. 78M for the aggregate size) and CRS-2 or CRS-2L/2P (latex/polymer-modified emulsion) for the emulsion type (NCDOT Standard Specifications for Roads and Structures 2002). The most commonly used size of aggregate for a single seal is a nominal maximum aggregate size (NMAS) of 3/8 in. (9.525 mm) (Gransberg 2005). Lightweight aggregate is often used as the aggregate material in AST construction in North Carolina because it provides a highly skid-resistant surface, good color contrast to improve visibility both in daylight and at night, a surface that reduces paint striping maintenance, and it completely eliminates windshield damage caused by flying loose aggregate, which is a major concern associated with chip seal surface treatments (Epps et al. 1974). In addition, the lightweight aggregate was found to be more efficient in reducing the aggregate loss and bleeding in chip seals (Kim and Lee, 2005).

2.3 AST Test Methods

Most of the AST test methods measure the ability of ASTs to retain aggregate particles. These test methods can be grouped into two categories, i.e., direct and indirect methods. The direct methods test the AST to measure the aggregate loss directly. The indirect methods measure aggregate embedment depth, which correlates closely to the aggregate loss. In the following, test methods in these two groups are reviewed.

2.3.1 Direct Methods

Tredrea (2008) researched the sources of horizontal stress and the factors that contribute to surface performance and determined that the three main factors that lead to the development of horizontal stress are:

- Wheel loading, tire type, tire pressure
- Wheel motion (acceleration, braking, turning)

- Coefficient of friction between the tire and the pavement

Horizontal stress is created within the pavement through longitudinal braking, acceleration and turning. Turning can also generate lateral forces, depending on the tightness of the turning radius and, unlike braking and accelerating, is not related to the power of the engine.

Once the origin and location of these stresses have been determined, the surface performance must then be assessed. Temperature, the binder at the interface and within the surface, and surface type are all important factors of surface performance. Temperature plays a large role in determining the age of surface failures. Whereas high temperatures (60°C) are associated with early life surface failures, low temperatures (6°C) are critical as the binder ages. With regard to the effect of the binder at the interface of the bituminous layers, viscosity proves to be the key property for reducing shear failure. The grade and type of the binder, the binder temperature, and the presence of diluents all contribute to the viscosity of the binder.

Tredrea (2008) used a wheel-tracking test apparatus with a skewed test wheel, as shown in Figure 4, to assess the material loss performance of four main surface types in Australia: high stress seals, high shear resistance asphalt, thin asphalt, and open-graded asphalt. The Tredea study then discusses performance measures in the laboratory using the skewed wheel test and provides a summary of potential test procedures. The study also discusses some of the issues associated with the sampling procedure, such as the positive aspects of the open-graded, high air voids systems, and the development of testing equipment in the laboratory. A negative aspect of Tredea's testing method is that the laboratory preparation of the sprayed seals is difficult due to the conditions and limitations of the currently available laboratory preparation procedure.

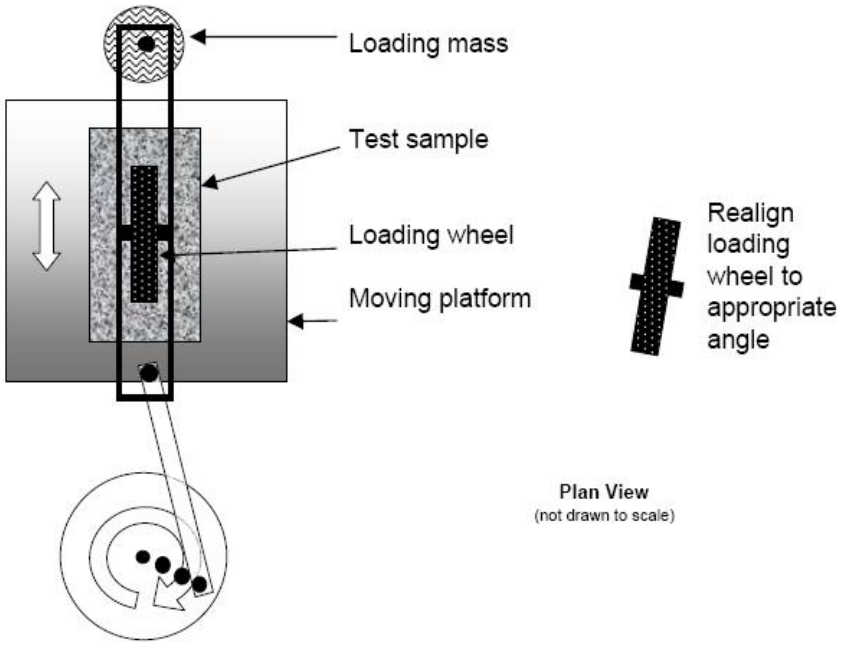

Figure 4 Wheel-tracking test apparatus showing the skewed test wheel and stroke control mechanism (Tredrea 2008)

Stroup-Gardiner et al. (1990) tried to identify potential construction problems that may affect the performance of a chip seal surface. Problems related to construction, such as aggregate pick-up by the rollers, may damage a section of road even before it is opened to traffic. Stroup-Gardiner et al. used the laboratory Vialit test to evaluate existing excess aggregate and the set rate of the emulsion. They fabricated samples for the Vialit testing on a small scale similar to that found in field construction, and tested these samples at various curing times.

Davis et al. (1991) researched the correlation between Vialit test results from the laboratory and from field tests conducted three months after construction and again after eleven months. The Vialit test samples from the field were collected from the pavement six feet from the center line after the last roller had passed and before the sweeping process. In order to prevent the metal Vialit plates flipping up and damaging the samples in the field, the roller speed was reduced to half its normal speed. A comparison of the aggregate retention results provided by the Vialit test between the laboratory and field testing shows that the differences in aggregate loss range from 10% to 35%. Davis et al. also conducted field studies near the field testing sites. They developed a composite condition index, on a scale of 1 to 10 with 10 being best, based on the overall condition, bleeding, and aggregate retention results.

Yazgan et al. (2004) researched a new test protocol that uses a performance-based method to determine the aggregate-binder compatibility for a seal coat using the Vialit test. Approximately one year after construction, they evaluated the performance of each test section and rated the field conditions on a scale of 1 to 5, with 5 being the best. Meanwhile, specimens taken from field test sections during construction were stored under laboratory conditions. Eleven of the twelve test sections showed agreement between the field performance and field specimen test results using this new testing protocol. Consequently, the new testing protocol appears to predict the field performance of seal coats.

Another raveling test device developed by LCPC in France, called a *tribometer* (referred to also by its French acronym, T2R), is shown in Figure 5. It is a biaxial hydraulic machine used to reproduce the phenomenon of surface degradation by loss of aggregates. Use of a load applicator, whose shape follows a logarithmic law, holds the force pair (i.e., vertical and horizontal forces on the pavement surface) at a near constant ratio and independently of the logarithmic pad position (Figure 6). In practice, a cyclic contact force with no sign change and of a predetermined angle of inclination is imposed in order to cause surface degradation by means of loss of aggregate.

The concept used by T2R to apply both horizontal and vertical forces is appealing. This device is the only one known in the literature that can apply both horizontal and vertical forces without involving some kind of accelerated pavement testing machine. However, developing a similar device that will work in the field under changing temperatures within reasonable complexity and cost is difficult.

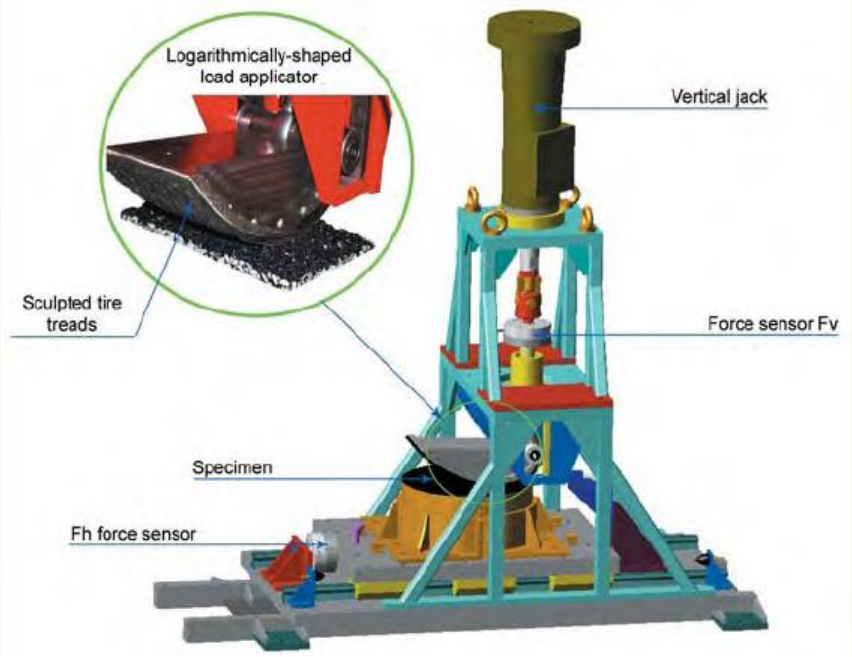

Figure 5 Overview of T2R for evaluating the resistance to tangential forces

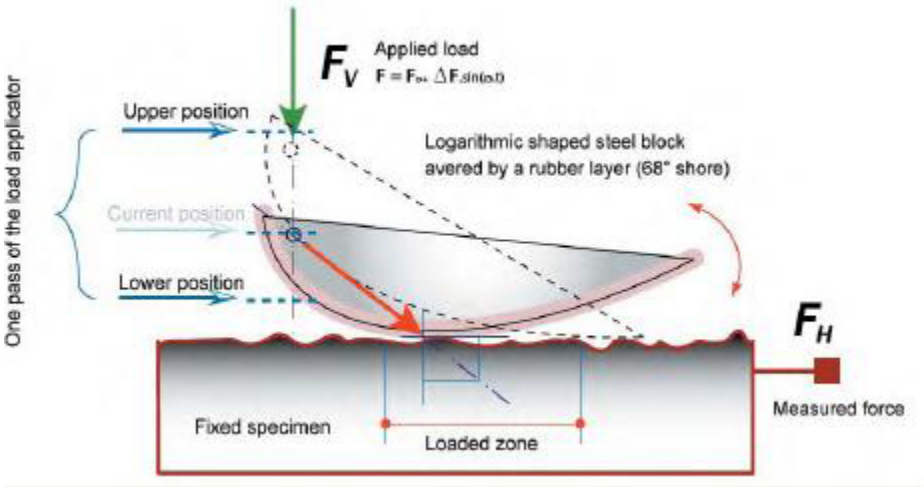

Figure 6 Principle of T2R

The Third Scale Model Mobile Load Simulator (MMLS3) simulates the traffic loading experienced by ASTs under field traffic loading conditions. The MMLS3 applies repeated wheel loads to the asphalt surface at a consistent and accelerated rate (990 wheel loads applied every 10 minutes) and causes the AST to respond similarly as it would under field loading conditions. Also, the MMLS3 has the ability to wander across the sample to simulate the actual wandering of vehicles across the wheel path. For the performance testing conducted in this project, the MMLS3 wandering feature was enabled. It takes approximately 10 minutes for the MMLS3 to wander across the whole 7 in. width of the chip seal specimens. For the aggregate loss testing,

the MMLS3 is placed inside a temperature chamber that allows the temperature to be controlled during testing, thus enabling the simulation of field temperature conditions during traffic loading in the laboratory. A maximum of three samples (at 12 in. lengths per sample) can be secured underneath the MMLS3 to be trafficked under MMLS3 loading conditions. The cumulative sample length (36 in. total) is the effective loading area for the MMLS3 tires. The MMLS3 testing procedure and equipment can be seen in Figure 7. The one departure from the picture shown in Figure 7 (d) during actual testing is that the top of the MMLS3 temperature chamber was covered to prevent heat escaping.

The MMLS3 test procedure involves a two-hour aggregate loss test conducted at 25°C. Prior to the test, each specimen is weighed to determine its weight prior to loading (i.e., at zero loading time). After mounting the samples and allowing the temperature chamber to reach the desired temperature, testing can begin, and the MMLS3 loading is applied for 15 minutes. Then, the test is stopped, and the specimens are removed from underneath the MMLS3 and weighed. This process is repeated at the cumulative testing times of 45 and 120 minutes. Thus, at the end of the two-hour test, specimen weights are available at 0, 15, 45, and 120 minutes. These weights are used to determine the aggregate loss for each specimen under MMLS3 traffic loading.

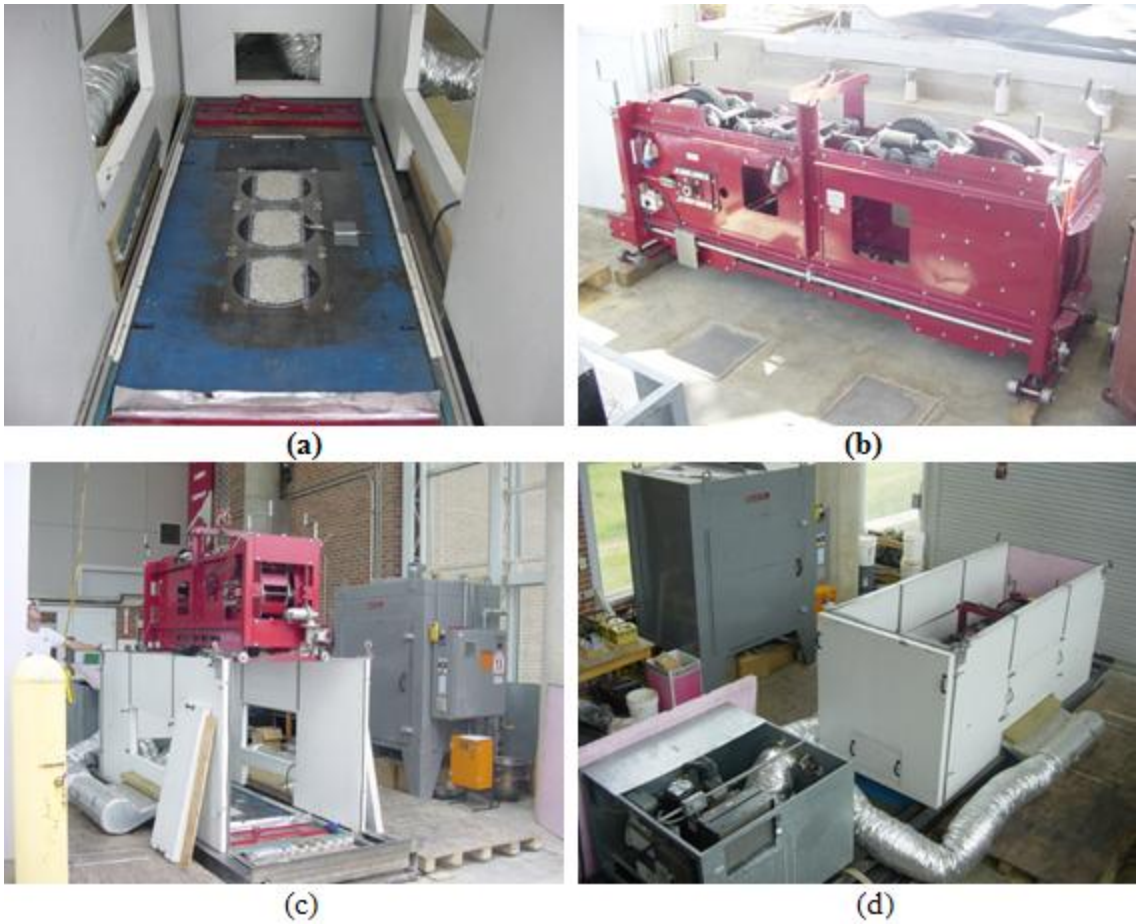

Figure 7 MMLS3 test preparation: (a) installation of specimens on a steel base, (b) side view of the MMLS3, (c) positioning the MMLS3 in the temperature chamber, and (d) complete MMLS3 test setup for testing

2.3.2 Indirect Methods

Aggregate exposure depth, and therefore aggregate embedment depth, is an important parameter for the adequate performance of ASTs. Distresses like aggregate loss, bleeding, and skid resistance all are strongly related to this physical parameter, and therefore measurements of embedment can serve as indirect indicators of such the probability of such distresses. Based on the comprehensive literature review and development efforts in the HWY-2004-04 and HWY-2006-06 projects, the modified sand circle test and laser profiler method were identified as test methods for the measurement of aggregate exposure depth. These methods are described below along with other alternatives. In each, the primary physical parameter of interest is the embedment depth. Visual and laser-based methods quantify this value directly whereas the sand-patch based/derived methods only qualify this value. The most common index for quantifying the average or representative embedment depth of an area of AST is the mean profile depth (MPD), which is a parameter that represents the exposed texture depth of a chip seal surface treatment and is inversely related to the embedment depth. Hypothetically speaking, as the EAR increases (as applied on a given single aggregate layer), the MPD will decrease, and where the EAR is decreased for a given aggregate structure, the MPD will increase. Transit New Zealand (2005) defines the MPD as:

$$MPD = \frac{Peak\ level\ (1st) + Peak\ level\ (2nd)}{2} - Average\ level \qquad (1)$$

The various chip seal parameters that make up Equation (1) are shown schematically in Figure 8.

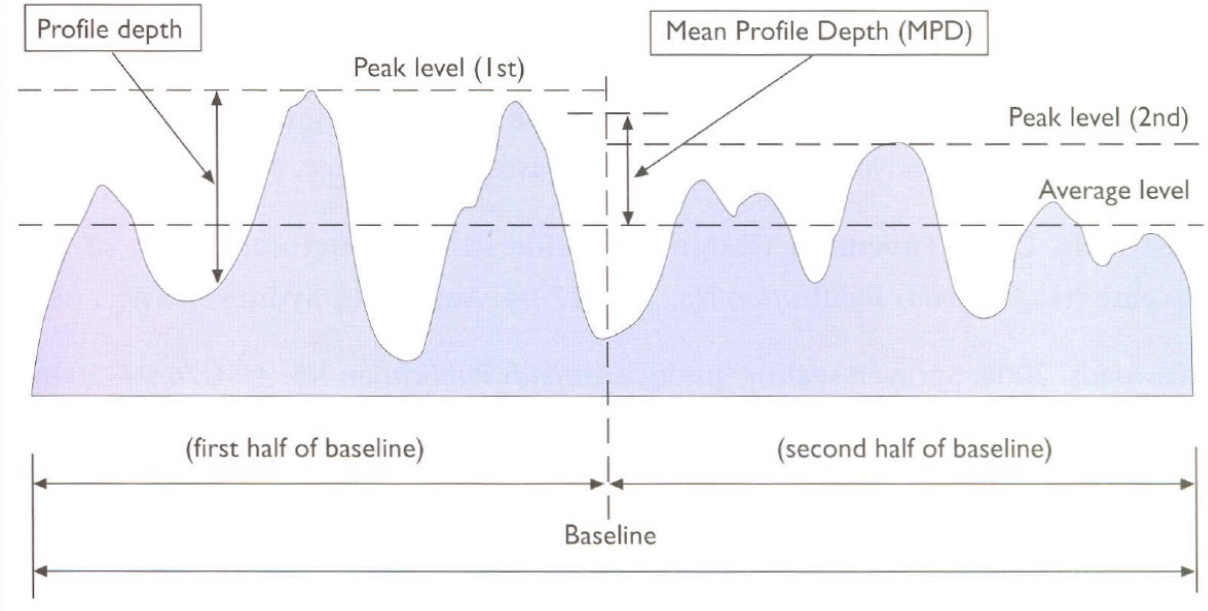

Figure 8 Schematic diagram of the mean profile depth determination

In the diagram, the MPD clearly indicates the roughness (i.e., macro-surface texture) and aggregate exposure depth of the chip seal. Roughness is important, because it provides the skid

resistance and friction needed for vehicles to brake adequately. The aggregate exposure depth is important because it is a function of the aggregate embedment depth, which is the most important factor that controls the aggregate loss and bleeding performance of chip seals. A small MPD value indicates the likelihood of bleeding and skid resistance problems. A large MPD value after construction indicates the possibility of excessive aggregate loss and, therefore, bleeding due to aggregate loss.

The MPD measurements taken from both the sand circle test and the laser profiler data were compared. From this comparison, the laser profiler was shown to be less operator-dependent than the sand circle test.

Sand Patch Test

The sand patch test is used by many state highway agencies in the United States to determine the AST texture depth and skid resistance and is a relatively simple test to perform (ASTM E 965). In New Zealand this test is called the sand circle test. The sand circle test is performed using a known volume of material and a spreading tool. The material traditionally used for this test is Ottawa sand, passing the #50 sieve and retained on the #100 sieve. The procedure for this test consists of placing a known volume of sand on the pavement surface and spreading it using a circular motion until the sand is dispersed over the voids in the pavement surface. The diameter of the area covered with the sand is measured, and this measurement is used to calculate the mean texture depth of the pavement macrotexture.

It has been reported that the results from this test are dependent upon the individual performing the test and, therefore, are not very repeatable (Meegoda et al. 2002). This finding has been confirmed by the NCSU research team in the previous HWY-2004-04 project. The major problem with this test method is the difficulty involved in maintaining a circle as the sand is being dispersed. During the HWY-2006-06 project, this test was modified to improve its accuracy and repeatability. This modified sand circle test is described in the next section.

Modified Sand Circle Test

The modified sand circle test uses a circular steel hollow cylinder (which has a constant diameter and specific height) and a loose unit mass of sand to determine the volume of sand that covers the AST surface inside the cylinder. This method starts by placing paper, which has a circle cut out from the middle, on top of the AST specimen. The diameter of the circular cut in the paper is the same as that of the cylinder. The cylinder is then placed on top of the circular cut. Enough sand is poured into the cylinder to cover the AST surface, and the cylinder is slowly removed from the AST. Excess sand is then removed from the AST surface to the paper using a straight edge. Calculating the difference between the weight of the AST specimen before and after the modified sand circle test yields the weight of the sand needed to cover the circle of the AST surface. The loose unit weight of sand can be used to determine the volume of sand. Currently, this test method is successfully used for the inverted AST specimen. The inverted AST specimen is fabricated by first applying hydro-stone epoxy on the AST surface to keep the exposed aggregate particles in place and then dissolving residue asphalt from the epoxy-reinforced AST specimen using kerosene. This inversion method exposes the embedded portion of aggregate particles and results in the inverted AST surface with even heights of aggregate particles. This even surface is important in the successful application of the modified sand circle method. The

accuracy of this method used for the original AST surface with uneven aggregate particles is in question, and additional work is needed to develop a more reliable test method.

Wallpaper Size Test

Page et al. (1998) developed an alternative test to replace the sand circle test that is traditionally used to indicate pavement texture depth in chip seal design and to measure skid resistance. Despite the fact that the sand circle test is widely used in the field, it is not very accurate. Page et al. adopted wallpaper *size* (a term used in the New Zealand specification to describe a jelly-like material) mixed with water as an alternative material because it is cheap, easy to prepare and store, has 'jelly-like' characteristics, low viscosity, good spreadability, and is not hazardous to the user or traffic, nor is it harmful to the environment. The Page et al. alternative test procedure is as follows.

1. Place a measured amount of wallpaper size in a mound on the road surface.
2. Place a Perspex plate and rubber mat over the mound of wallpaper size; the operator stands on the rubber pad for 3 seconds.
3. Lift the rubber pad and Perspex plate.
4. Measure the diameter of the resulting wet patch in four locations and use the average of these diameters to *indicate* the mean profile depth (MPD).

Carpet Tile Test

Hegarty (2008) presented Institute of Asphalt Technology (IAT) guidelines for surface dressing (chip seals) in Ireland at the first Sprayed Sealing Conference in 2008. As part of an ongoing evaluation of this process, the surface dressing guidelines for Ireland were revised for publication of the second edition. This second edition covers all aspects of surface dressing, including recent developments such as the use of polymer-modified binders, slot-jet spray bars, multiple layer dressings, and recommendations for sealing unbound and cold mix layers; these various techniques were provided to reflect current practice. Two test methods detailed in EN 12272-1 are described in Hegarty (2008) to measure, calibrate and properly maintain both aggregate and emulsion application rates (AARs and EARs). In order to check both binder and spread aggregate rates easily in the field, the so-called carpet tile test, as shown in Figure 9, was conducted, and the rate-of-spread box, as shown in Figure 10, was examined. Figure 11 shows the rate of the spread of aggregate in terms of liter per square meter. This method is a simple check to carry out and helps in establishing a useful database. If the optimal rate of spread for a particular source and size of aggregate can be determined using the box measurement to give adequate coverage without unnecessary aggregate excess, then this information can be transferred and used for the same source and size of aggregate in actual construction. A quick check of the rate of spread at the commencement of the work can then result in considerable savings of material.

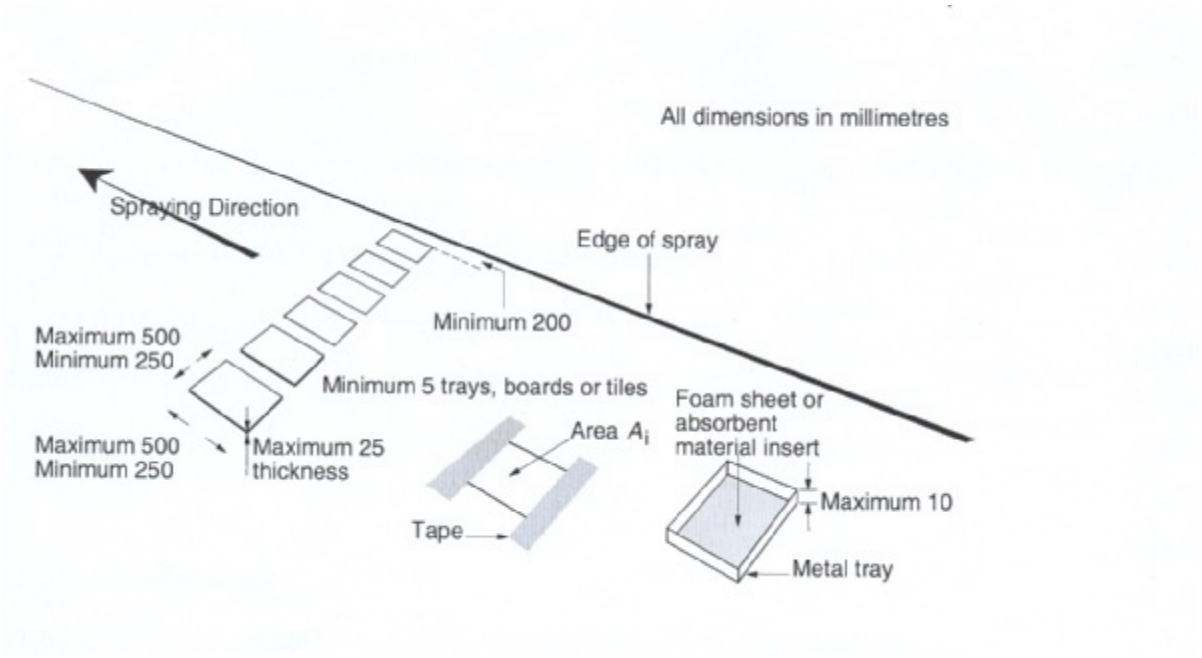

Figure 9 Carpet tile (or metal tray) test for binder rate of spread (Hegarty 2008)

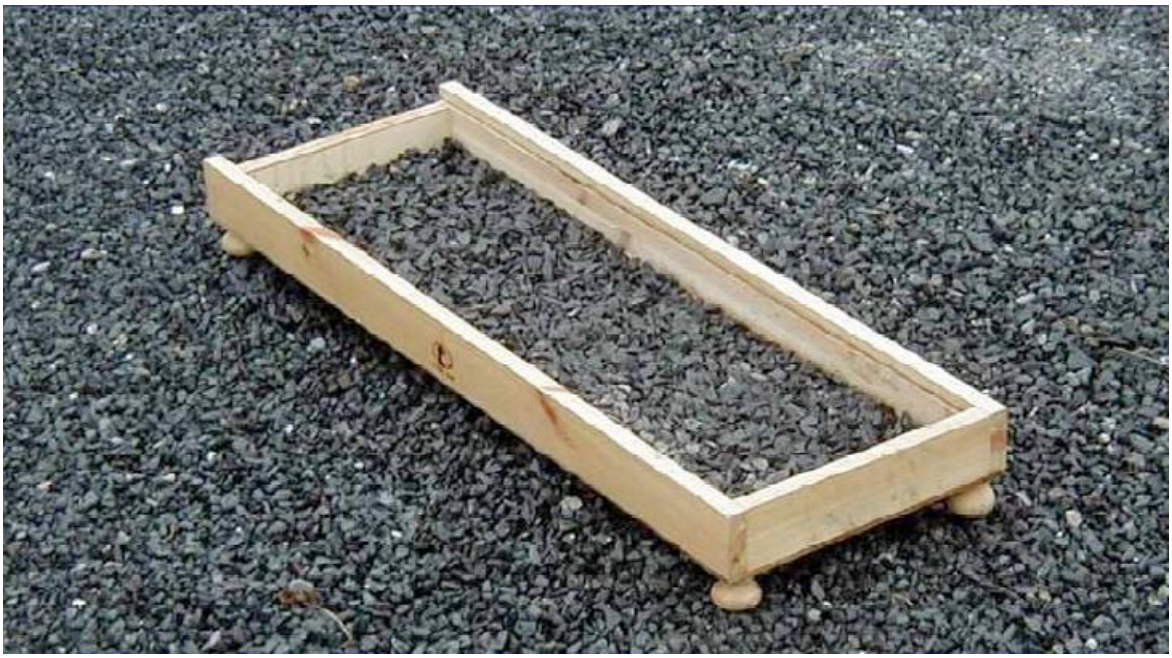

Figure 10 Rate-of-spread box (Hegarty 2008)

Figure 11 Rate of spread in liters per square meter (Hegarty 2008)

Digital Imaging Test

Pidwerbesky et al. (2006) researched digital imaging technology to measure chip seal surface texture. The major goal of the Pidwerbesky et al. research was to prove that a relationship exists between chip seal texture (as measured by the sand circle test) and digital image output (as measured by a function of the fast Fourier transform (FFT) of the digital image) and therefore to replace the imprecise sand circle test. They sought correlations in both directions, i.e., texture versus FFT and FFT versus texture. Additionally, the texture component was examined in two ways, i.e., using the sand circle diameter and using the computed texture depth.

Pidwerbesky et al. found a number of strong correlations between image output and physical measurements, including the correlation between the road texture measured by the sand circle test and that measured by the fast Fourier transform (FFT) of the digital image of the surface taken at the same spot as for the sand circle test. A statistical correlation was found using linear regression analysis with a coefficient of determination of 80% between the digital image processing output and the sand circle measurements taken at the same spot. Based on this correlation between the road surface texture measurements obtained from digital image processing and from FFT analysis, Pidwerbesky et al. (2006) developed:

- "an accurate, repeatable method of measuring texture to replace the sand circle method"; and
- "a fast, safe method of measuring texture to reduce the hazard of road surface texture measurement and minimize disruption to traffic."

Research by McGhee et al. (2003) validated high-speed texture measuring equipment for use in highway applications. They evaluated two high-speed systems and a new static referencing device. This study was conducted on 22 runway and taxiway test sections at the National Aeronautics and Space Administration (NASA) Wallops Flight Facility and on seven surfaces from Virginia's Smart Road. Table 1 shows the information for the texture measuring system used in this study. The two high-speed systems were evaluated by collecting texture data obtained from various airfield and highway surfaces and comparing them with data obtained using static referencing devices.

The texture determined by the International Cybernetics Corporation (ICC) and the MPD measured using the MGPS system show a very good correlation based on measurements taken at Smart Road. However, the ICC values are generally 50% larger than those determined using the MGPS system. Also, a strong correlation between the MGPS system and the circular track meter (CTM), which is discussed in the next section, was also observed.

Table 1 Characteristics of the texture measuring systems included in the McGhee et al. study (McGhee 2003)

Type of System	Frequency of Measurement	Name	Background	Measures
High speed (dynamic)	Semi-continuous to continuous	ICC (International Cybernetics Corporation)	Developed by private company	Proprietary texture estimate
		MGPS-Surface	Developed by FHWA (commercial outcome of ROSAN project)	Mean profile depth (ASTM E 1845)
Referencing device (static)	Discrete	Volumetric (sand patch)	Traditional	Mean texture depth (ASTM E 965)
		CTM	Developed by Nippon Sangyo Co. of Japan	Mean profile depth and root mean square

Laser Profiler Test

Cackler et al. (2006) measured and analyzed formal texture variations and grinding techniques and their respective surface characteristics, particularly with respect to tire-pavement noise for concrete pavements. For this research, Cackler et al. (2006) developed and implemented a robotic texture measurement system, RoboTex, as seen in Figure 12. RoboTex is a six-wheel, remote-controlled robot that creates 3-D textural information for concrete pavement surfaces through the use of LMI Selcom's innovative Roline line laser. General lasers (point lasers) that measure texture and smoothness rely on a single-point laser that captures elevations along a single path on a roadway. In contrast, the Roline laser projects a laser line approximately 100 mm wide, with the ability to capture 100 or more elevations across the entire line at a rate of 1 kHz. The line laser mounted on the RoboTex moves along a road surface at walking speed, thus providing a 3-D texture map with a lateral resolution of 0.5 mm to 1.0 mm, and a vertical resolution of 0.01 mm. The example figure from RoboTex is shown in Figure 13.

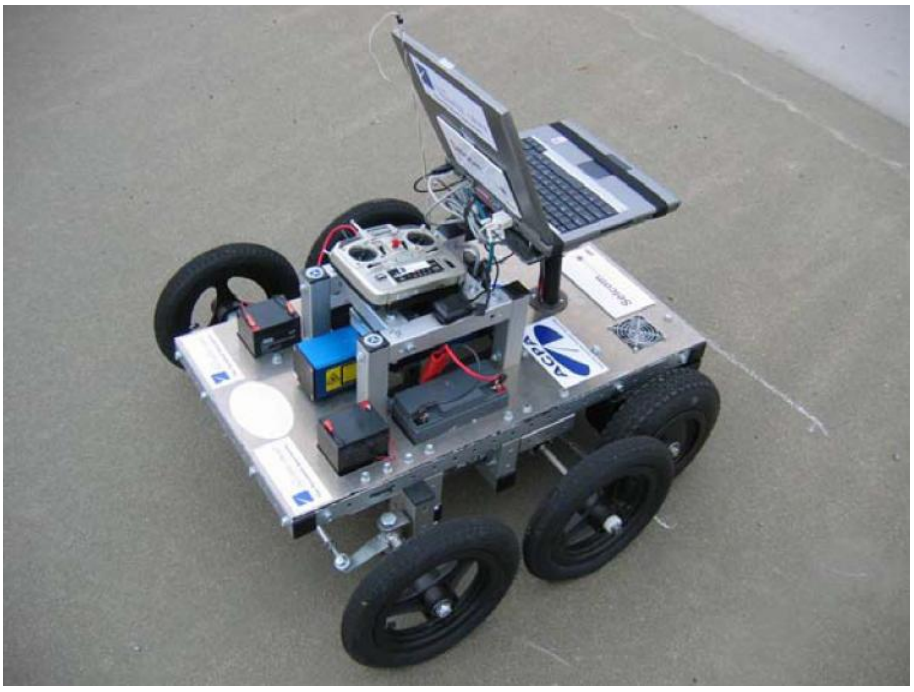

Figure 12 RoboTex with laser technology

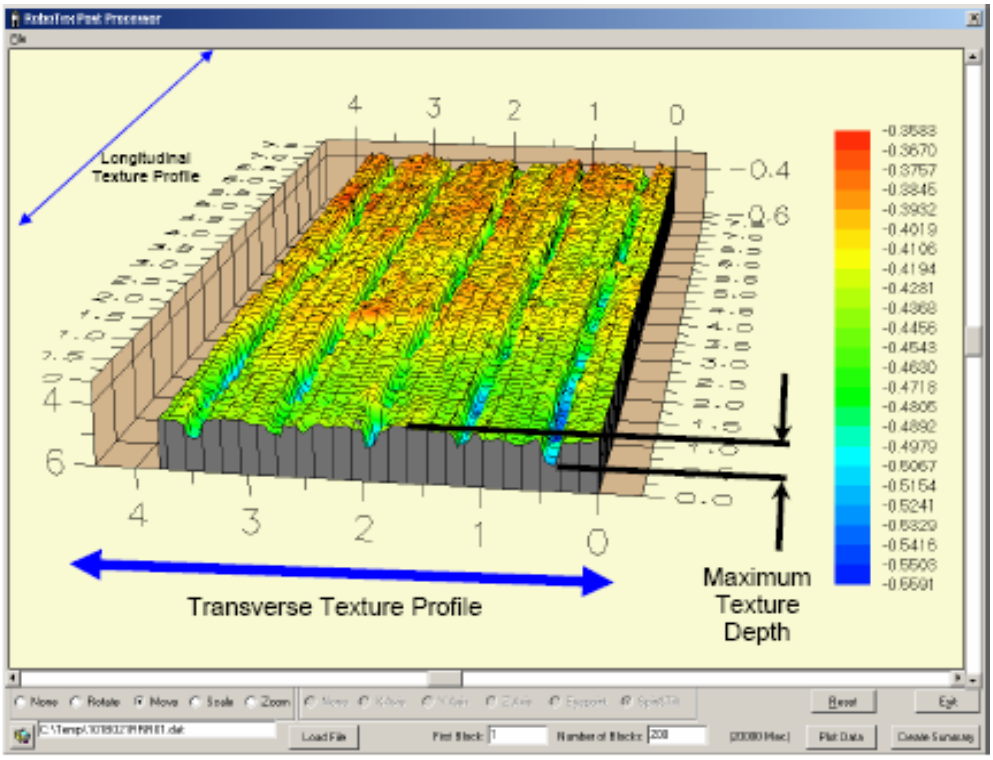

Figure 13 3-D surface texture presentation, by RoboTex

Hanson et al. (2004) evaluated the CTM (ASTM E 2147) that is used to take texture measurements of pavement surfaces, as shown in Figure 14. The CTM is a laser-based device for measuring the MPD of pavement at a static location. In order to provide comparative results for the CTM, the sand patch method (ASTM E 965) was adopted to measure the mean texture depth (MTD). Both the MPD measurements obtained from the CTM and the MTD measurements obtained from the sand patch test were collected at five random locations in each of 45 sections of the 2000 National Center for Asphalt Technology (NCAT) test track. Four different surface types in the NCAT test track were included: coarse and fine dense-graded Superpave mixes, Hveem mixes, stone mastic asphalt (SMA) and Novachip. The CTM produced comparable results to those obtained from the sand patch test (ASTM E 965). Hanson et al. developed an equation to relate the fineness modulus to the macrotexture. This equation was proved using independent data collected by the Virginia Transportation Research Council.

Figure 14 Circular texture meter (CTM)

The NCSU research team developed a laser profiler that can measure the surface texture of ASTs across a surface area, therefore called the three dimensional (3-D) laser profiler. The laser profiler that has been designed is composed of three parts: a laser, a frame, and a motor. A laser sensor is mounted on the frame, and the motor speed is set to achieve a constant traverse speed to read the distance between the sensor and the AST surface; this measurement can then be analyzed to determine the surface texture of ASTs.

Figure 15 provides the schematic diagram of the measurement system of the laser. The basic concept is that the technology measures distance without coming into contact with a variety of

surface materials. 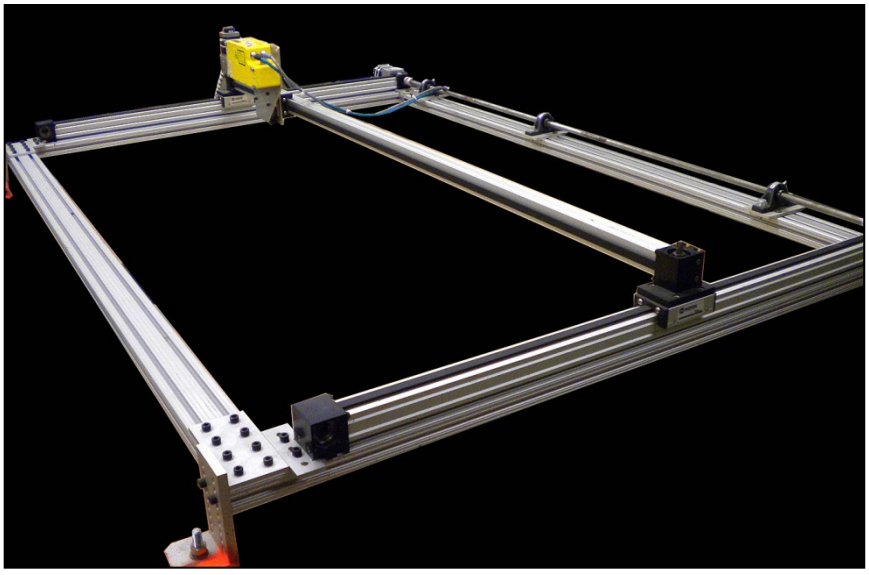

Figure 16 shows the frame for the laser profiler. The laser sensor is affixed to the top bar and can be moved transversely by a motor at a constant speed to scan the surface texture of the AST. The actual travel length of the laser is 172.7 cm. A gear drive moves the laser sensor slightly in the longitudinal direction. Therefore, the transverse movement provides data along the X coordinate (along the transverse direction of the road), and the longitudinal movement determines the Y coordinate (along the longitudinal direction of the road).

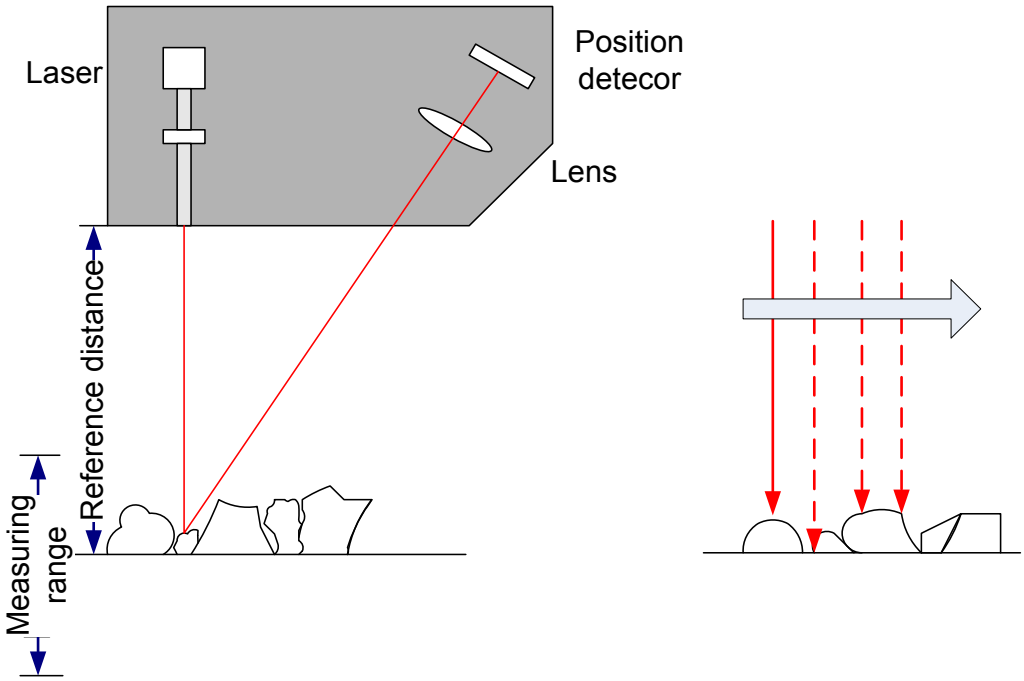

Figure 15 Schematic representation of surface texture laser

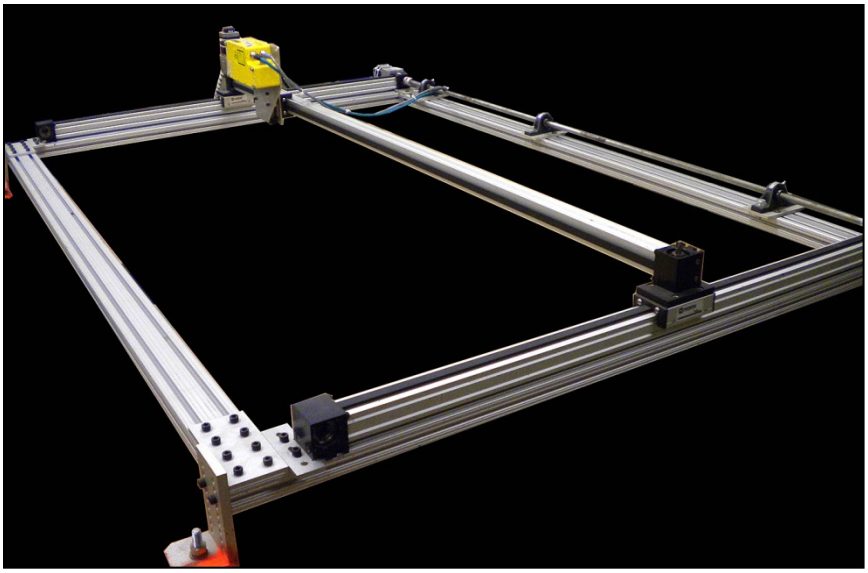

Figure 16 Schematic diagram of laser profiler frame

According to Austroads Technical Report AP-T112/80, the preferred vehicle-based laser measurement is the MPD. In looking at different types of laser profilers on the market, the research team was able to compare measurement criteria with costs, portability and feasibility in order to determine if the 3-D laser profiler should be developed further, or if another profiler already exists that would meet the measurement needs. The Mini Texture Meter (MTM), developed by a British company, WDM, Ltd., has a surface operating range of 20 mm with a surface texture resolution of 0.01 mm. The latest version of the MTM, seen in Figure 17, can produce both MPD as well as sensor measured texture depth (SMTD).

Figure 17 WDM, Ltd.'s Mini Texture Meter

Although the MTM has a smaller range than NCSU's 3-D laser profiler as well as other laser profilers on the market, its portability and simple design make it easy to use. These characteristics were applied to the design of the 3-D laser profiler in order to improve its user-friendliness.

The stationary laser profilometer (SLP) is similar to the 3-D laser profiler developed by the research team. The SLP was developed by Transit New Zealand and consists of a laser 0.5 mm in diameter that travels along a track and provides a cross-section of the aggregate surface. As seen in Figure 18, the SLP has a similar design to that of the NCSU 3-D profiler, but uses a point laser, rather than a line laser, to measure the surface.

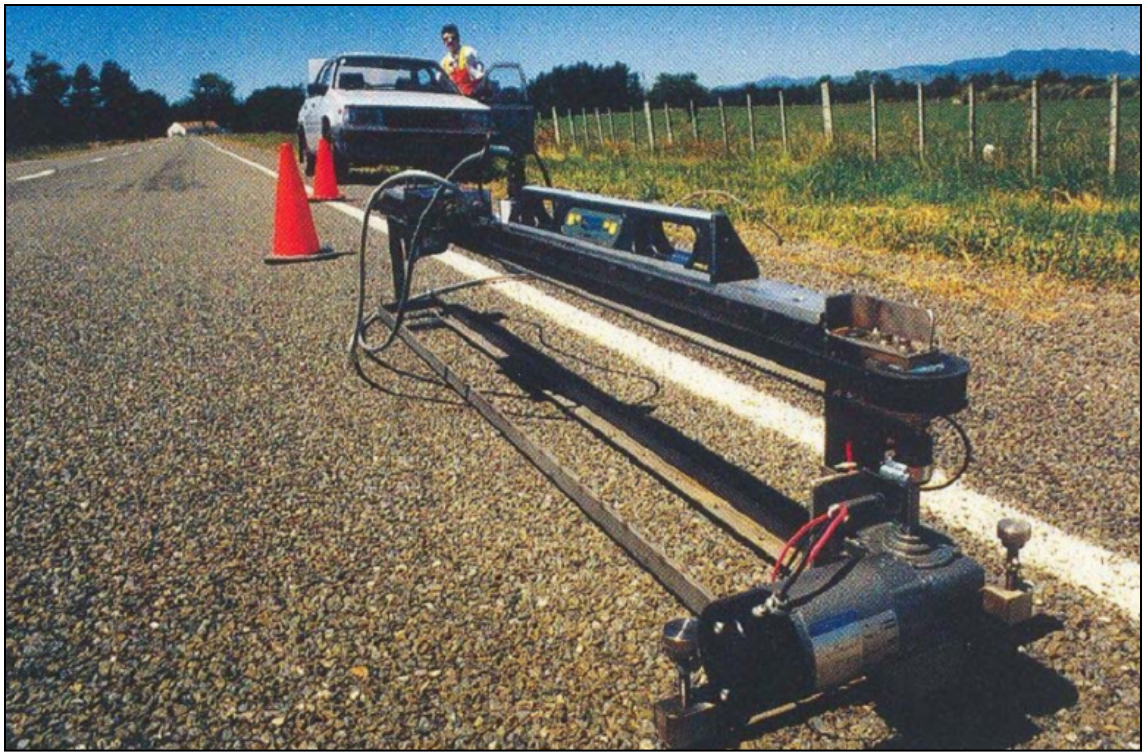

Figure 18 Stationary laser profilometer (SLP)

Figure 19 Hawkeye 2000 digital laser profiler

The ARRB Hawkey 2000 digital laser profiler (DLP) is capable of measuring MPD as well as SMTD at speeds up to 90 km/h, or 55.9 mph. The DLP is mounted on a truck and positioned

over the wheel path, as seen in Figure 19, so as to capture relevant information, and is capable of measuring profile data at 1 mm intervals. Although the DLP offers impressive features, the research team determined that the convenience and ease of collecting the necessary data do not outweigh the estimated $160,000 of the vehicle-mounted laser. Although the DLP can collect a vast amount of information within a few minutes, it was deemed more beneficial to keep the costs down and collect fewer, but more relevant, data points.

3. DEVELOPMENT OF 3-D LASER PROFILER FOR THE IN SITU PERFORMANCE TESTING OF ASTS

3.1 Original 3-D Laser Design

The original 3-D laser profiler, shown in Figure 20, was designed by the NCSU research team to measure the distance between the laser sensor and the pavement surface in both the longitudinal and transverse directions of the pavement to produce a 3-D map of the pavement surface texture. Specifically, the laser scans a 97 mm line on the pavement surface in the longitudinal direction and obtains one distance measurement per millimeter along that 97 mm line. The resulting data, separated into 1 mm increments along the 97 mm line, provide an accurate picture of occurrences at the microscopic level of the surface of the field sections and laboratory test specimens. Then, the laser moves in 2 mm increments in the transverse direction, perpendicular to the wheel traffic direction, and takes another 97 mm line scan to the end of the travel length of the field section or specimen. This procedure is displayed in Figure 21.

From this procedure, 3-D data are obtained that are then manipulated to determine the MPD for that particular field section or specimen. This procedure involves taking the raw data from the scan of a particular section or specimen and determining the overall MPD value using Equation (1). That is, the height information collected from each 97 mm line is used to determine the MPD value for that line. This operation is repeated every 2 mm in the transverse direction to determine the MPD values for numerous 97 mm scans along the transverse direction of the pavement. Then, all the 97 mm MPD values are averaged to obtain a final MPD value for that section or specimen.

Figure 22 displays the micro-texture data obtained from scanning a field test section that has been trafficked under real field traffic conditions for two days after the initial construction of the test section. These data are representative of all the data obtained from the scan and were not processed at all prior to being graphed. Figure 22 illustrates the ability of the 3-D laser to capture the micro-texture of each aggregate particle in addition to that of the overall wheel path; such accuracy is essential in determining the surface texture and the MPD changes that occur under traffic loading over time. Figure 22 is color-coded based on height to depict the wheel path more clearly. The graph shows the two 97 mm-wide scans that were performed on one particular location of Section 3.

Figure 20 Photo of the 3-D laser profiler scanning a chip seal field section

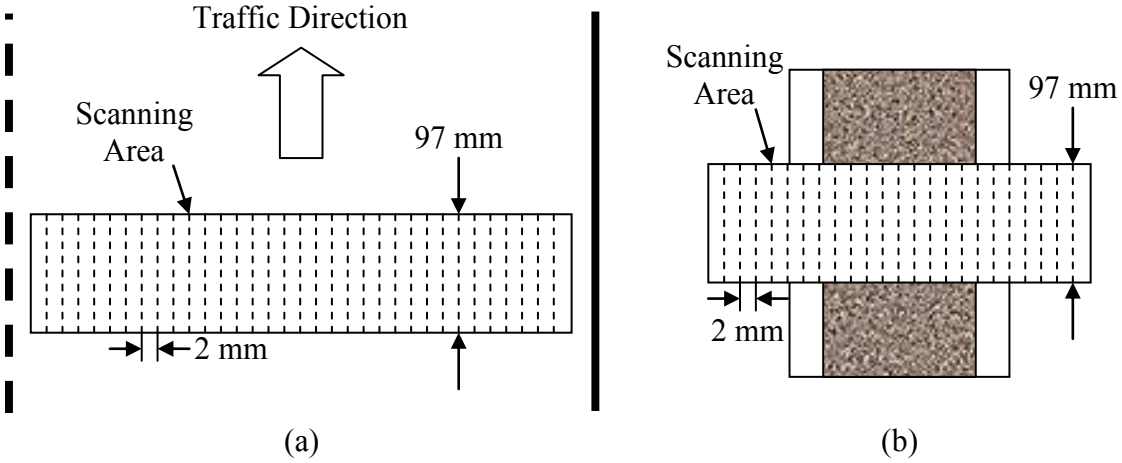

Figure 21 Schematic diagram of the laser scanning procedure: (a) for the field section and (b) for the MMLS3 sample

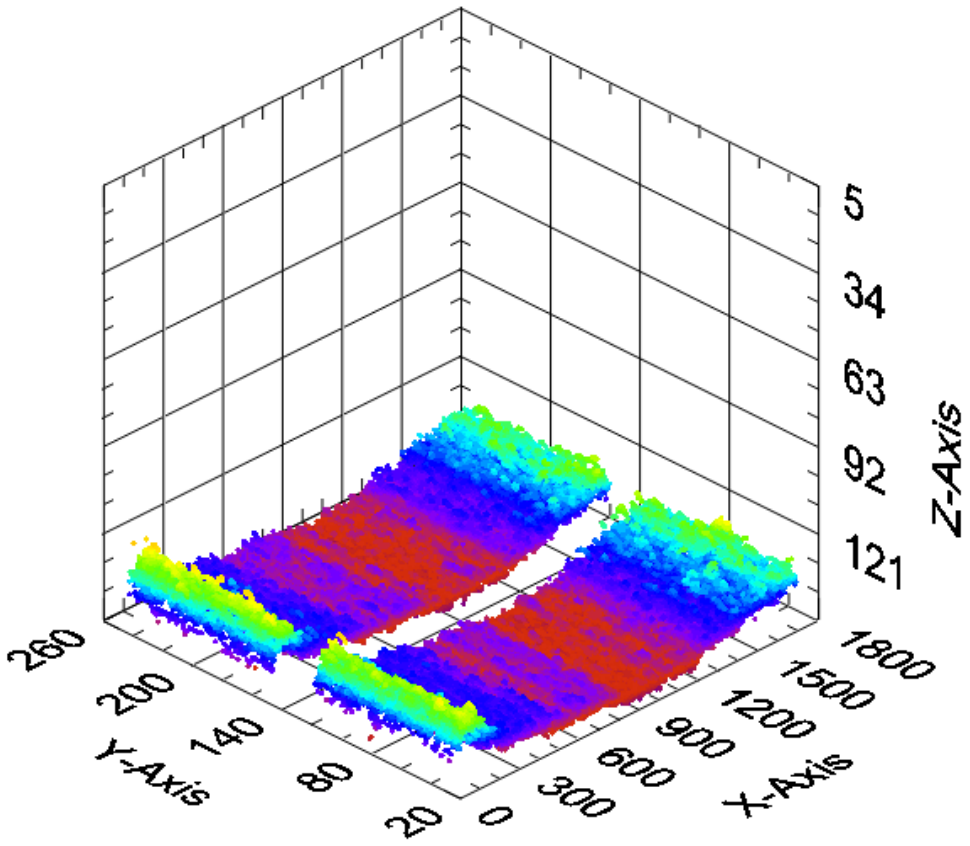

Figure 22 3-D laser profiler graph of a chip seal pavement

The 3-D laser profiler first measures the distance between the laser sensor and the pavement surface in both the longitudinal and transverse directions of the pavement and produces a 3-D map of the pavement surface texture, displayed in Figure 22. The distances measured along the 97 mm line are processed to determine the minimum (valleys) and maximum (peaks) points in the AST profile. Figure 23 displays an example output of the surface profile measurements, transverse to the traffic flow, taken eleven days after construction at the medium traffic volume test road. This test road was built to support the research under NCDOT project HWY-2008-04. This section has a double seal constructed with granite 78M aggregate for the bottom layer and lightweight aggregate for the top layer. The maximum and minimum profile depths are shown in green and blue, respectively, and red represents the average profile depth. (Note: Although the research team recognizes that the readers will not be able to distinguish these colors in their monochromatic copies, the presentation of three complex profiles in one graph necessitates the use of colors in developing the graphs for this report.) The area highlighted by the rectangle represents the measured wheel path after trafficking.

The rutting due to traffic loading can be seen from these transverse profiles. Because the profiles shown in Figure 23 are drawn with data points 2 mm apart, they can be used to determine the macro-profile (such as rutting) of the pavement surface rather than the micro-textural profile. The micro-profile was determined using the 1 mm separated data along the longitudinal direction

of the pavement and was needed to determine the aggregate exposure depth, which is an important parameter in developing the void reduction model for NCDOT project HWY-2008-04.

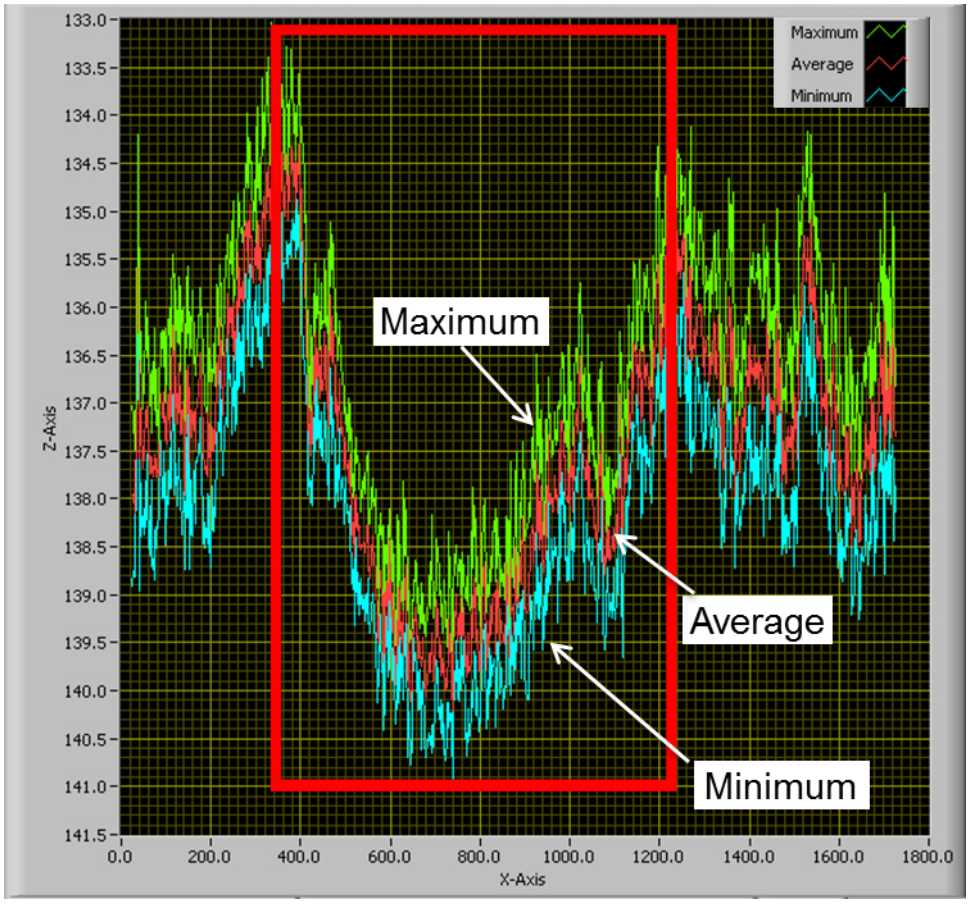

Figure 23 Software data presentation of surface profiles

Unfortunately, not all the field scans obtained from the 3-D laser profiler are as clear as that shown in Figure 23. The lowest point on the scan, ideally the middle of the wheel path, was extremely hard to locate in some cases. Thus, the width of the wheel path was almost impossible to determine, and the data were difficult to decipher. In order to keep the scans relatively consistent between placements, the edge of the 3-D laser profiler was placed on the outside lane marking each time. However, because the wheel path is determined by the driver, the wandering area can fluctuate dramatically which, in turn, affects the distance from the outer lane markings. Hence, the location of the wheel path is difficult to determine when looking at the surface profile scan.

As seen in Figure 24, the wheel path is also difficult to locate depending on the quality of the scan itself. In this specific example, the profile depth is clearly lower on the left-hand side of the graph, but the locations of both the wheel path and the low point on the graph are hard to specify. The quality of these scans could be due to poor execution by the 3-D laser or could be the result

of skewed placement on the pavement. A poor or unusable scan usually is indicated by a severe spike in the surface profile graph.

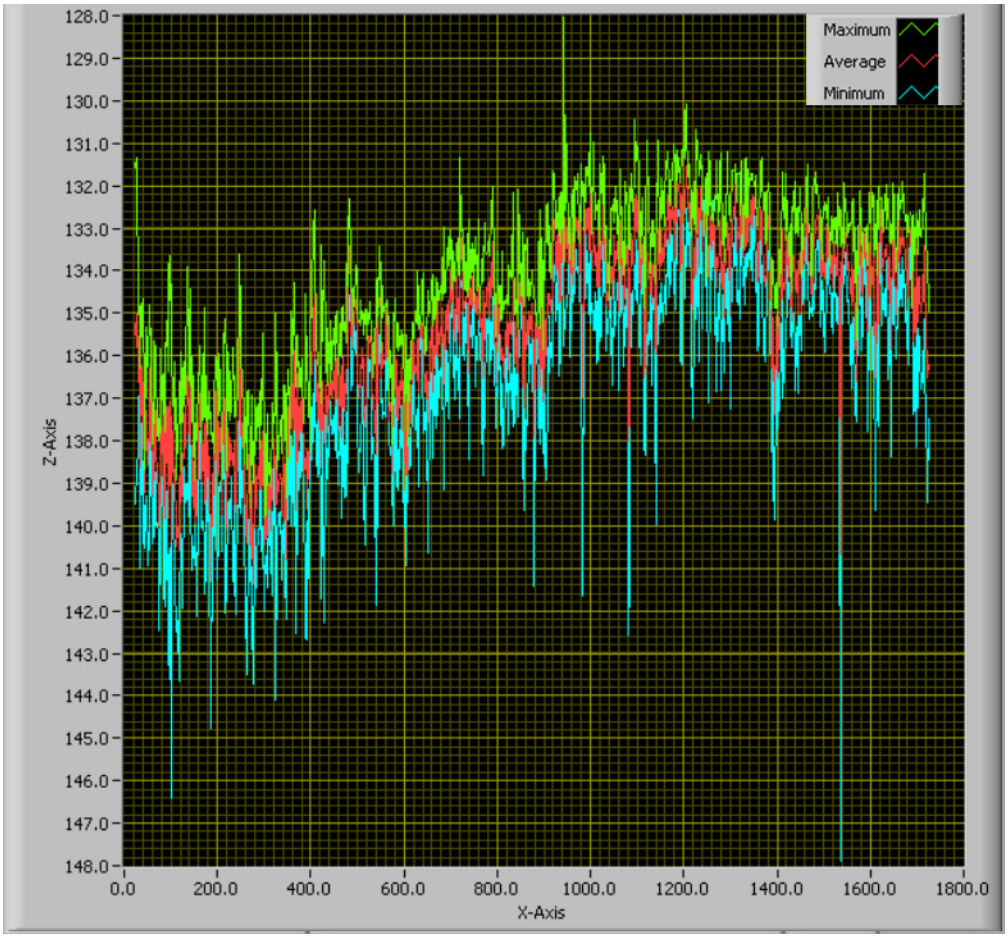

Figure 24 Failed software output of the surface profile

Figure 25 clearly shows a spike of nearly 110 mm in the profile depth. This reading indicates (erroneously) that the scanner passed over aggregate nearly 4.33 inches high and only 0.39 inch wide. If such an error occurred in only one or two of the field scans, the research team might have been able to attribute the spike to debris in the roadway, but these spikes appeared in numerous scans throughout the dataset, rendering the scans useless when determining the wheel path width and aggregate exposure depth. Such errors can most certainly be attributed to a fault in the 3-D laser profiler's performance.

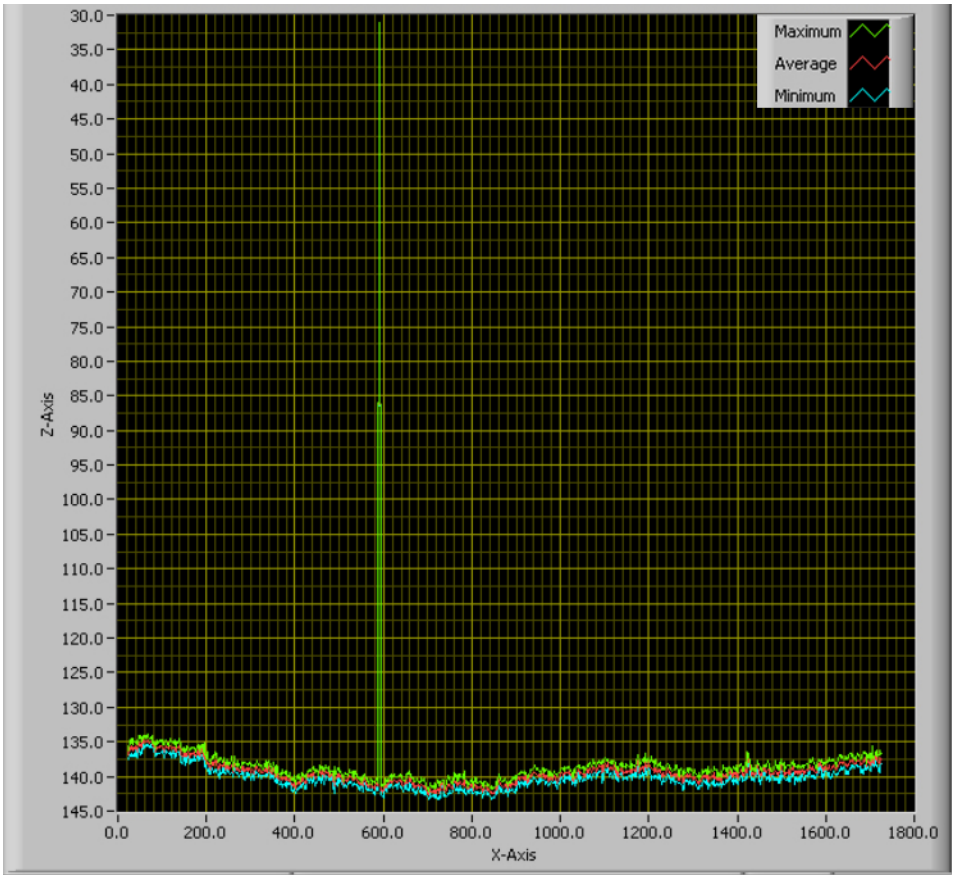

Figure 25 Failed software output due to a spike in the surface profile

3.2 Capturing the Wheel Path

The frame of the 3-D laser profiler that is shown in Figure 20 is 1,524 mm wide and 1,727 mm long, which made the profiler too heavy and too large to transport. Because the primary objective of the laser profiler is to determine the micro-texture of the pavement surface rather than the transverse profile of the entire lane width, the research team decided to downsize the profiler so that it would fit within the wheel path. Aside from lane changes and severe wandering, vehicles stay primarily within the wheel path, which causes this area to have the most noticeable change in MPD. In order to downsize the unit properly, the research team needed to better appreciate the amount of laser scan data needed in order to make statistically valid conclusions. Upon understanding this aspect better, a practical and useful device and associated protocol could be suggested.

The original 3-D laser (i.e., that shown in Figure 20) required that a portion of the collected data needed to be extracted in order to isolate the wheel path data. However, reducing the laser scan distance and fitting the laser within the wheel path caused each data point collected to be relevant and useful, so no extraction was necessary. This change allows the data collection time to be reduced significantly.

Determination of the wheel path width and exposure depth hinges upon the accuracy and reliability of the laser profiler. Although the research team had been pleased with the profiler's

performance overall, errors such as the spikes in the surface profile graph had to be corrected before the design could be finalized. The field testing system must be error-free in order to be user-friendly and accurate outside of the lab. Importantly, the final design must be reliable and provide data that can be interpreted without fear of inherent errors.

The research team then worked to determine the optimal length for the 3-D laser profiler, based on the width of the wheel path. Aside from lane changes and severe wandering, a vehicle should occupy the wheel path for most of its travel time. Therefore, the wheel path is the most important aspect of the paved surface when measuring characteristics such as aggregate exposure depth, skid resistance, aggregate loss and bleeding. The 3-D laser profiler measured 1,703 mm in the transverse direction to the roadway. After examining all the data gathered from field measurements, the research team determined that 1,703 mm, or 67 inches, was not enough distance to capture both the inner and the outer wheel paths simultaneously.

After measuring the width of the scanned wheel path for numerous field sections under varying degrees of traffic load, the average wheel path width was found to be 1,158 mm, or nearly 3.8 feet. The research team then decided that scanning only the outer lane wheel path was sufficient for analyzing AST distresses. The outer wheel path is known to show extreme deterioration and effects of trafficking due mainly to its location near the shoulder, as well as the effects of transverse grade and water runoff. Therefore, measurements obtained from the outer wheel path, and the conclusions reached as a result of those measurements, can be considered conservative. The laser profiler, as it is seen in Figure 20, was then modified to capture only the outer wheel path, rather than try to span the distance of nearly 12 feet to capture both wheel paths. This modification also served to improve the portability and ease-of-use of the laser profiler. Portability is a major criterion when developing the field testing system for ASTs. Initially, the length and width of the frame were too large for one person to handle the profiler alone. By reducing the size of the laser profiler, it should become much easier for one person to transport.

The final scanning width of the laser profiler was determined using the field data. The field scans conducted in the fall of 2008 were performed by two side-by-side passes of the laser in the direction transverse to the traffic flow. The team determined that two passes, each measuring 4 inches across, would provide plenty of information for analysis. Therefore, the laser profiler was narrowed to be wide enough for two passes of the laser. By reducing both the width and the length of the laser profiler frame, both portability and efficiency have been improved substantially.

The surface profile data captured from only one wheel path (the outer wheel path) of a field section that is in the early stage of the life using the original 3-D laser profiler are shown in Figure 26 through Figure 29. The information displayed in the graphs was obtained from the same spot in the medium volume field section (approximate ADT of 4,500 vehicles) on September 22 (the initial construction date), September 23, September 24, and October 3, all in 2008. This section was a single seal section using 78M aggregate. It is important to note that because the profile depths shown are calculated as distances from the laser to the surface, the graphs should be analyzed upside down in order to see the wheel path and non-wheel path areas of the profile.

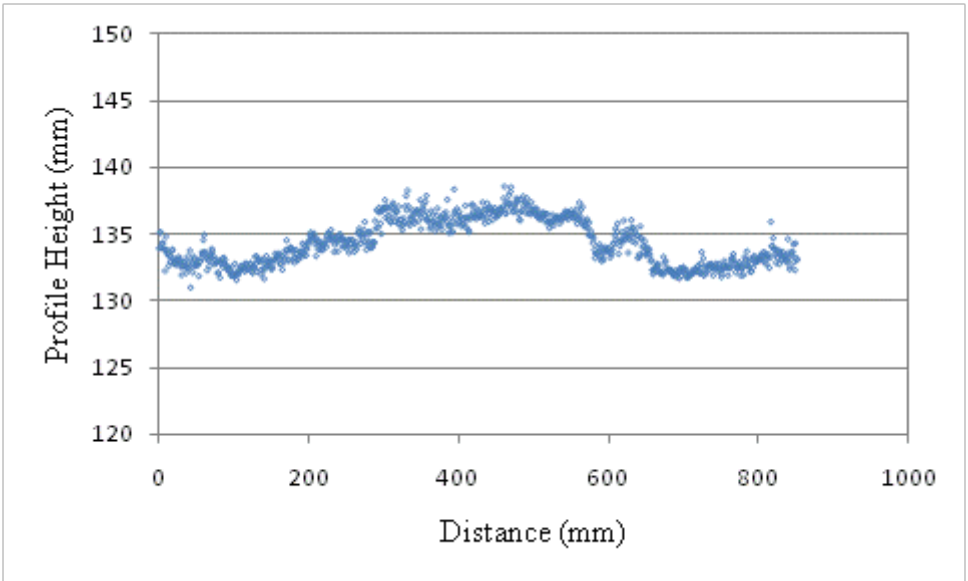

Figure 26 Surface profile on 9/22/2008

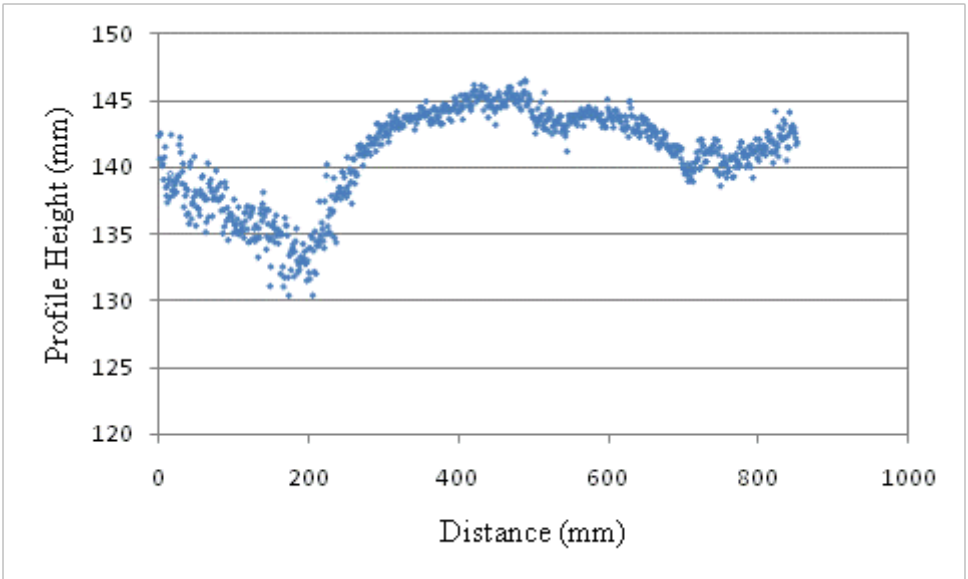

Figure 27 Surface profile on 9/23/2008

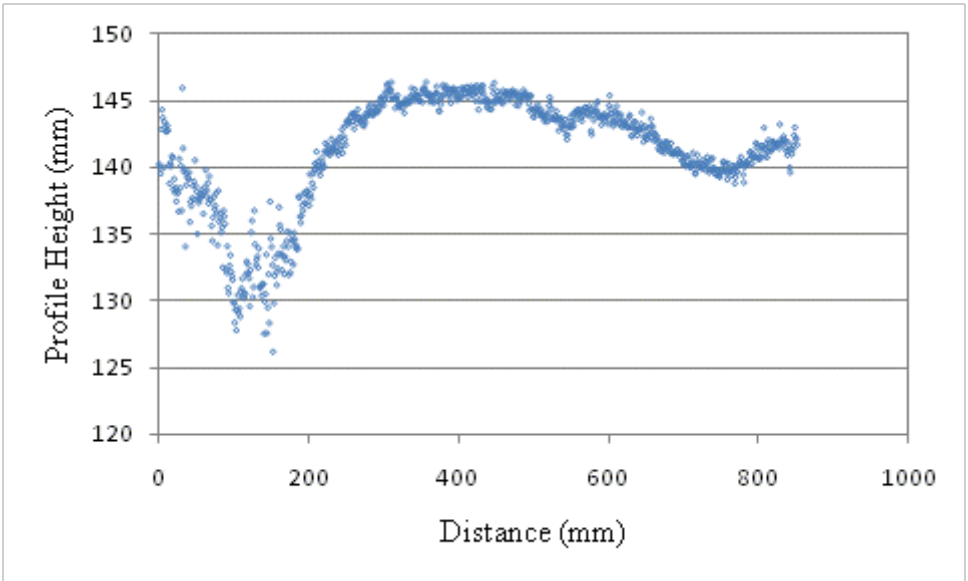

Figure 28 Surface profile on 9/24/2008

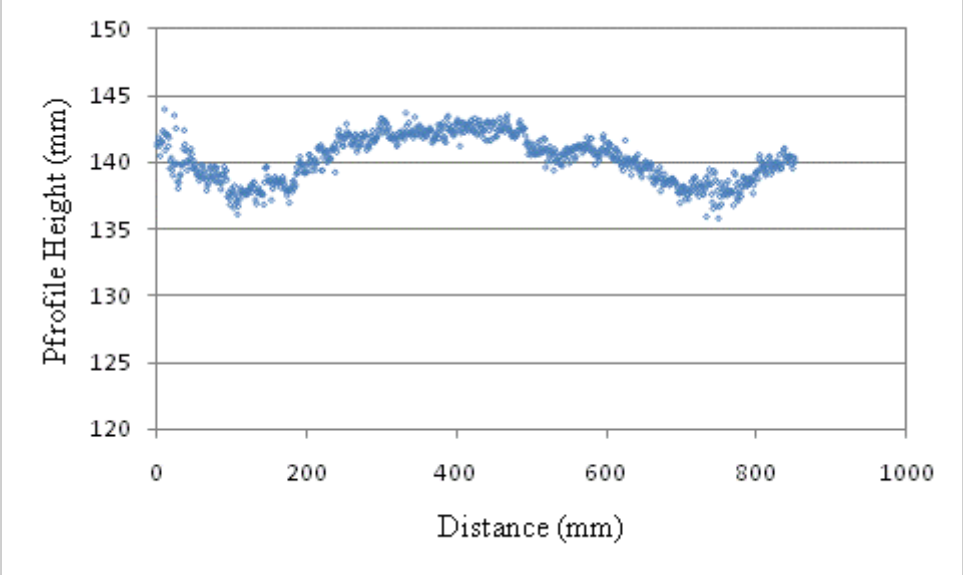

Figure 29 Surface profile on 10/3/2008

Figure 26 shows the surface profile immediately after the chip seal was constructed. At this point, the test section had not been subjected to any traffic loading. The next figure, Figure 27, presents the scan of the section after one day of traffic loading on the test section. This figure shows a wheel path that is deeper and more definitive than the un-trafficked wheel path scanned on the initial test section construction date. Figure 28 shows a clearly defined non-wheel path area. The section of the graph that is spiky, that is between 100 and 200 mm (on the x-axis), represents the non-wheel path area between the two wheel paths in the traffic direction. The other side of the wheel path (in the range of approximately 650-900 mm on the x-axis) moves

towards the unpaved shoulder in this section. Figure 28, in comparison to Figure 27, shows the surface profile one day later. The lowest reading of the wheel path is still around 145 mm (as read from the y-axis), but the profile of the non-wheel path area between the two wheel paths is 5-7 mm higher as a result of the asphalt mass shifting under loading. A reverse trend is found in Figure 29, which shows the scan that was taken nine trafficked days after Figure 28 was scanned. Most notably, the profile of the non-wheel path area between 100 and 200 mm is significantly lower than it is in Figure 28 that shows the scan taken nine days earlier. This difference is probably due to the wandering of vehicles into the non-wheel path area over the course of those nine days, which caused some of the asphalt mass that accumulated there to be pushed into the wheel path area. This movement of mass from the non-wheel path area into the wheel path results in the increase of the profile in the wheel path by approximately 5 mm from 145 mm (as read from the y-axis) on September 24, 2008 to 140 mm (read from the y-axis) on October 3, 2008. The non-wheel path peak drops about 15 mm as a result of this shift in mass.

3.3 Sensitivity Analyses

In order to determine the necessary scan width, sensitivity analysis was conducted using the laser scan data obtained from the chip seal pavements tested during the HWY-2008-04 project. The objective of this analysis is to determine the optimal scanning width that is small enough to be embedded within the wheel path and large enough to capture the representative exposure depth of the wheel path. First, the location of the lowest point in the wheel path is found for each section scan. From that point, the average MPD is determined for twelve different scanning widths, as indicated in Table 2 and Table 3.

Table 2 Sample sensitivity analysis for 12 different widths: Section 3, Spot 50 (medium traffic)

	Total Wheel Path MPD (mm)											
Date	**±300**	**±250**	**±200**	**±150**	**±114**	**±100**	**±86**	**±70**	**±56**	**±42**	**±28**	**±14**
9/22/08	3.08	3.09	3.10	3.15	3.11	3.12	3.08	3.08	3.08	3.10	3.20	3.15
9/23/08	3.22	3.15	3.02	2.85	2.68	2.66	2.68	2.69	2.74	2.76	2.81	2.89
9/24/08	2.34	2.33	2.33	2.33	2.33	2.33	2.35	2.36	2.38	2.47	2.55	2.66
10/3/08	2.25	2.25	2.27	2.23	2.23	2.24	2.19	2.16	2.16	2.17	2.15	2.27
4/8/09	1.97	1.96	1.92	1.86	1.78	1.77	1.73	2.03	2.00	2.01	2.01	1.99

Table 3 Sample sensitivity analysis for 12 different widths: Section 1, Spot 50 (medium traffic)

	Total Wheel Path MPD (mm)											
Date	**±300**	**±250**	**±200**	**±150**	**±114**	**±100**	**±86**	**±70**	**±56**	**±42**	**±28**	**±14**
9/22/08	3.52	3.48	3.46	3.43	3.45	3.44	3.43	3.46	3.52	3.55	3.73	3.91
9/23/08	1.82	1.87	1.90	1.94	2.02	2.05	2.05	2.05	2.03	1.93	1.87	1.92
9/24/08	3.12	3.08	3.02	2.91	2.73	2.61	2.60	2.55	2.49	2.44	2.29	2.20
10/3/08	1.95	1.94	1.96	1.98	1.99	2.02	2.05	2.06	2.04	1.99	1.99	2.00
4/8/09	1.88	1.89	1.89	1.90	1.87	1.86	1.86	1.87	1.86	1.87	1.90	1.85

Using Equation (1) to calculate the MPD, the peak value is found among the first 48 points of a line scan as well as the second 49 points. Because the 3-D laser profiler measures the distance from the laser to the pavement surface, the peak value is actually the lowest number when observing the raw data. The average of all 97 data points is then subtracted from the average of the two peak values. This number is the MPD for that 97 mm scan. The MPD values are determined for each scan within a sampling width.

The results shown in Table 2 and Table 3 suggest that the average MPD values remain relatively constant for scan widths greater than 56 mm and smaller than 150 mm. Based on this observation, further sensitivity analysis was carried out for each sampling width of +/- 150 mm, +/- 124 mm, and +/- 100 mm from the lowest point in the wheel path. Partial results are displayed in Table 4 through Table 7.

Table 4 MPD data from Section 3, Spot 60 (medium traffic level)

	Total Wheel Path MPD		
Date	**±150 mm**	**±124 mm**	**±100 mm**
9/22/08	2.89	2.92	2.92
9/23/08	2.52	2.38	2.33
9/24/08	2.17	2.17	2.15
10/3/08	2.16	2.21	2.20

Table 5 MPD data from Section 8, Spot 55 (medium traffic level)

	Total Wheel Path MPD		
Date	**±150 mm**	**±124 mm**	**±100 mm**
9/22/08	3.40	3.41	3.44
9/23/08	2.51	2.53	2.53
9/24/08	2.08	2.09	2.08
10/3/08	2.14	2.13	2.14

Table 6 MPD data from Section 9, Spot 50 (medium traffic level)

	Total Wheel Path MPD		
Date	**±150 mm**	**±124 mm**	**±100 mm**
9/22/08	3.18	3.22	3.28
9/23/08	2.62	2.59	2.59
9/24/08	2.29	2.28	2.23
10/3/08	2.15	2.10	2.21

Table 7 MPD data from Section 2, Spot 60 (medium traffic level)

	Total Wheel Path MPD		
Date	**±150 mm**	**±124 mm**	**±100 mm**
9/22/08	3.56	3.55	3.55
9/23/08	2.16	2.16	2.15
9/24/08	1.95	1.96	1.96
10/3/08	1.90	1.93	1.91

For each MPD analysis, a graph was created to help visualize the trends of the MPD as a function of the sampling width. As shown in Figure 30 to Figure 32, these graphs show how significantly the MPD changes over time, as well as how sensitive the MPD value is to different scan widths (200 mm, 248 mm, and 300 mm).

The graphs in Figure 30 and Figure 31 are considered 'normal' in that the MPD values decrease continuously from 9/22/08 until 10/3/08. Although this outcome could be expected, this steady decrease is not always the case. In many cases, as in Figure 32, an increase in the MPD can occur at a later date. According to the scan presented in Figure 32, the MPD values actually increase from 9/22/08 to 9/23/08. After looking at a number of medium and low volume readings, it is not uncommon for the second day to have higher MPD readings than the construction day. One reason for this occurrence could be due to the movement of the dislodged aggregate particles. As vehicles drive over the newly constructed chip seal, the excess aggregate may be pushed toward the rutted wheel path and, therefore, cause a buildup of excess aggregate within the wheel path. In most cases, however, the MPD measurement continues to drop after the second day, regardless of an increase or decrease during the first 24 hours of trafficking.

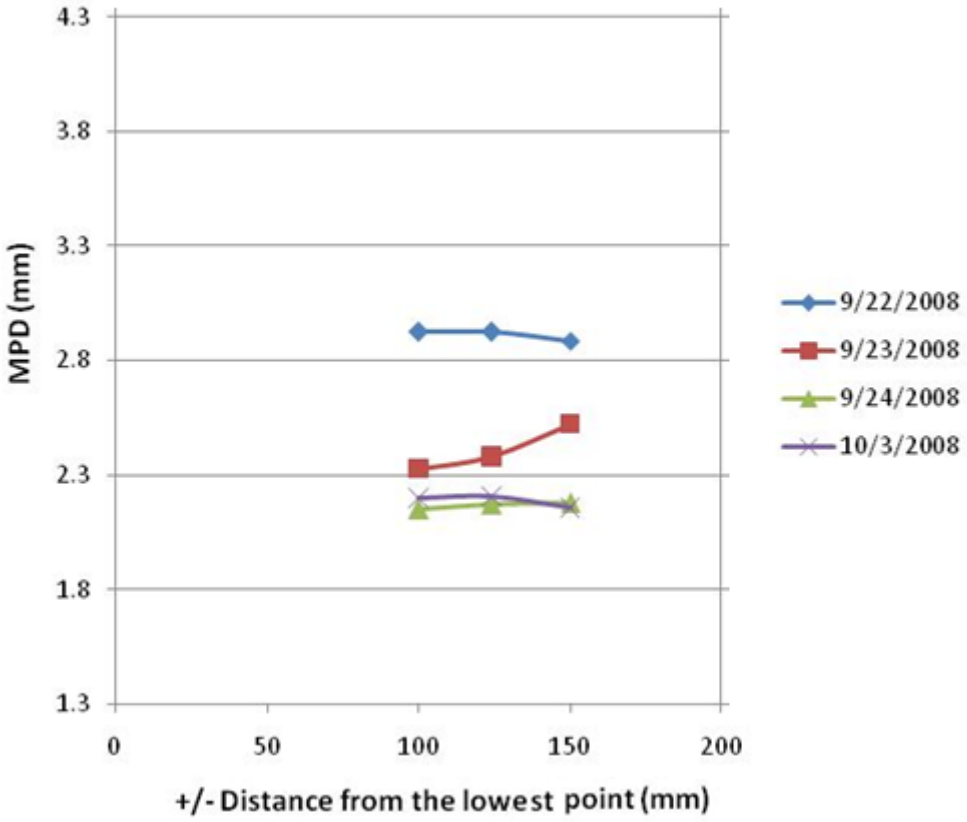

Figure 30 MPD graph for Section 3, Spot 60 (medium traffic level)

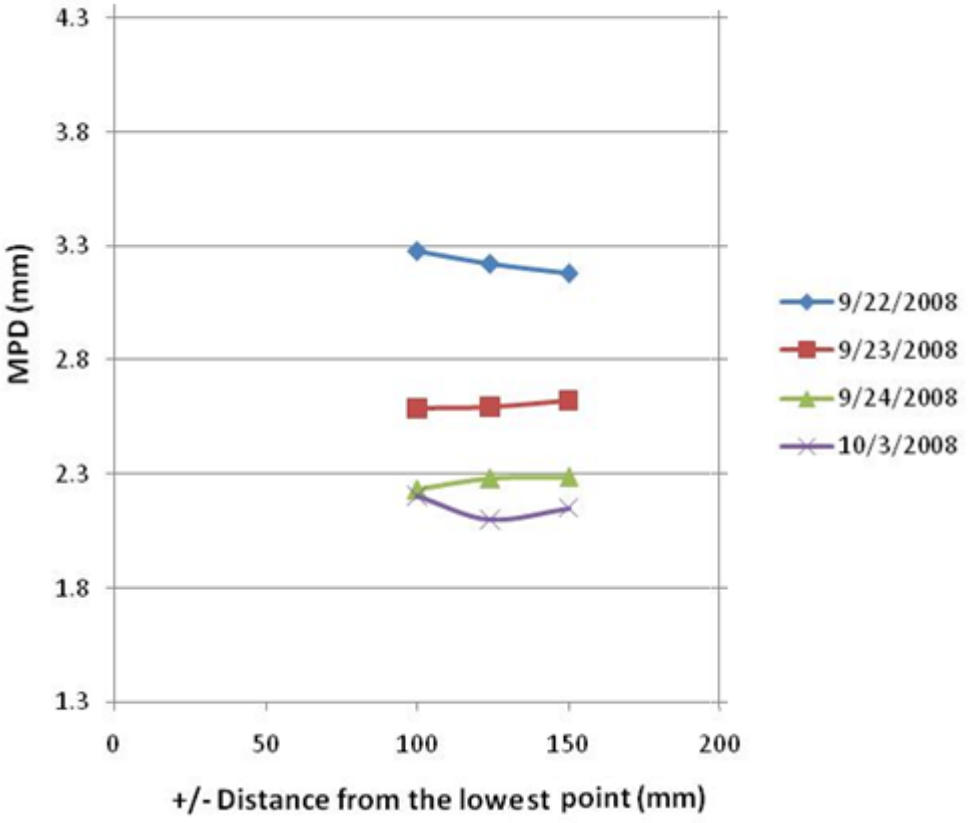

Figure 31 MPD graph for Section 9, Spot 50 (medium traffic level)

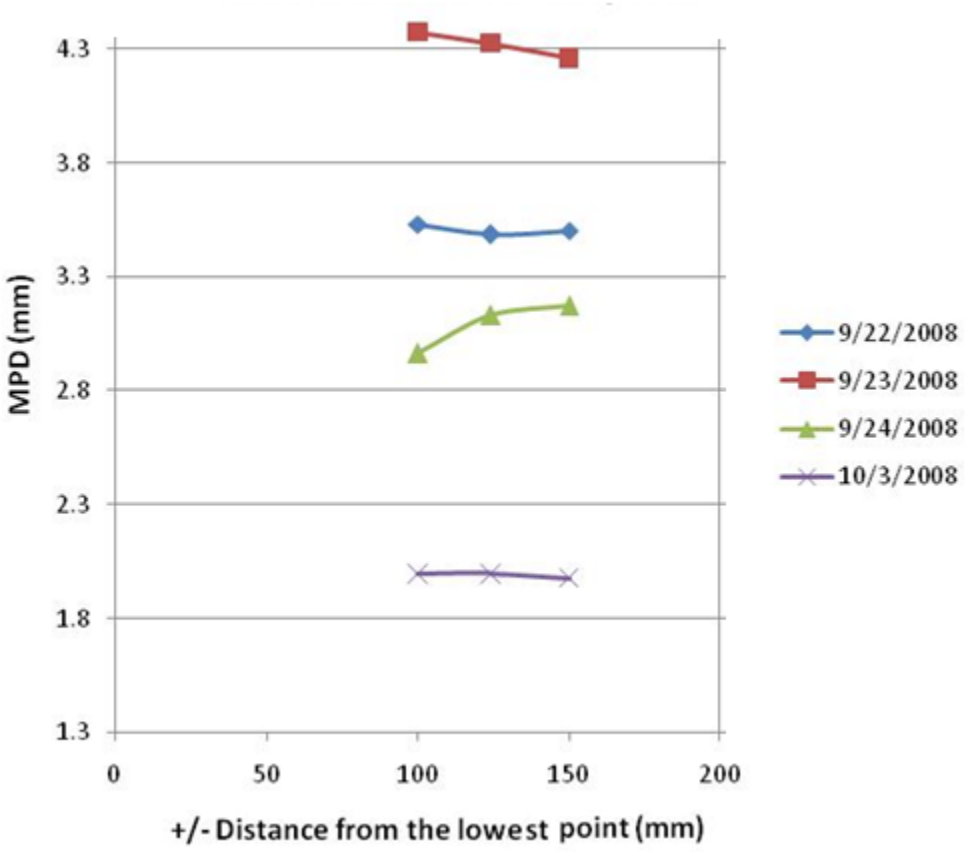

Figure 32 MPD graph for Section 1, Spot 55 (medium traffic level)

After completing this second sensitivity analysis for each spot within each section, it was determined that +/- 124 mm from the lowest point is the optimal scanning width. This width includes enough data points to create a representative sample of the wheel path, but is small enough to fit easily within the wheel path.

The two sensitivity analyses for width of the wheel path were carried out on all the low volume and medium volume sections. The high volume data proved to be a bit troublesome in that the wheel path was not captured accurately in most of the scans. The placement of the laser was the same as in the low and medium volume sections, but the wheel path generally appeared to be much wider and less defined within the high volume readings. As a result, the entire wheel path could not be captured by the laser, although this problem was not discovered until three or four scans had already taken place. Because of this issue, the sensitivity analysis could not be completed accurately for many of the high volume sections; however, sufficient data were obtained from the low and medium volume sections for which the same width of +/- 124 mm applies as for the high volume road.

One reason for the wider wheel path in the high volume road compared to the low and medium volume roads could be a slight failure in the sub-base. The high volume road could have a

weaker base and subgrade than the lower volume roads. Thus, the wheel paths that were once two well-defined wheel paths have become one wide dip in each lane.

3.4 Final Design of the 3-D Laser Profiler

3.4.1 Housing Frame

As was discussed in the previous sections, the original 3-D laser profiler was much too heavy and much too large to be considered portable. Also, the research team determined that only the data obtained from within the wheel path needed to be analyzed, rather than the entire lane width as originally thought. After conducting sensitivity analyses, the research team determined the wheel path to be approximately 280 mm wide. Based on these findings, the 3-D laser profiler was then redesigned to make the testing device much more portable and much smaller, as shown in Figure 33.

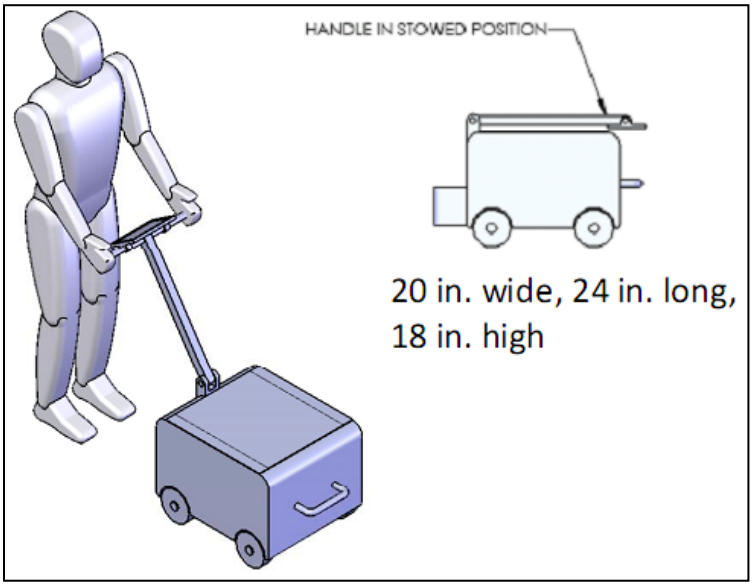

Figure 33 Redesigned laser profiler

The new laser profiler design includes the following features: XY Gantry robot, encoders, GPS, PC (Windows XP compatible), external USB interface, rubber wheels, touch screen LCD, stowaway handle, carrying handles, graphical user interface (GUI), rechargeable battery, and AC power.

The final design of the 3-D laser profiler weighs approximately 100 lbs, and the scan time, although variable, takes about five minutes to complete, which is faster than the previously used Selcom RoLine FP1000 line laser.

3.4.2 Laser System

In order to finalize the redesign of the 3-D laser profiler, the research team needed to determine the type of laser to be used for data collection. In the earlier design, the team selected the Selcom RoLine FP1000 line laser to collect the embedment depth data. This method of collecting data is quite effective for 3-D laser images and modeling, but is somewhat excessive for the simple embedment depth readings that are of specific interest to the research team. Line lasers are, in general, more costly than simple point lasers, and the research team wanted to optimize the cost as much as possible. In order to determine if a point laser could collect sufficient data, the MPD was calculated using different numbers of data points and plotted against the number of data points. By investigating the changes in MPD as the number of data points increases, the minimum number of data points necessary to determine the representative MPD could be found. The research team selected six different field sections for analysis, and the results are shown in Figure 34 through Figure 39.

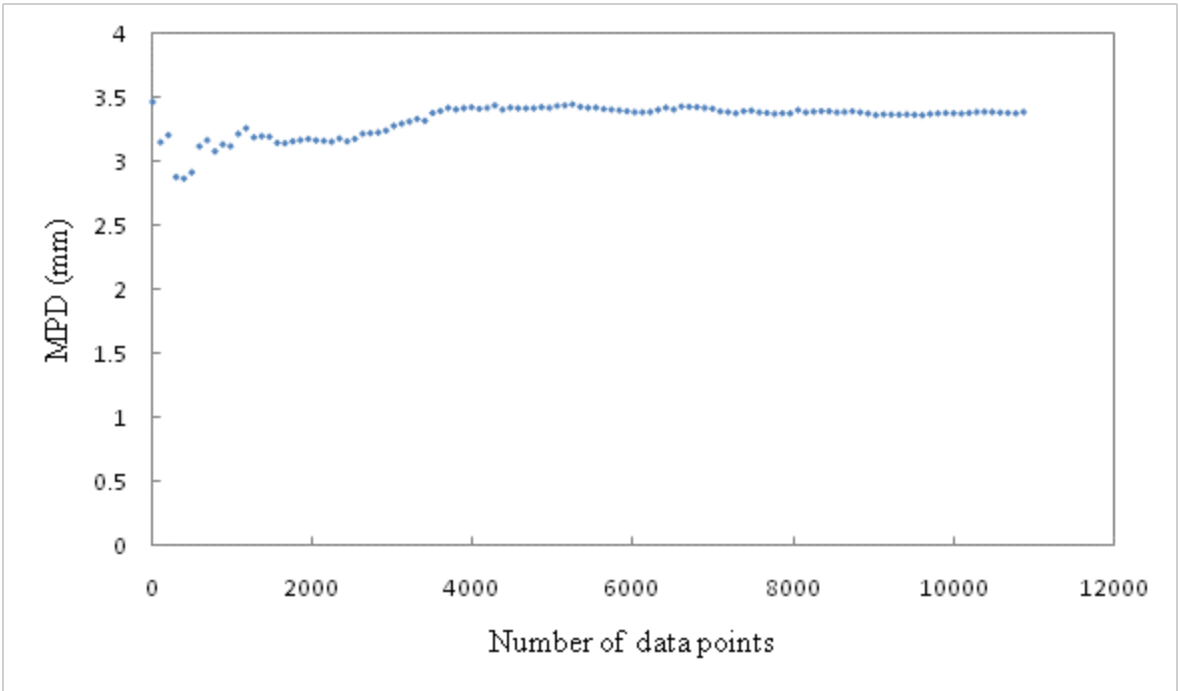

Figure 34 MPD vs. number of data points along Section 8 (medium volume), 9/22/2008 (day 1 of trafficking)

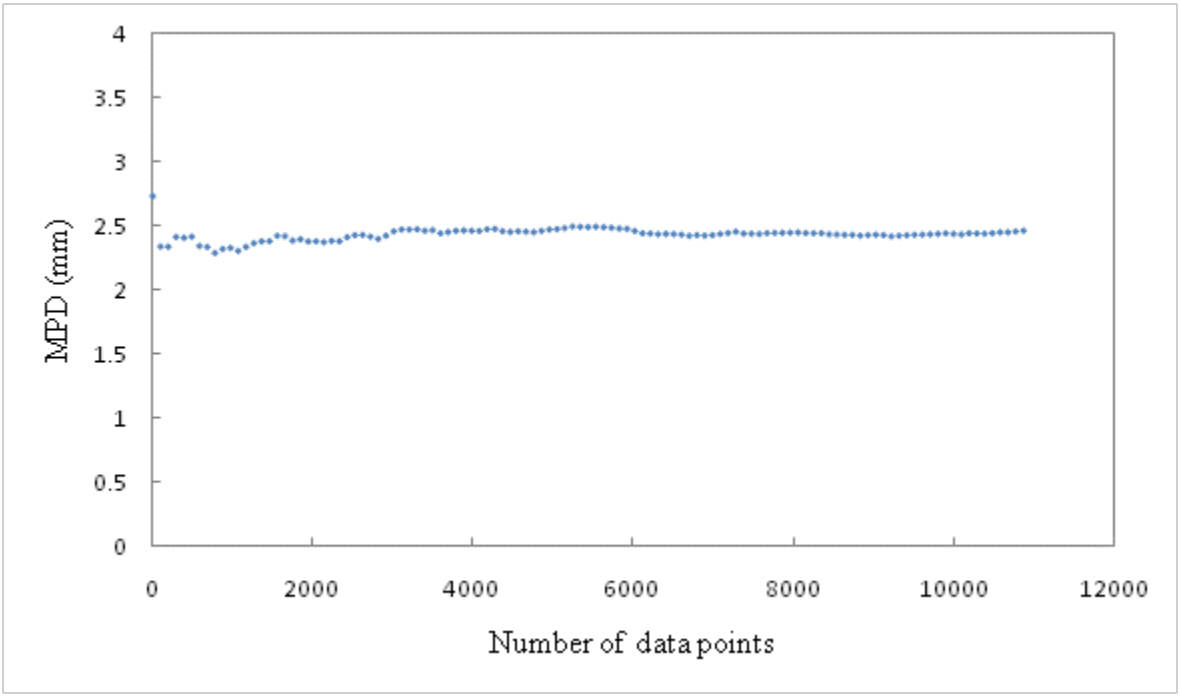

Figure 35 MPD vs. number of data points along Section 8 (medium volume), 9/23/2008 (day 2 of trafficking)

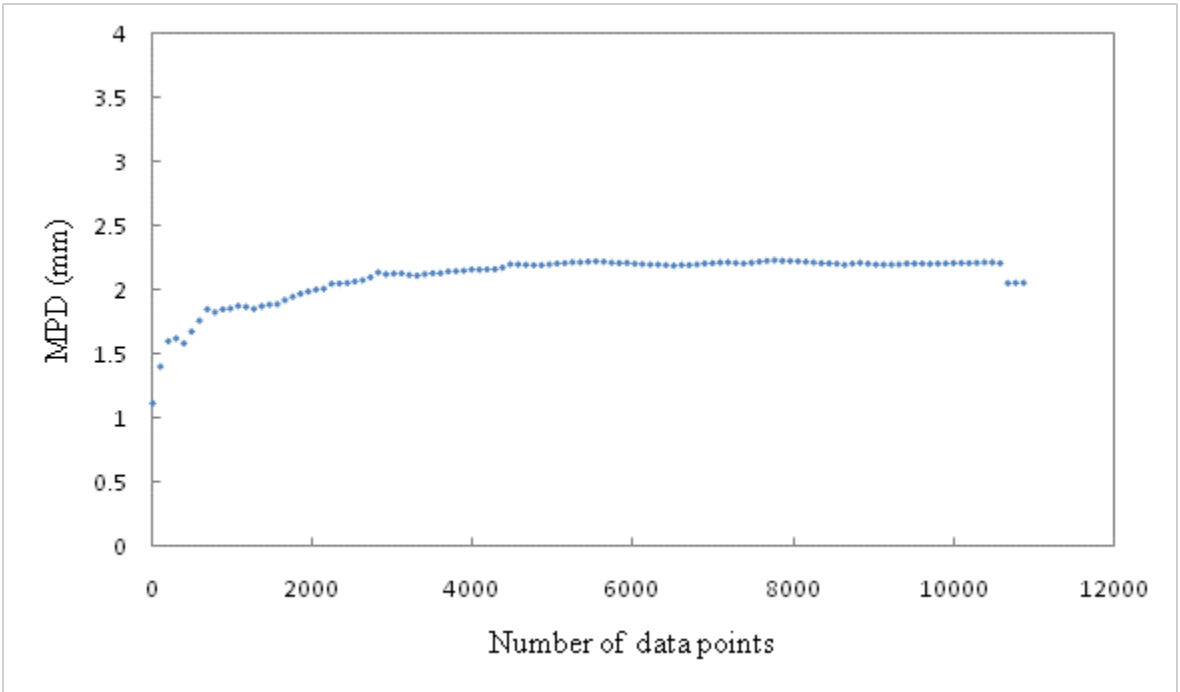

Figure 36 MPD vs. number of data points along Section 8 (medium volume), 9/24/2008 (day 3 of trafficking)

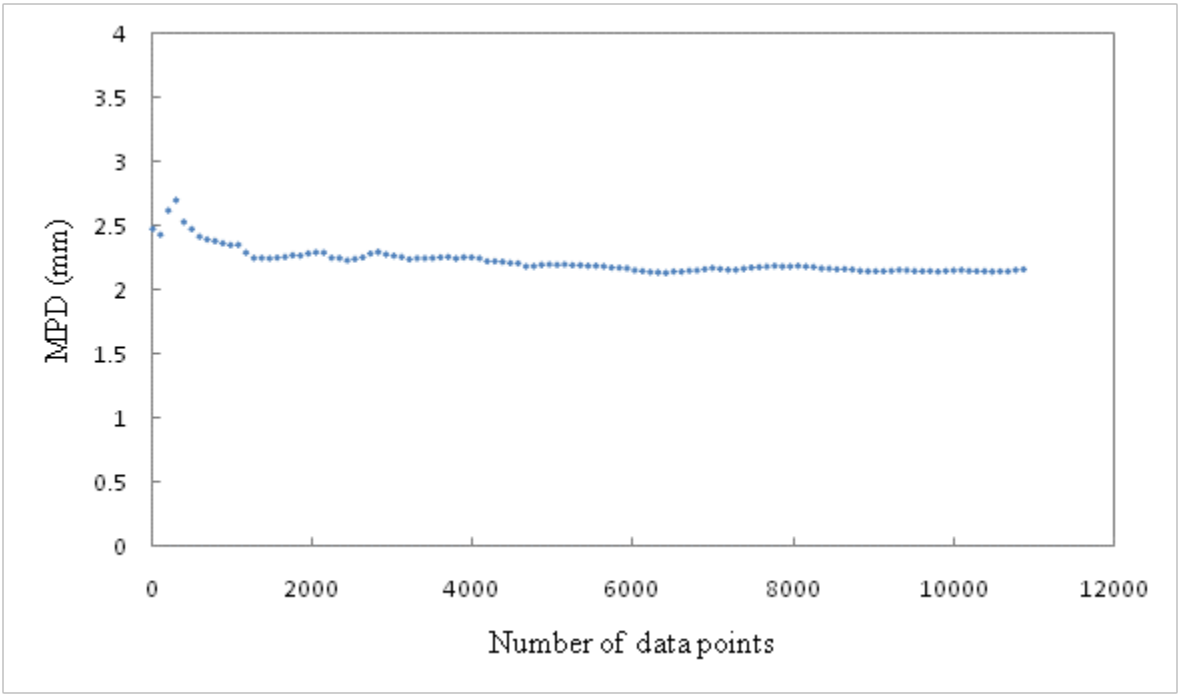

Figure 37 MPD vs. number of data points along Section 8 (medium volume), 10/3/2008 (day 12 of trafficking)

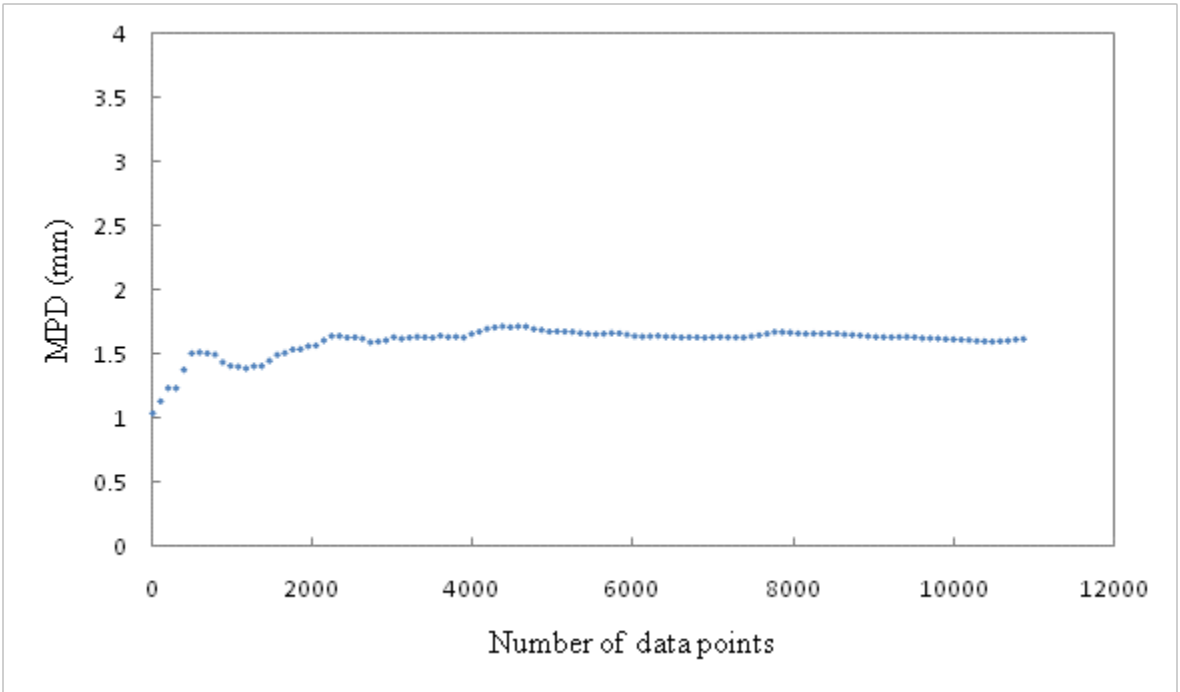

Figure 38 MPD vs. number of data points along Section 21 (medium volume), 8/25/2008 (day 1 of trafficking)

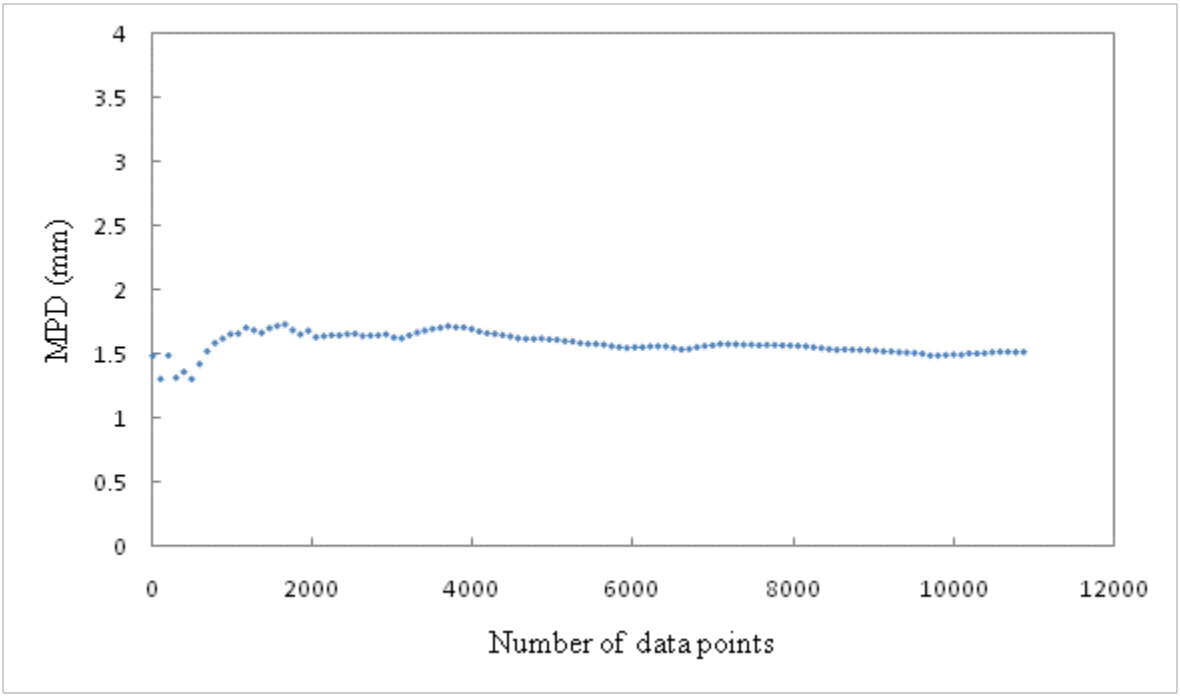

Figure 39 MPD vs. number of data points along Section 21 (high volume), 9/3/2008 (day 10 of trafficking)

In each of the graphs that plot the MPD versus the number of data points, the MPD has been calculated as a running average, i.e., where the total MPD is recalculated for each new data point. As shown in each of the six graphs, the MPD fluctuates between 0 and 4,000 data points as the formula adjusts for new peak levels.

Because the MPD formula takes peak values into account, a threshold must be set for the number of data points used in the calculation. Without defining a specific number of data points to be used in the MPD equation, the 'peak average', as calculated in the first part of the formula, continues to rise as new, larger peaks are collected as data. This occurrence results in a large difference between the peak average and the average level. In order to avoid this misrepresentation of the embedment depth, ASTM E 1845, *Standard Practice for Calculating Pavement Macrotexture Mean Profile Depth*, defines the minimum profile requirements as ten evenly spaced profiles of 100 mm (3.9 in.) in length, or a total of 1,000 data points.

By following these guidelines, the research team recalculated the total MPD for each new data point that was added. A representative MPD was calculated for each 100 mm profile (100 data points), and these values were then averaged to determine the overall MPD. As each new data point was added, the MPD became more representative of the entire sampling area. It is for this reason that a large amount of fluctuation exists in the MPD within the first 2,000 data points.

Although ASTM E 1845 requires at least 1,000 data points, the research team increased that requirement based on the data analysis. By collecting at least 5,000 data points, the researchers

believe that the MPD formula represents the sampling area evenly yet still accounts for a factor of safety, should some outliers occur.

Based on this analysis, the research team has determined that, within the sampling area, the number of data points collected is more critical than the manner in which they are collected (point vs. line). As a result, it is no longer necessary to collect the data using a line laser. The same information can be collected using a less expensive point laser, without compromising the quality of the analysis. When compared to a line laser, the point laser decreases the scanning time significantly, as well as the overall weight of the laser profiler. Also, the point laser is ~$7,500 less expensive than the newest Selcom RoLine laser. The research team chose to install Micro-Epsilon Model ILD1700-100, a single-point triangulation laser with a 100 mm measuring range.

3.4.3 Photoelectric Sensor

The digital imaging technique was used in the HWY-2004-04 project, *Optimizing Gradations for Surface Treatments*, to quantify the amount of bleeding present in a chip seal construction. This process records a digital image of a chip seal specimen and then analyzes that photo based on a threshold grayscale value. The darkest pixels of the photo represent emulsion in the chip seal, and the percentage of dark pixels present in the entire sample indicates whether or not the chip seal has a bleeding problem.

The research team compared various combinations of camera, zoom, lighting, and distance factors between the camera and the chip seal specimen to determine the best setup for the digital imaging. However, it was found that none of the images captured from the digital camera were better than earlier images captured using the scanner in previous projects. By turning the scanner upside-down and placing the screen on top of the chip seal specimen, as shown in Figure 40, the image could then be converted and analyzed to determine the grayscale threshold and the bleeding percentage within the specimen. When compared to the digital photo option, the research team determined that the scanner method is much simpler and more reliable in the laboratory and that testing and development could be completed much sooner. The scanner method also has the potential to be much less expensive than the digital camera option. Therefore, it was decided to incorporate the scanner-like mechanism into the laser profiler for the in-situ bleeding evaluation.

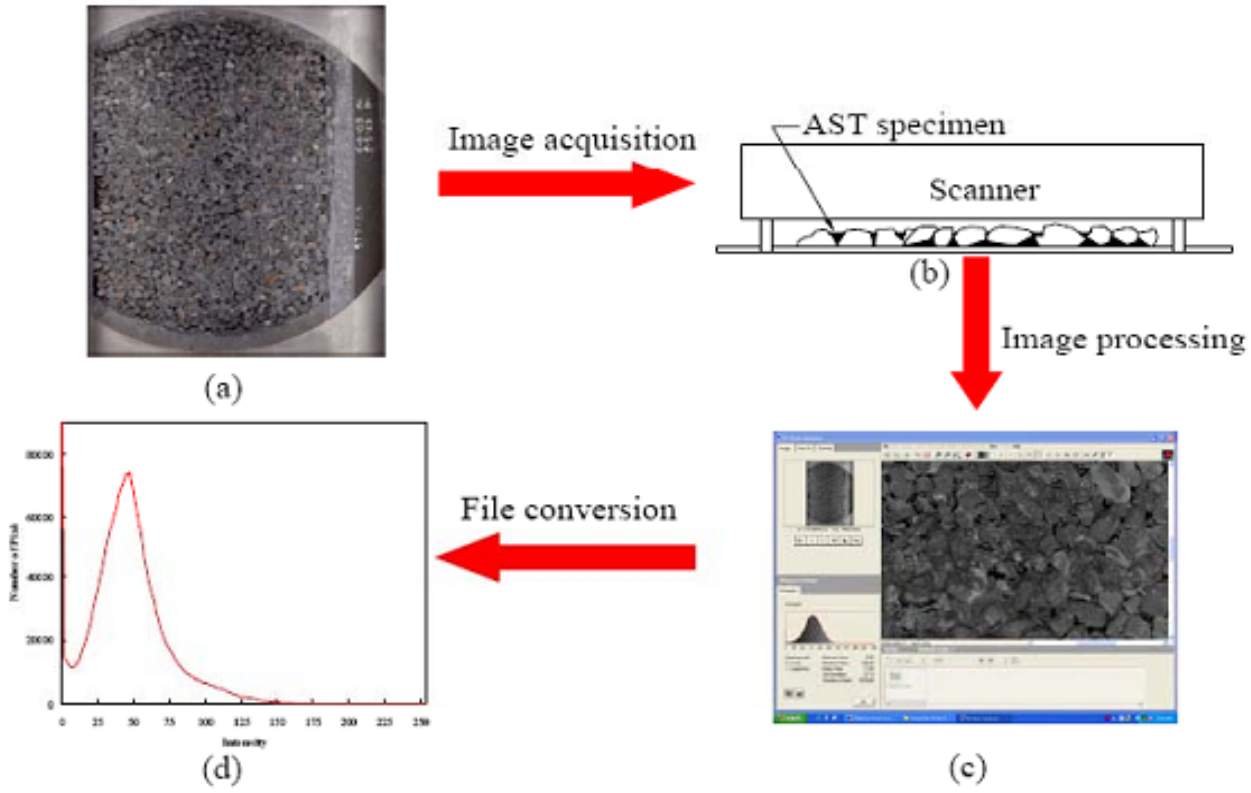

Figure 40 Bleeding evaluation process using a scanner

Through discussions with scanner manufacturers, the research team became aware of the BVS ConVis photoelectric sensor, developed by Balluff. This photoelectric sensor, or camera, can be mounted alongside the laser in the undercarriage of the profiler and can be used to capture digital images of the AST. The lens on this camera is designed with a small focal length, much like a computer scanner, and moves along with the laser. Using this camera sensor and technique, the user can merge the images together and create a digital image of the entire scanned surface. This image can then be analyzed to determine if the chip seal surface is too dry or too wet. This analysis is conducted based on a threshold grayscale value. As shown in Figure 41, the camera compiles a grid of digital images that are analyzed to determine if the chip seal is too wet, which signifies bleeding.

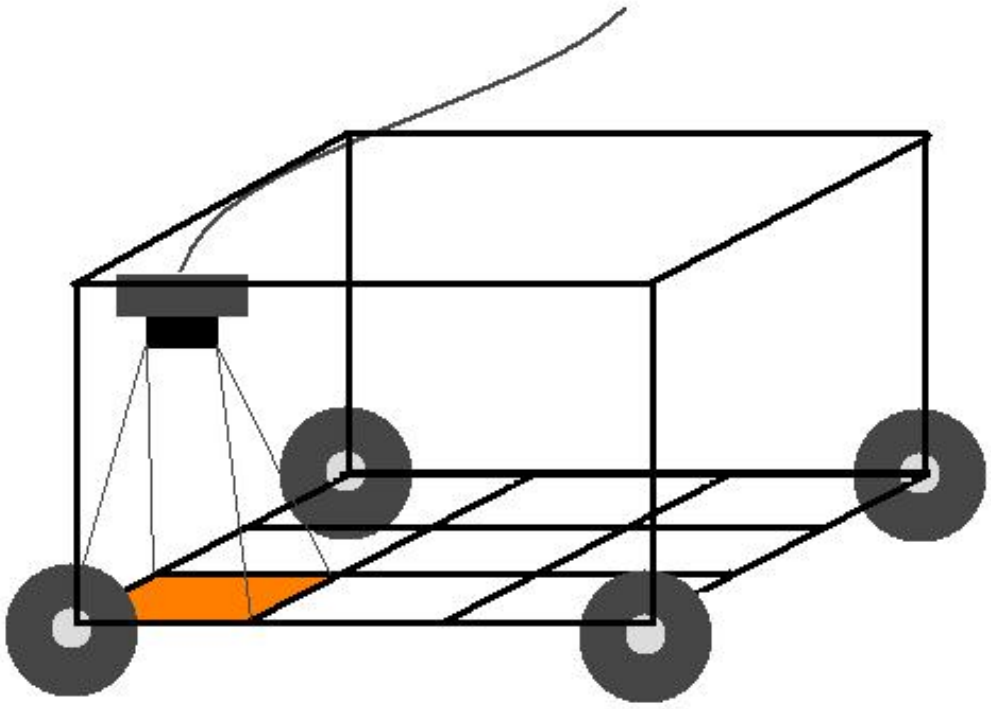

Figure 41 Schematic of the undercarriage of the profiler, with a photoelectric sensor mounted to analyze the bleeding percentage

With assistance from technicians at Balluff and the Scott Equipment Company, the research team determined that the 12 mm Balluff Sharpshooter is the optimal photoelectric sensor for this application. The 12 mm focal length sensor, as opposed to the 8 mm or 6 mm sensors, provides clear, focused images at a height that falls within the physical boundaries of the testing device.

Factors such as lighting, brightness, contrast and focal length all contribute greatly to the quality of the image. Figure 42 and Figure 43 show a sample digital image and the image processed by the National Instruments Vision Assistant (NIVA) software, respectively.

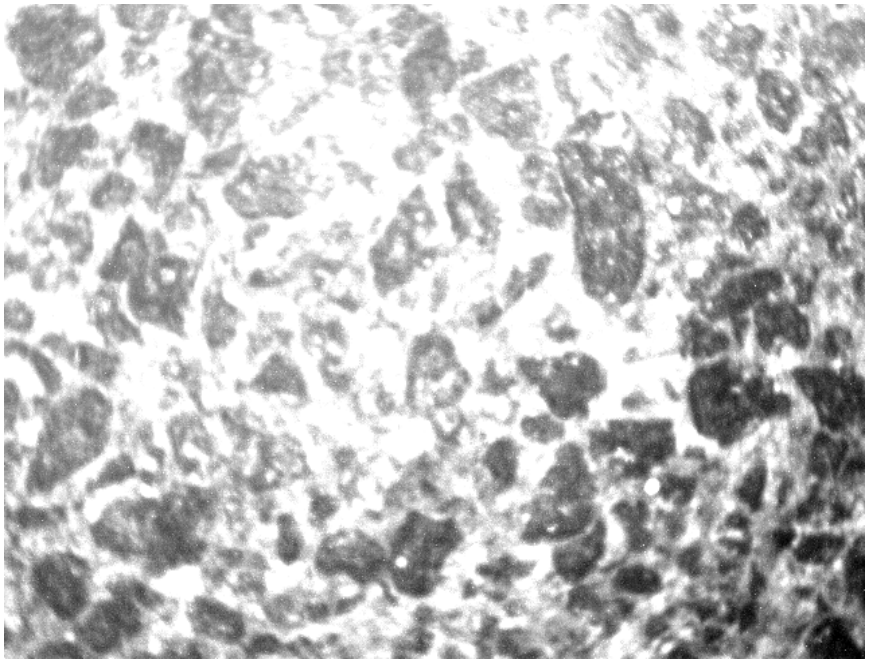

Figure 42 Sample image acquired from the Balluff Sharpshooter 12 mm photoelectric sensor

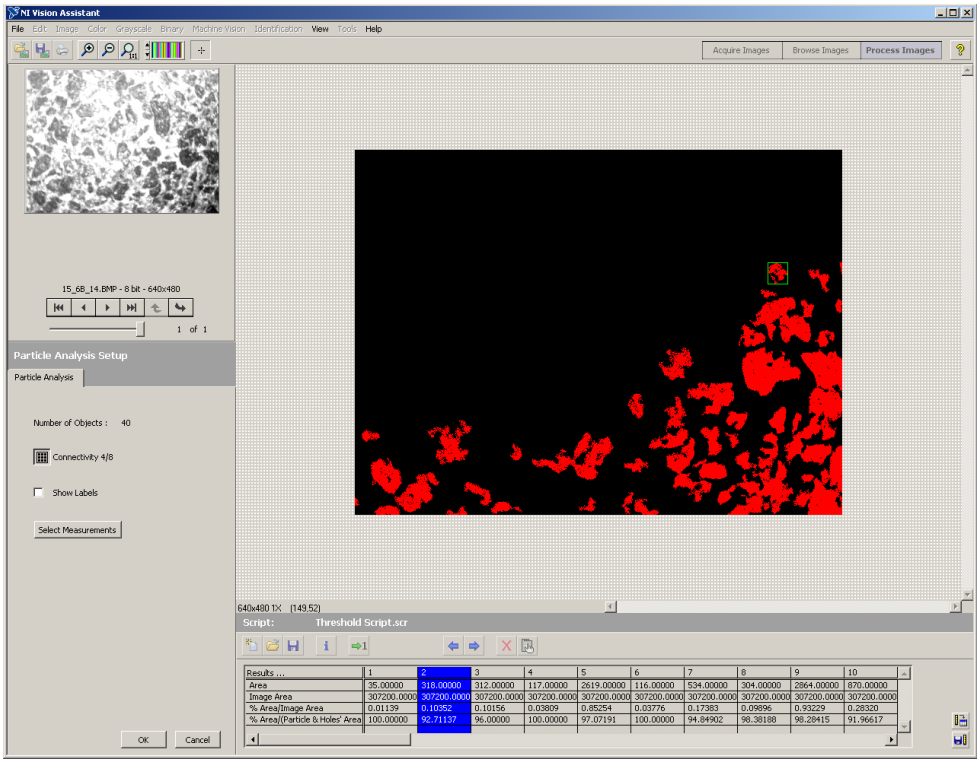

Figure 43 Screenshot from the National Instruments Vision Assistant software analyzing the chip seal sample shown also in Figure 42

The digital imaging technique also was applied to the determination of the aggregate embedment depth. The research team first poured gypsum plaster over the fabricated chip seal sample (7 in. x 12 in.) in order to prevent aggregate loss and to 'freeze' the sample for cutting. The sample was then sliced into 1-inch wide strips, thus exposing cross-sections of the surface treatment, shown in Figure 44. Using the photoelectric sensor and NIVA, the research team then captured the cross-sectional images, seen in Figure 45, which were used in turn to conduct further research to determine the aggregate embedment depth.

Figure 44 Cross-sectional image of a chip seal sample

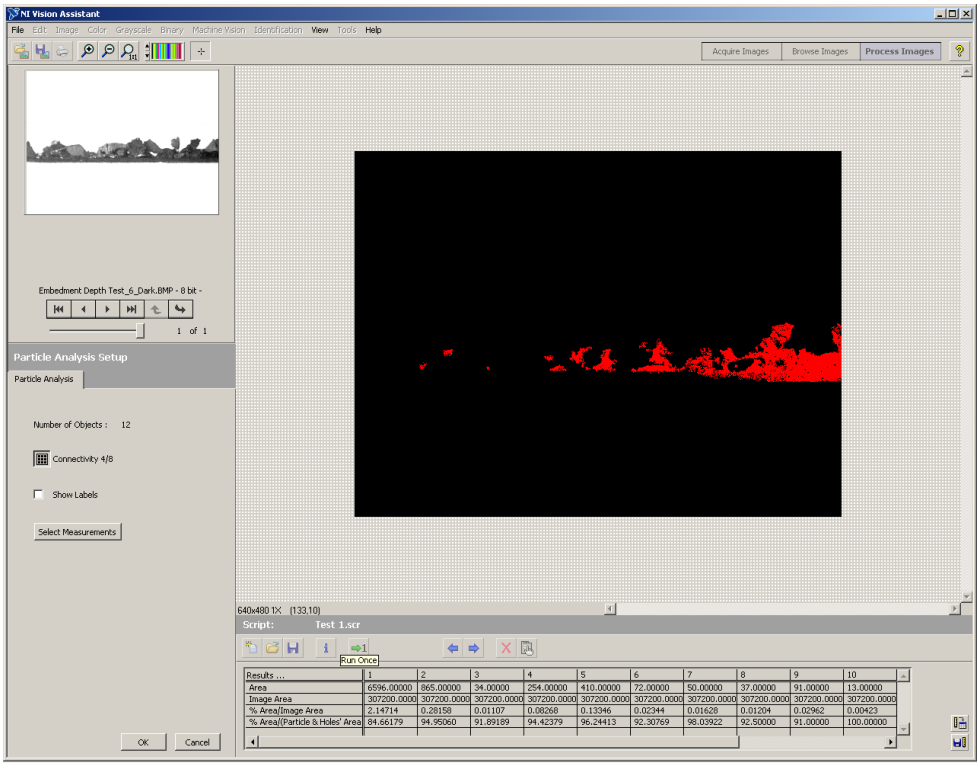

Figure 45 National Instruments Vision Assistant software analysis of the chip seal cross-section shown in Figure 44

4. DEVELOPMENT OF MODIFIED SWEEP TESTER

In order to evaluate the aggregate retention for different chip seal samples, the research team relied upon the sweep tester, as specified by ASTM D7000. This sweep tester uses a stiff-bristled brush to gently sweep the surface of the aggregate as the brush rotates about the center of the sample. Although this test does apply a significant amount of shear force while brushing the aggregate surface, the research team felt that the brush attachment was not forceful enough to agitate or dislodge loose aggregate in the same way that a vehicle tire would do. To simulate this scenario, the researchers wanted the ability to apply both horizontal *and* vertical shear force to the aggregate surface, in the same manner as front wheels of a vehicle stress the pavement surface when turning. To gain this ability, the research team replaced the brush head with a free-rolling, free-spinning rubber wheel, similar to a grocery cart wheel, as seen in Figure 46.

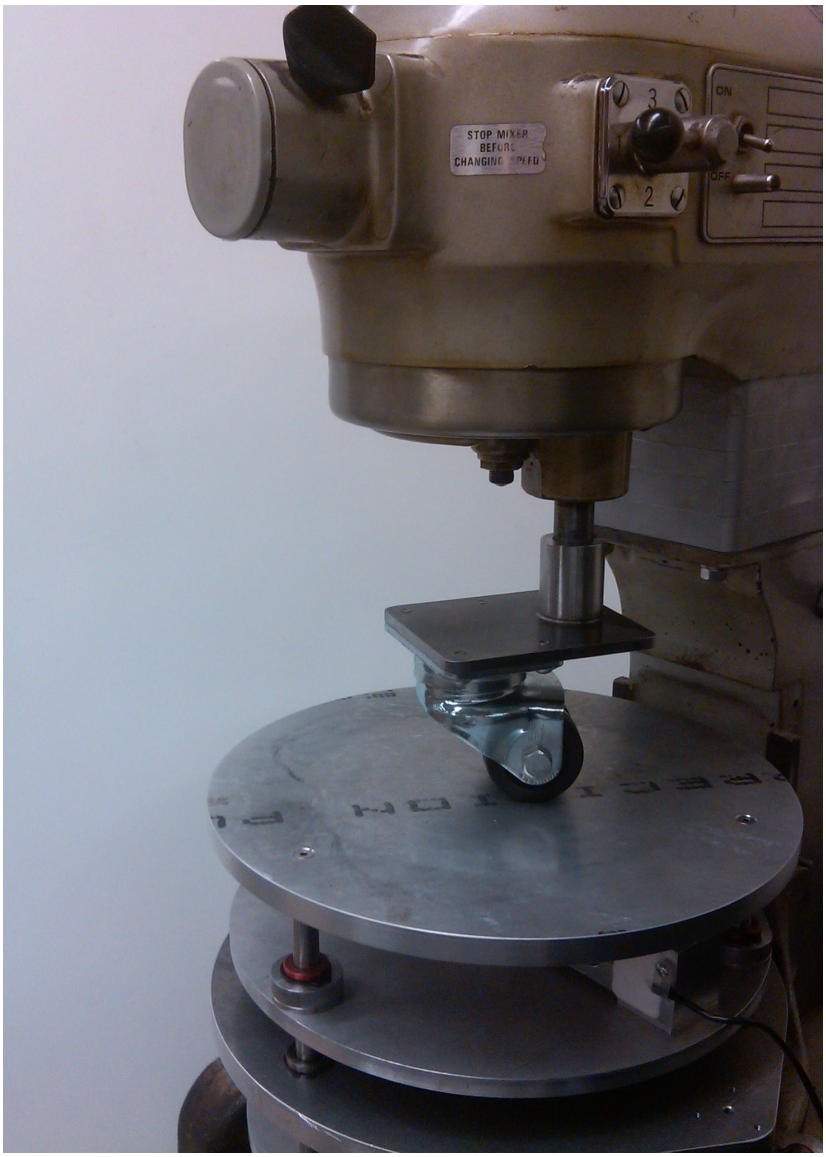

Figure 46 Modified sweep tester showing the free-rotating wheel on top of the adjustable platform

The researchers also noticed that as the brush head wore down over multiple tests, or when aggregate sources with different sizes were used, the applied pressure to the aggregate surface changed. To combat this variation in testing, the research team designed the sample platform so that the height is adjustable. In this way, the sample can be raised or lowered to the same position each time. Specifically, the researchers wanted the vertical pressure applied by the modified sweep test to be measurable and adjustable depending on the aggregate type and the gradation of the sample. To accomplish this capability, the research team included a single-point load cell in the center of the plate as well as a strain gauge to measure the vertical force applied. The load cell and strain gauge can be seen in Figure 47.

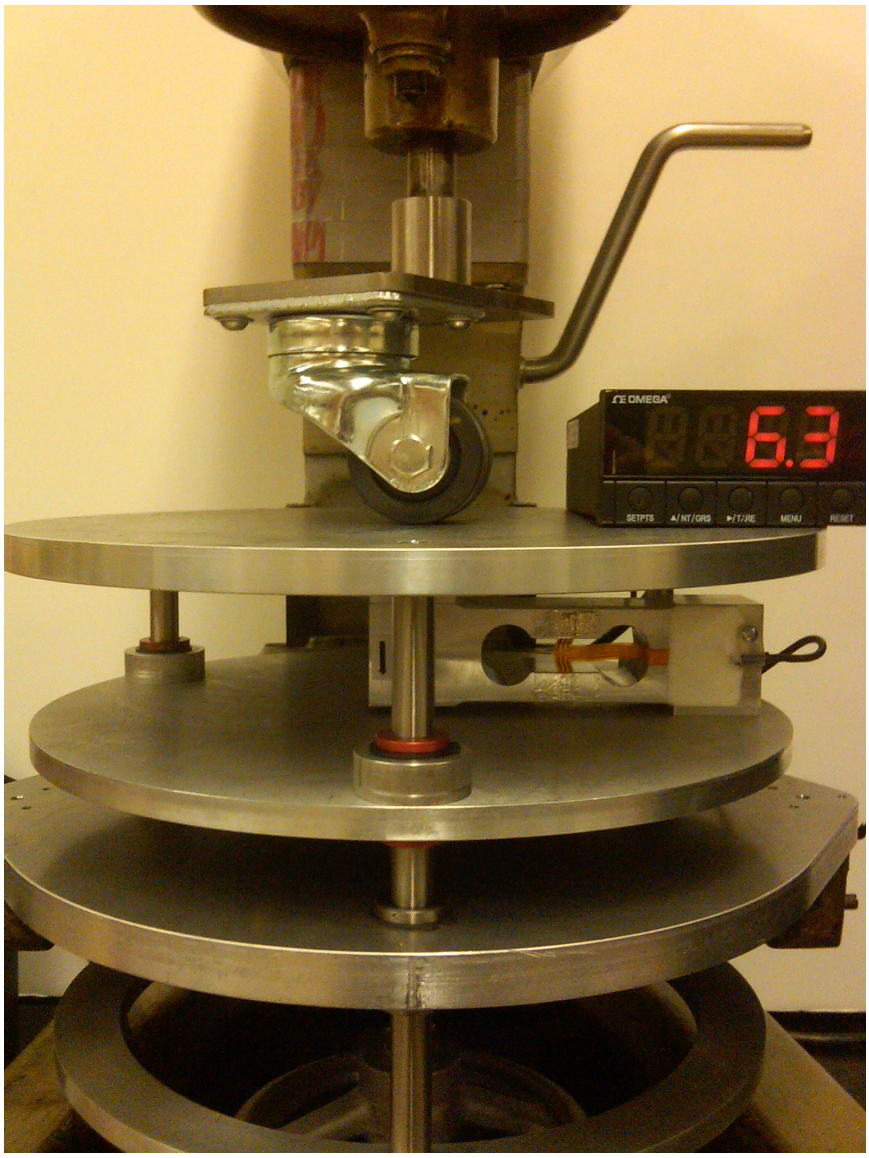

Figure 47 Modified sweep tester showing the single-point load cell and strain gauge

All modifications that have been made by the NCSU research team are interchangeable with the current sweep test specifications, should the research team need to run tests using the brush in the future.

5. EVALUATION OF THE BITUMEN BOND STRENGTH TEST

The bitumen bond strength (BBS) test method that uses the pneumatic adhesion tensile testing instrument (PATTI) was identified during review of the ongoing national research into emulsion testing. The BBS test measures the adhesion between the binder and the aggregate and the cohesive strength of the binder. PATTI, seen in Figure 48, is specified in ASTM D4541, *Pull-Off Strength of Coatings Using Portable Adhesion Testers*, and applies a true axial (relative to the sub-axis) tensile pull.

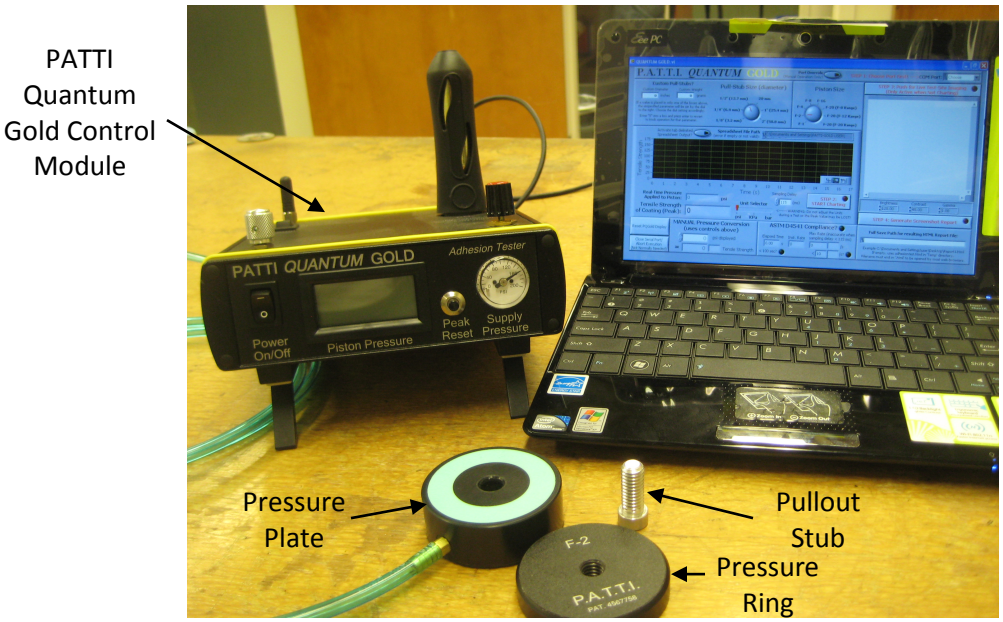

Figure 48 PATTI Quantum Gold device

The tensile values obtained from PATTI quantitatively measure the bond between the emulsions (i.e., cohesion) or between the emulsion and the aggregate substrate (i.e., adhesion), depending on the failure mode. The stiffness and strength properties measured by the Dynamic Shear Rheometer and PATTI can be used to ensure proper aggregate retention performance even prior to construction of the chip seals. Through this test, the researchers were able to demonstrate the ability of PATTI as a tool for determining the adhesion between the aggregate and emulsion, that is, as a tool for compatibility testing. The research team updated PATTI and refined the BBS test devices based on the AASHTO BBS procedure standard.

To develop the final PATTI and updated BBS procedure, the research team developed a research plan that includes three types of aggregate and four types of emulsion. The aggregate types include lightweight and granite aggregates. The emulsion types include CRS-2 and CRS-2L.These materials were subjected to PATTI testing, and the chip seal specimens composed of these materials were tested using the Vialit test and the MMLS3 test for aggregate retention performance. The findings from PATTI were compared against the aggregate loss results from

the Vialit test and the MMLS3 test. The research team refined the procedure of the BBS test by using CRS-2 as the emulsion and Vialit test steel plates as the substrate.

After testing the bitumen bond strength using CRS-2 as the emulsion and Vialit test steel plates as the substrate, the research team used 6 in. x 8 in. lightweight plates and 12 in. x 12 in. granite plates for the aggregate substrate and CRS-2 and CRS-2L as the emulsions for the database.

Based on the updated AASHTO standard, 40 mm x 40 mm silicone molds with no backing and with a 20 mm diameter hole and 0.8 mm (approximately 1/32 in.) thickness were fabricated to allow the binder to be placed directly on the substrate and also to limit the emulsion from spreading too much over the aggregate substrate. Pullout stubs 20 mm in diameter were fabricated to fit in the original F-2 piston. Because of the increased length of the pullout stub, a supporting ring also was introduced to the test and, thus, the piston no longer directly contacted the substrate. This supporting ring was fabricated with a height of 12.7 mm and an inside diameter of 25.4 mm. The cohesive strength between the emulsions and the adhesive strength between the emulsion and aggregate both could be determined by simply observing the failure conditions optically.

In order to remove residual particles from the substrate surfaces prior to testing, an ultrasonic cleaner, FS60D, with inside dimensions of 6 in. x 11.75 in. x 6 in. (tank interior D x W x H) and 5.7 L capacity, was purchased. Distilled water was used as the solution for completely submerging the substrate in the cleansing sink. The temperature of 60°C was maintained during the cleaning operation. Throughout the BBS test procedure, a 280-grit silicon carbide material on a standard lapidary wheel was applied in an attempt to maintain a consistent finish on the solid aggregate substrates (granite and lightweight aggregate). This process not only removed saw marks, but also ensured a consistent surface roughness. Because the granite plates came from the supplier sized as 12 in. x 12 in., the decision was made to cut the granite aggregate substrate (to 6 in. x 10 in.) to fit the aggregate plate into the ultrasonic cleaner. For the lightweight aggregate substrate, the original size of 6 in. x 8 in. was maintained to allow the substrate to be submerged completely in the solution.

CRS-2 emulsion from Seaco-Columbia and CRS-2L emulsion from Asphalt Emulsions-Dunn are the emulsions that were chosen by the NCDOT for adhesion testing. Prior to executing the BBS test, the research team first studied the relationships among failure strength, failure type and the effective pressure applied to the pullout stub during the curing procedure.

PATTI requires very little emulsion for each test, and the researchers chose to store the emulsion in 2-oz plastic bottles in order to minimize emulsion waste. A digital camera was used to capture the failure type for future analysis. Six replicates were applied for each test on the same granite substrate in order to limit the surface roughness variance. Figure 49 illustrates a simple image of the BBS test setup after curing.

Figure 49 Pullout stubs on top of granite substrate with CRS-2L emulsion, after curing

During the BBS test curing procedure, the researchers applied different loads to the pullout stubs in order to study the relationship between effective pressure and failure tensile strength. Each load placed on the pullout stubs was applied evenly for three minutes. Results from six replicates for each load show that as effective pressure increases, the average failure tensile strength increases as well. However, the ultimate average failure tensile strength was not reached; therefore, the effective pressure was increased continuously until stability could be reached. However, from the research conducted, it was found that the effective pressure does not affect the failure type in terms of cohesive or adhesive failure.

The BBS test procedure is summarized below:

- Place 2 oz of CRS-2 emulsion (Seaco, Columbia) into oven for 1 hour.
- Clean the aggregate substrate for 60 minutes in an ultrasonic cleaner containing distilled water at 60°C to remove residual particles on the plate surface and dry it.
- Place emulsion on top of the mold and let it cure for 20 minutes.
- At the same time, place pullout stub into oven at 60°C.
- Place heated pullout stub on emulsion and apply fingertip pressure to allow pullout stub to sit completely and evenly on the emulsion.
- Place the substrate with pullout stub into a 25°C environmental chamber for 1 hour.
- Connect PATTI to the software via a USB.
- Separate the piston body (bottom of piston) from the reaction plate (top of piston), exposing the gasket. Ensure that the gasket is free of dirt and other debris.

- Place the piston body that is covered by tape over the pullout stub, with the felt side resting on the emulsion.
- Thread the reaction plate clockwise onto the pullout stub until light contact is made with the piston body.
- Unscrew the reaction plate counter-clockwise 90° to seal the gasket, and align the reaction plate perpendicular to the axis of the pullout stub.
- Connect the blue hose from the control module to the piston.
- Turn on the PATTI software.
- Make sure the "Piston Pressure" display is 0 psi (+/-1 psi).
- Close the "Rate Valve".
- Start the software.
- Push and hold the red "Run" button.
- Once the piston assembly and attached pullout stub detaches from the test surface, release the "Run" button.
- Repeat the test on all the samples on the substrate.
- Conduct post-test operations (disconnect, clean, etc.).

During the PATTI procedure, Goldwave software was used to catch the popping sound that indicates the bond failure in order to determine failure stress. Figure 50 shows the cohesive failure image and failure stress for the CRS-2 emulsion with granite substrate on PATTI.

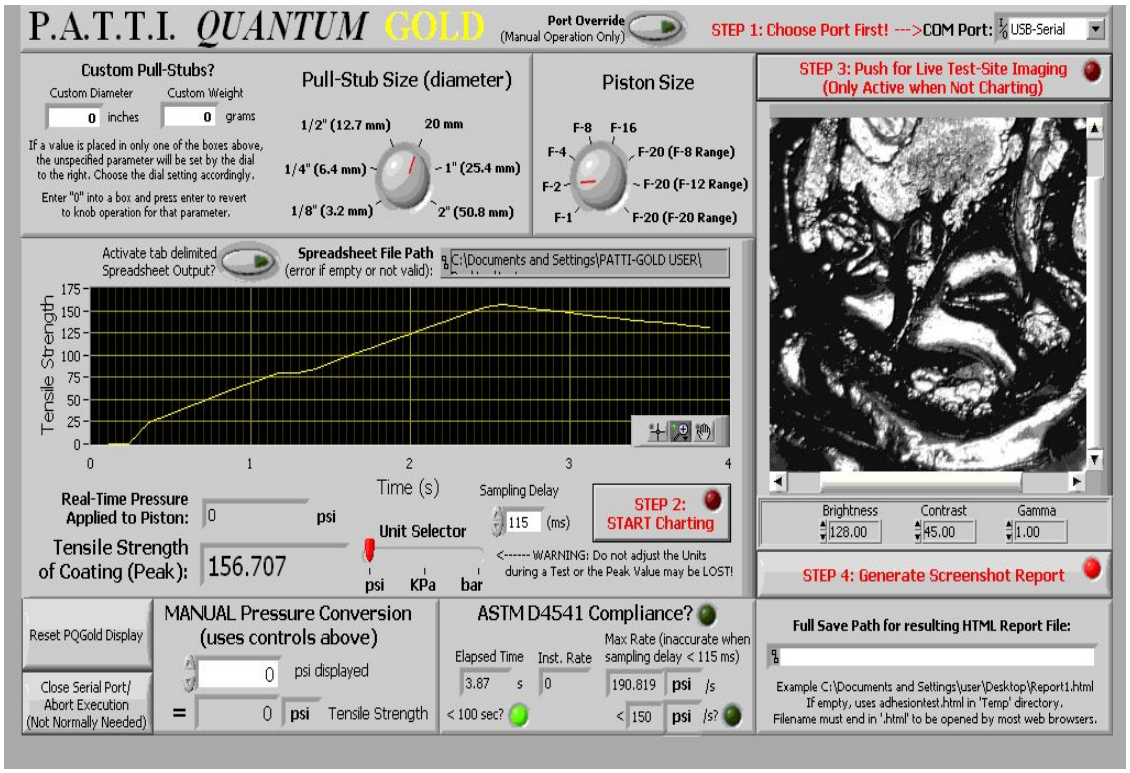

Figure 50 Cohesive failure image and failure stress for CRS-2 emulsion with granite substrate, as shown on PATTI

Via the BBS test, the research team was able to demonstrate the ability of PATTI to be employed as a tool for determining the cohesion among different emulsions and adhesive bonding between the aggregate and emulsion. Figure 51 shows a sample output from the PATTI testing procedure. The peak value represents the point at which failure occurred.

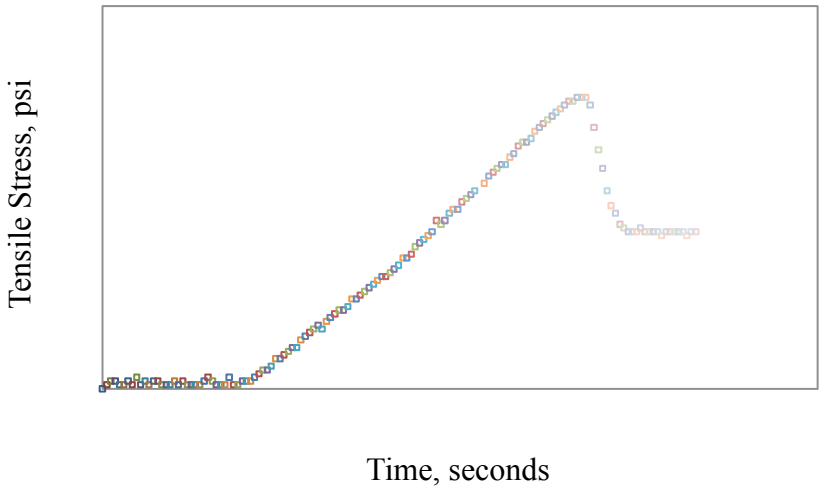

Figure 51 Sample output from PATTI test procedure

Figure 52 illustrates the failure stress for the CRS-2 emulsion with both granite and lightweight substrates. Figure 53 illustrates the failure stress for the CRS-2L emulsion with both granite and lightweight substrates. For both the CRS-2 and CRS-2L emulsions, the failure stress for the granite substrate is higher than that for the lightweight substrate. However, cohesive failure is found for the granite substrate, and adhesive failure is found for the lightweight substrate.

Figure 54 illustrates the failure stress for the granite substrate with both CRS-2 and CRS-2L emulsions, and Figure 55 illustrates the failure stress for the lightweight substrate with both CRS-2 and CRS-2L emulsions. From the observations and analyses, it is not difficult to predict that the CRS-2L emulsion with both granite and lightweight substrates results in higher failure stress than the CRS-2 emulsion.

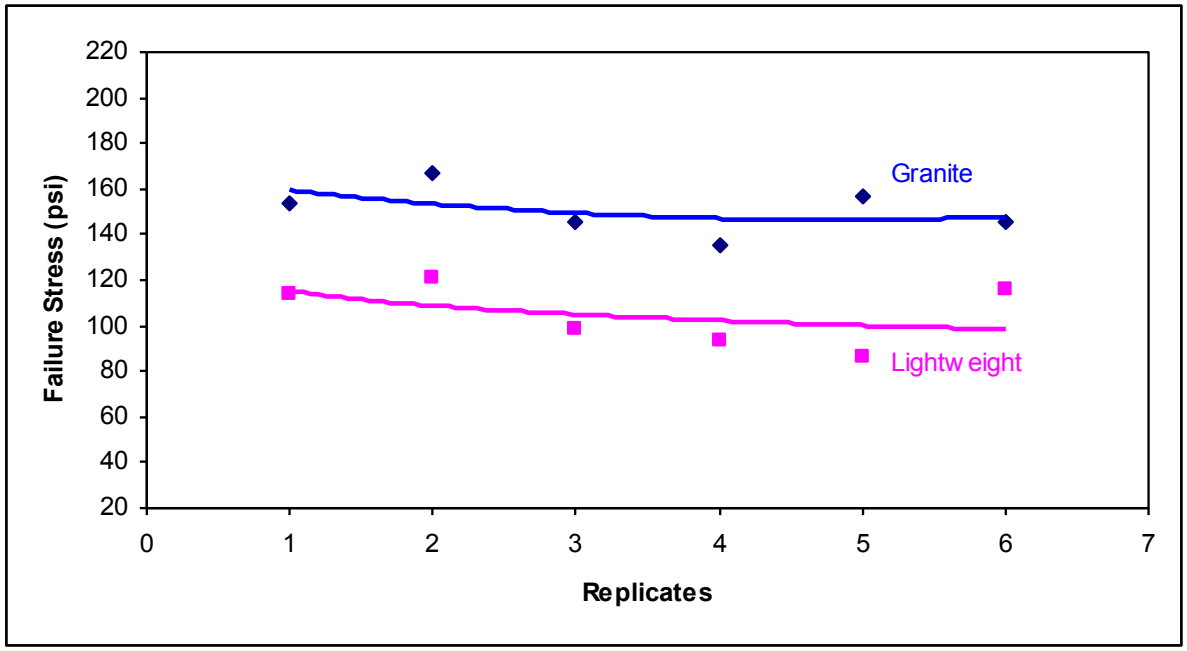

Figure 52 Failure stress for CRS-2 emulsion with granite and lightweight substrates

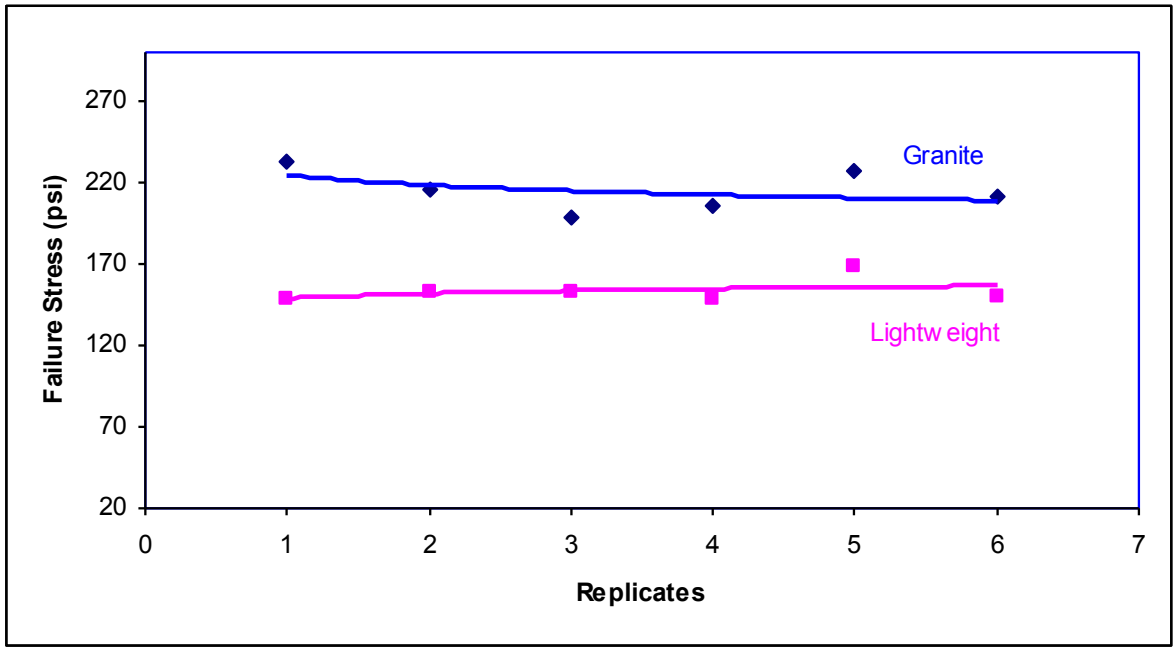

Figure 53 Failure stress for CRS-2L emulsion with granite and lightweight substrates

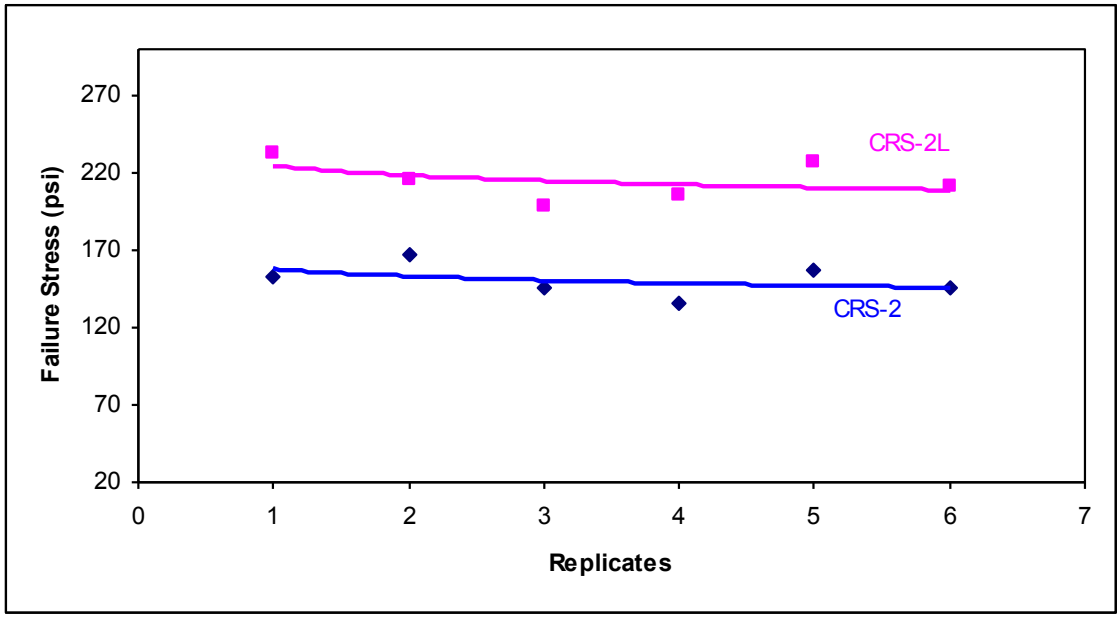

Figure 54 Failure stress for granite substrate with both CRS-2 and CRS-2L emulsions

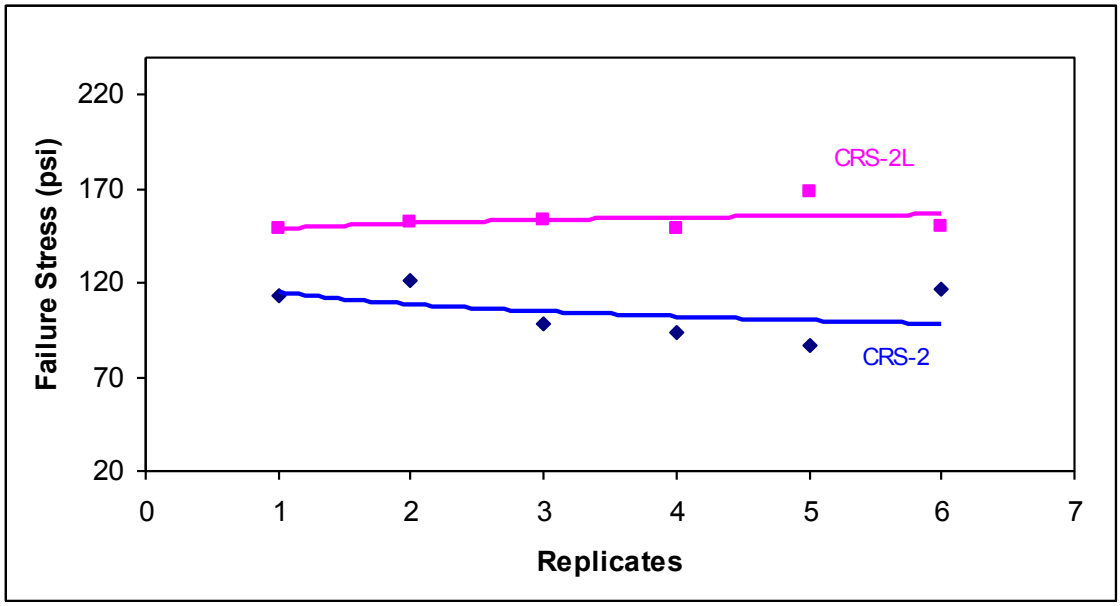

Figure 55 Failure stress for lightweight substrate with both CRS-2 and CRS-2L emulsions

6. PRELIMINARY INVESTIGATION OF AGGREGATE EMBEDMENT DEPTH DETERMINATION

In this project, an attempt is made to understand the relationship between the surface profile measured by the 3-D laser profiler and the aggregate embedment depth. In order to fully understand aggregate embedment within the emulsion for a single chip seal layer, the research team created theoretical chip seal layers using the surface profiles of raw aggregate particles in the board test measured by the 3-D laser profiler. A theoretical fabrication of a single-seal surface treatment was necessary due to the extremely sensitive measurement analysis and the nature of the chip seal itself. In the field, it is observed that the EAR and AAR used to construct the "same" surface treatment from one section to another actually vary a great deal depending on the variability of the construction equipment, construction day conditions, and operator accuracy, among other factors. Although these factors can be controlled with much greater precision in the laboratory than in the field, a significant amount of variability from sample to sample is evident nonetheless with regard to embedment depth and compaction behavior.

One factor that *is* reliable throughout the entire fabrication and observational process is the ability of the laser to report the exact surface texture of the surface treatment. The research team was able to discover a wide range of differences among similar EAR and AAR construction samples due to the precision with which the laser measured and reported the surface profile measurements. The main benefit to creating a theoretical chip seal specimen is that the researchers could view the entire surface texture, from the top of the exposed aggregate to the bottom of the sample depth, and measure this height difference at all points along the profile. For this reason, the researchers decided to construct theoretical chip seal samples using the measurements obtained from laser scans of aggregate without emulsion.

The research team constructed a single-layer aggregate board test within an 8 in. x 8 in. steel plate, as seen in Figure 56. The steel board includes a lip that is high enough to contain the aggregate and ensure that the aggregate matrix would not shift or dislodge due to transport or movement. The board, including the single layer of aggregate, was then scanned using the point laser. The research team set up the laser so that an aggregate height was captured every 0.1 mm in the transverse direction, thus creating a fine resolution scan of the raw aggregate within the 8 in. x 8 in. steel board. This procedure was carried out for both lightweight aggregate and 78M granite aggregate, and three separate gradations were constructed for each aggregate type. These gradations are generically referred to as Gradation A, Gradation B, and Gradation C.

For each board scan, only the raw, single-layer aggregate structure was scanned, and the structure did not include any emulsion. The researchers then averaged the valleys of the entire scan. A valley is defined here as the point at which the slope of the scan changes from a negative value to a positive value. The research team captured the lowest points, calling them "valleys", and then found the average of these points. This averaged value is referred to here as the "valley average", or the average height at which the aggregate particles touch one another. It was then assumed that if the emulsion level reaches (i.e., fills to) this value, the aggregate would be 50% embedded. A diagram of this definition is presented in Figure 57.

Figure 56 Single-layer aggregate board test using 8 in. x 8 in. steel plate

Figure 57 Schematic representation of the board test scan with red points representing the valleys

It is noted that the 3-D scan of the board filled with raw aggregate particles captures empty spaces between two aggregate particles. The laser readings from these empty spaces represent the distance between the laser sensor and the top of the empty board. These readings violate the definition of the valleys displayed in Figure 57 and, therefore, need to be corrected. This correction is made by converting all the zero height data points in between the two aggregate particles (i.e., data points collected from the top of the empty board) to the height of the last non-zero data point, which is about midway of the aggregate particle that is adjacent to the empty space.

An example of each aggregate gradation scan with the theoretical embedment depth profile can be seen in Figure 58 through Figure 63. To create a theoretical chip seal sample that is 60% embedded, the valley average is multiplied by 1.2 to increase the lowest point. It is then multiplied by 1.4, 1.6, 1.8, and 2.0 to create the 70%, 80%, 90% and 100% embedment line, respectively.

By creating laser scan data of the aggregate particles that are embedded theoretically at 50%, 60%, 70%, 80%, 90%, and 100%, the researchers could then use these data to represent the exposed surface area of the chip seal, similar to the data that could be collected directly in the field.

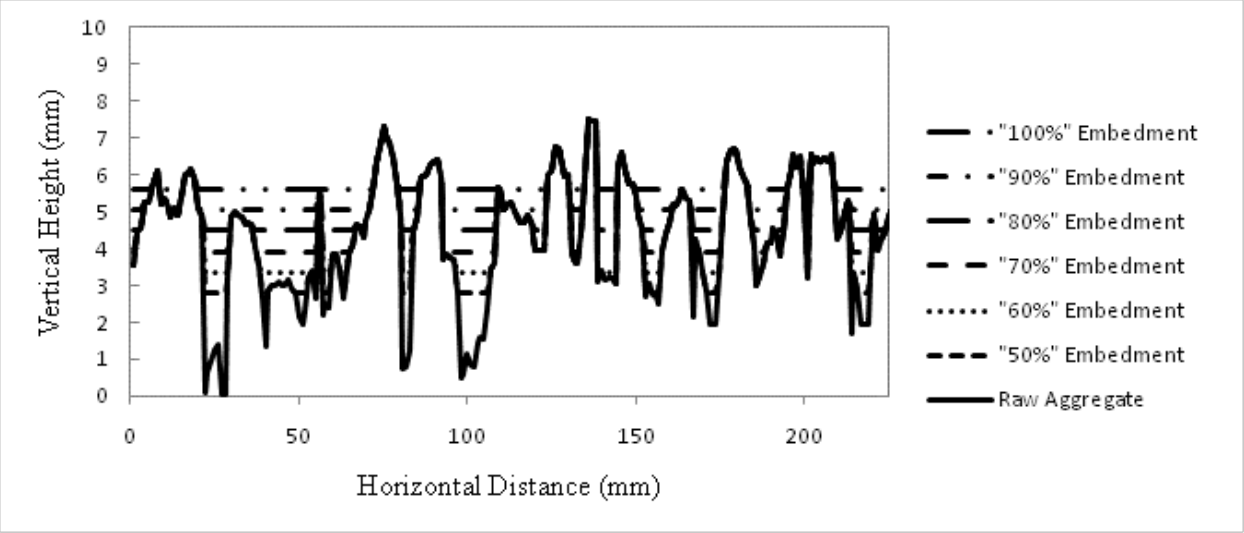

Figure 58 Example of granite 78M Gradation A board test scan, including theoretical embedment depths

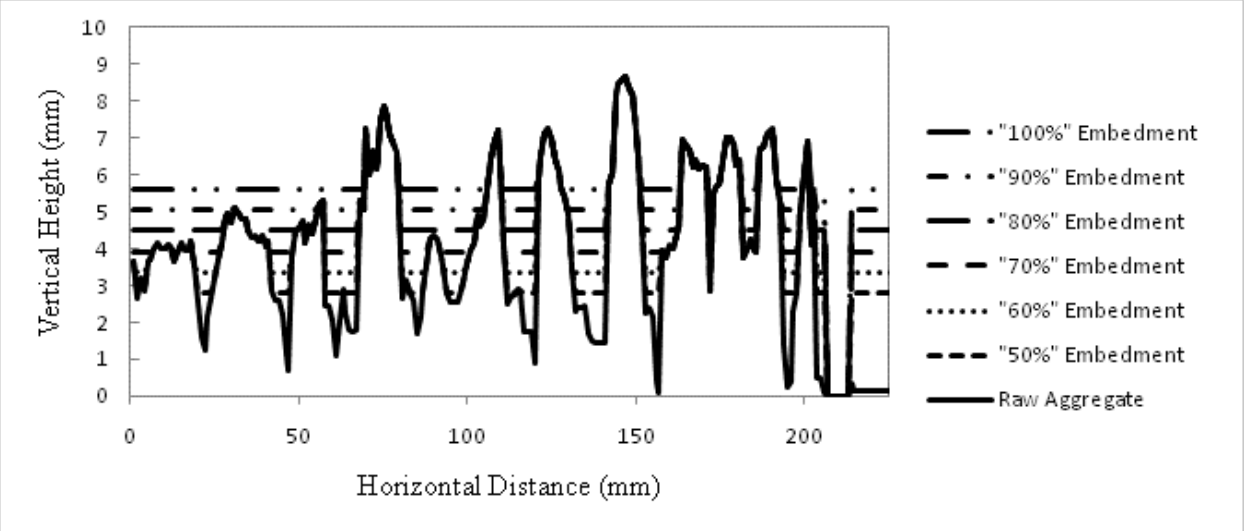

Figure 59 Example of granite 78M Gradation B board test scan, including theoretical embedment depths

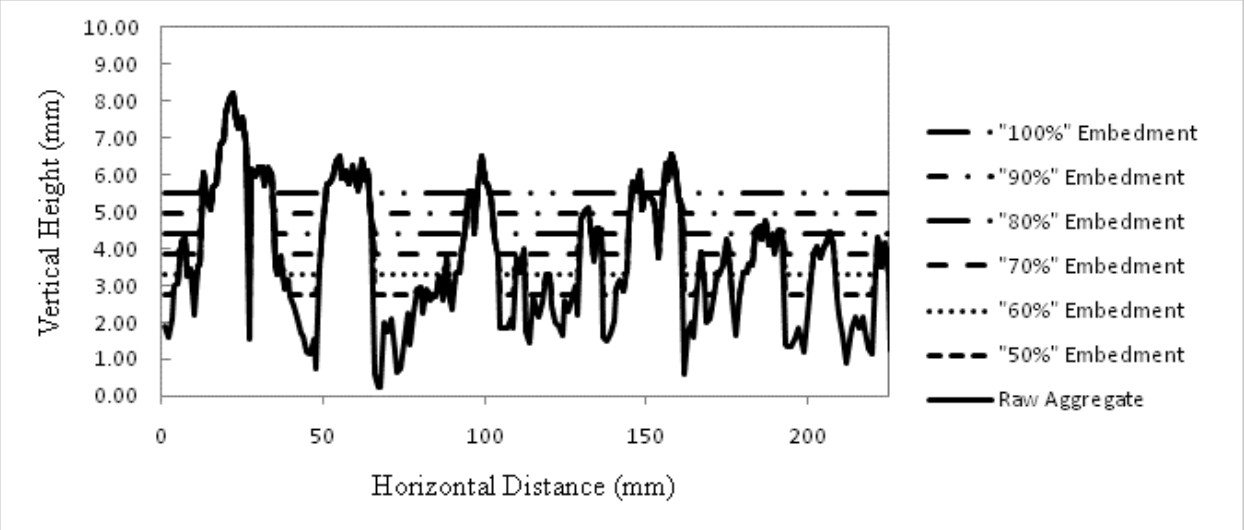

Figure 60 Example of granite 78M Gradation C board test scan, including theoretical embedment depths

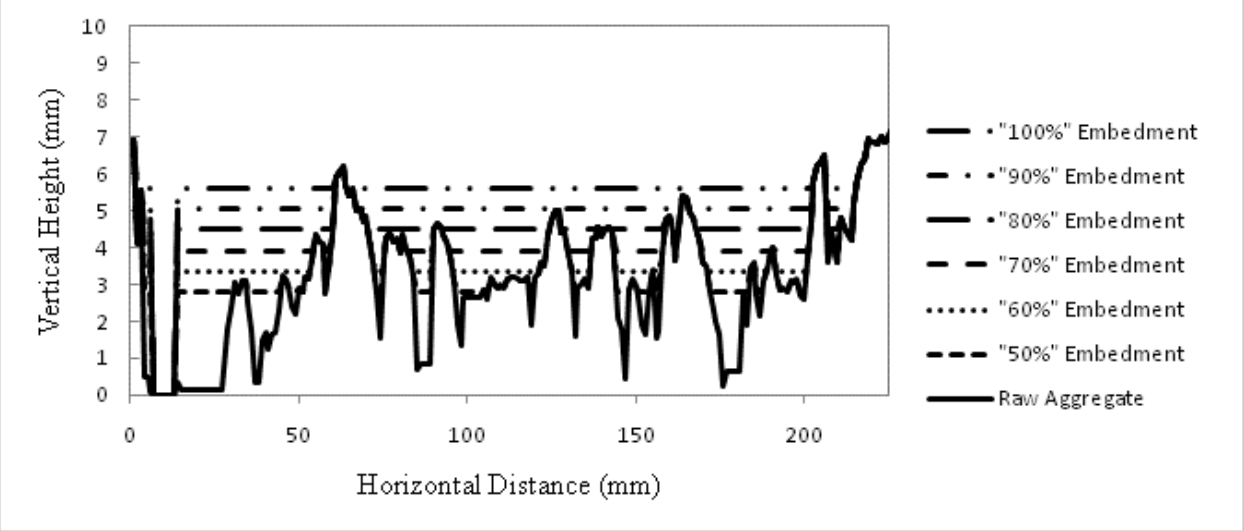

Figure 61 Example of lightweight Gradation A board test scan, including theoretical embedment depths

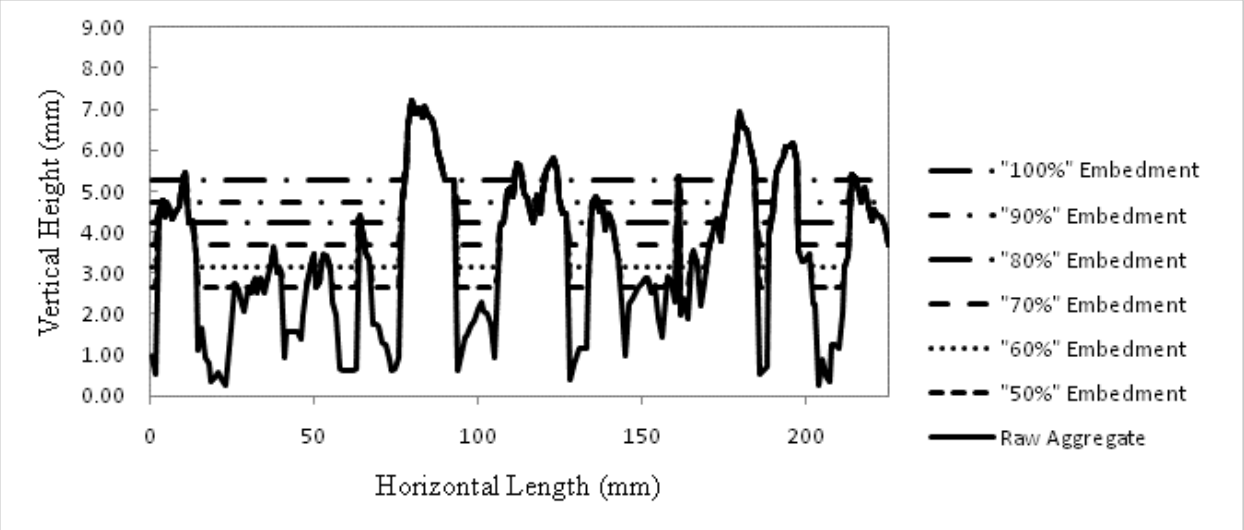

Figure 62 Example of lightweight Gradation B board test scan, including theoretical embedment depths

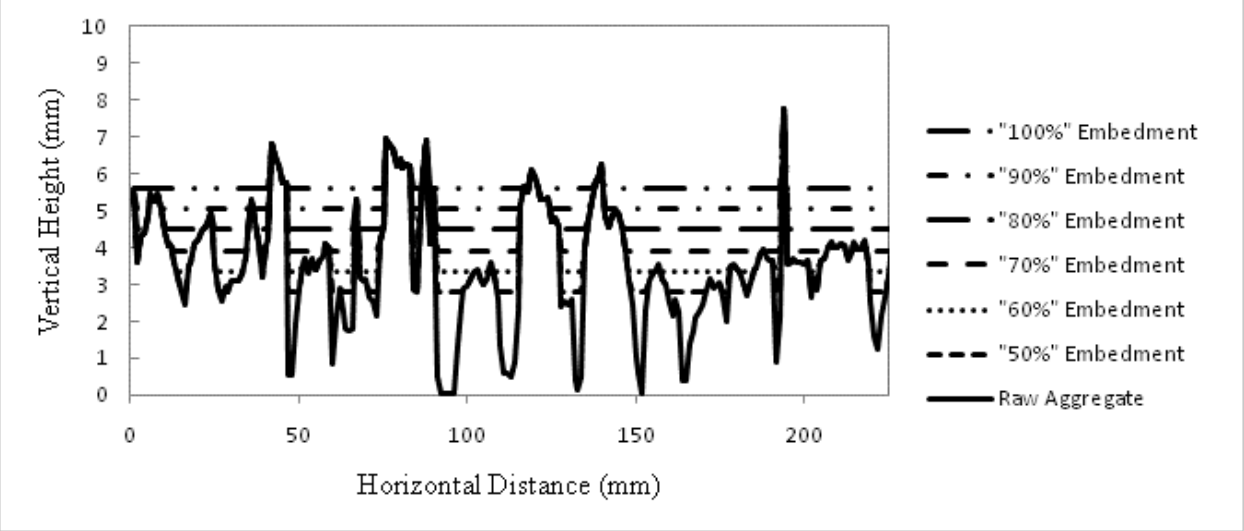

Figure 63 Example of lightweight Gradation C board test scan, including theoretical embedment depths

The theoretic 100% valley average parameter, or twice the height of the valley average, intrigued the research team when this value was compared to the percentage passing plots of the six different gradations (3 lightweight and 3 granite). Observational analysis proved that the height at which the valley average is multiplied by two always falls on the gradation curve very near the 50% passing point. That is to say, by knowing the sieve size at which 50% of the aggregate passes the sieve, the researchers could predict the 100% valley average value of a raw aggregate single-layer board scan. The 100% valley average can be converted to other percentages of valley average via a simple arithmetic equation. Table 8 summarizes the 100% valley average values for different aggregate types and gradations. These values are plotted on top of the

percentage passing gradation plots for different aggregate types and gradations in Figure 64 through Figure 69.

Table 8 Summary of theoretic 100% valley average values for six separate gradations

	"100%" Valley Average
78M Gradation A	5.86 mm
78M Gradation B	5.06 mm
78M Gradation C	5.52 mm
LW Gradation A	5.6 mm
LW Gradation B	5.26 mm
LW Gradation C	4.99 mm

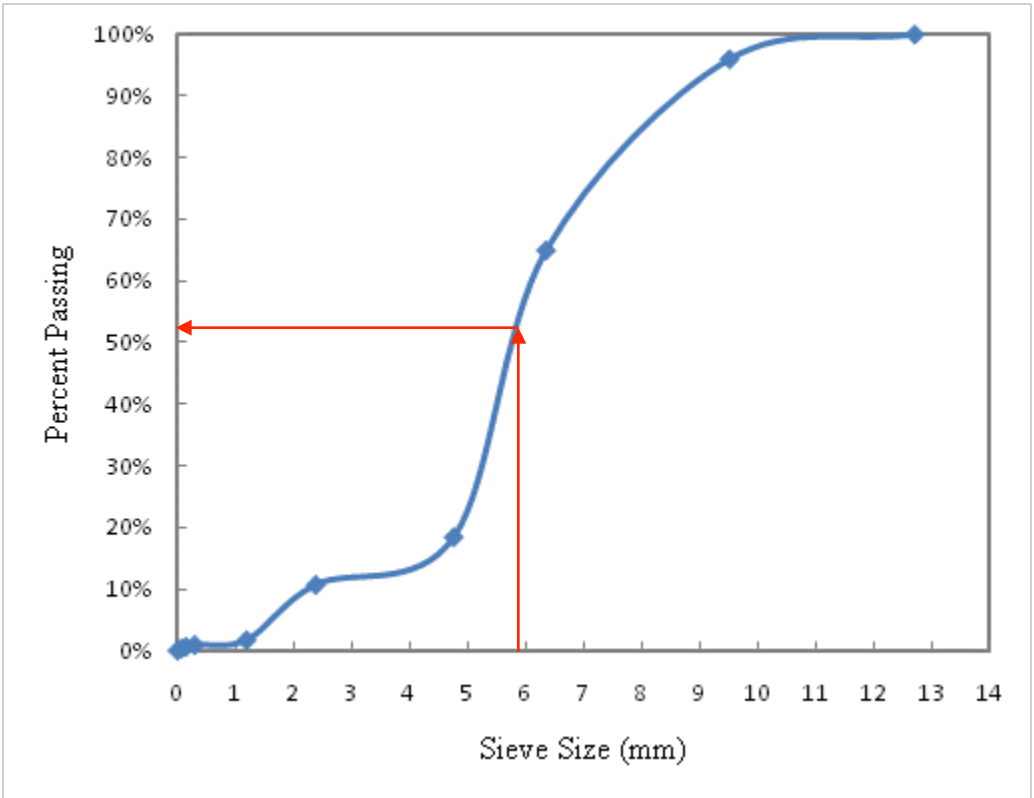

Figure 64 Percentage passing plot for granite 78M Gradation A

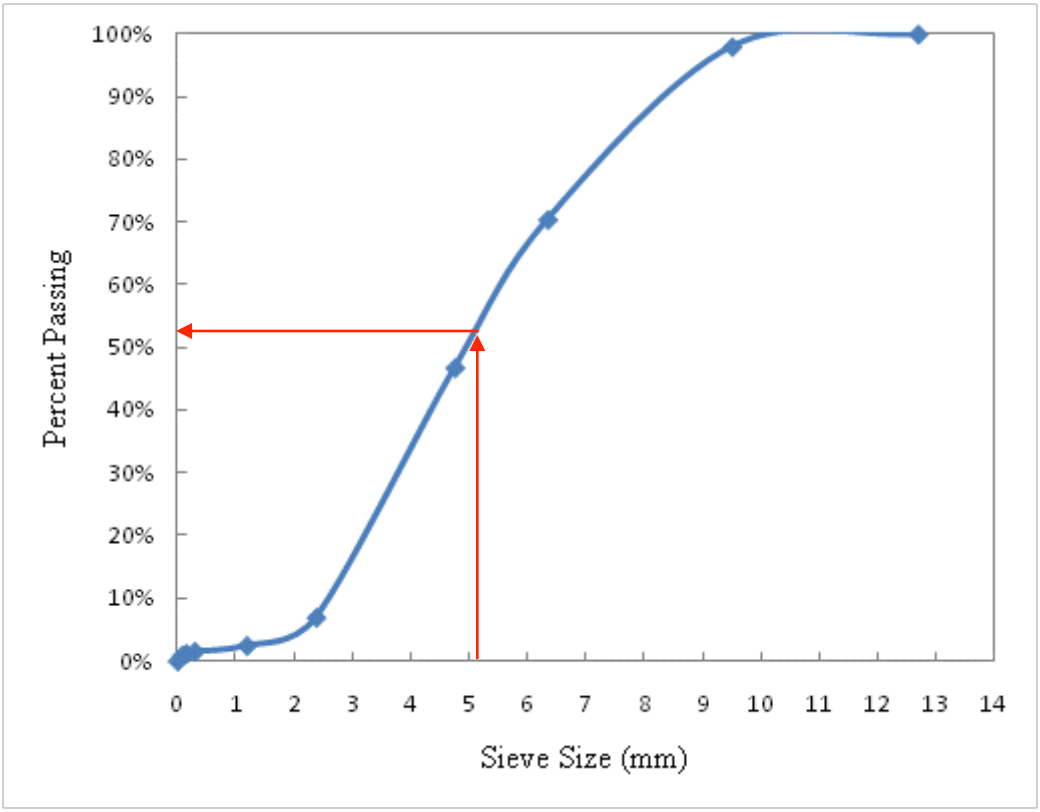

Figure 65 Percentage passing plot for granite 78M Gradation B

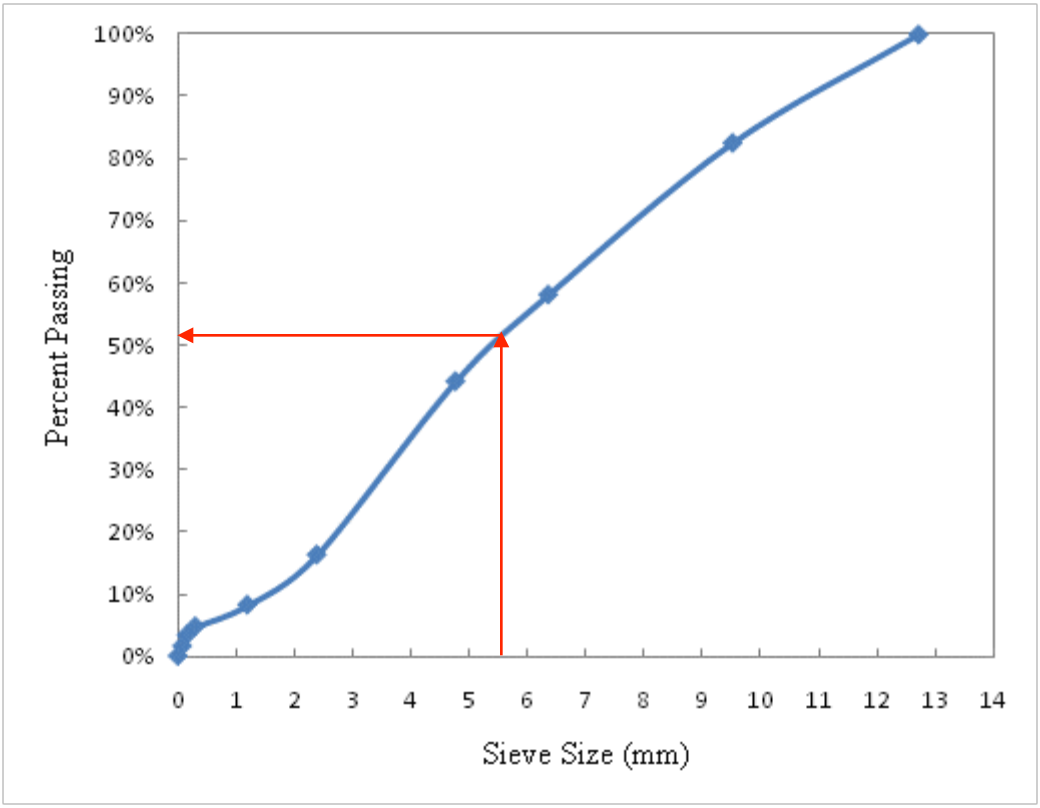

Figure 66 Percentage passing plot for granite 78M Gradation C

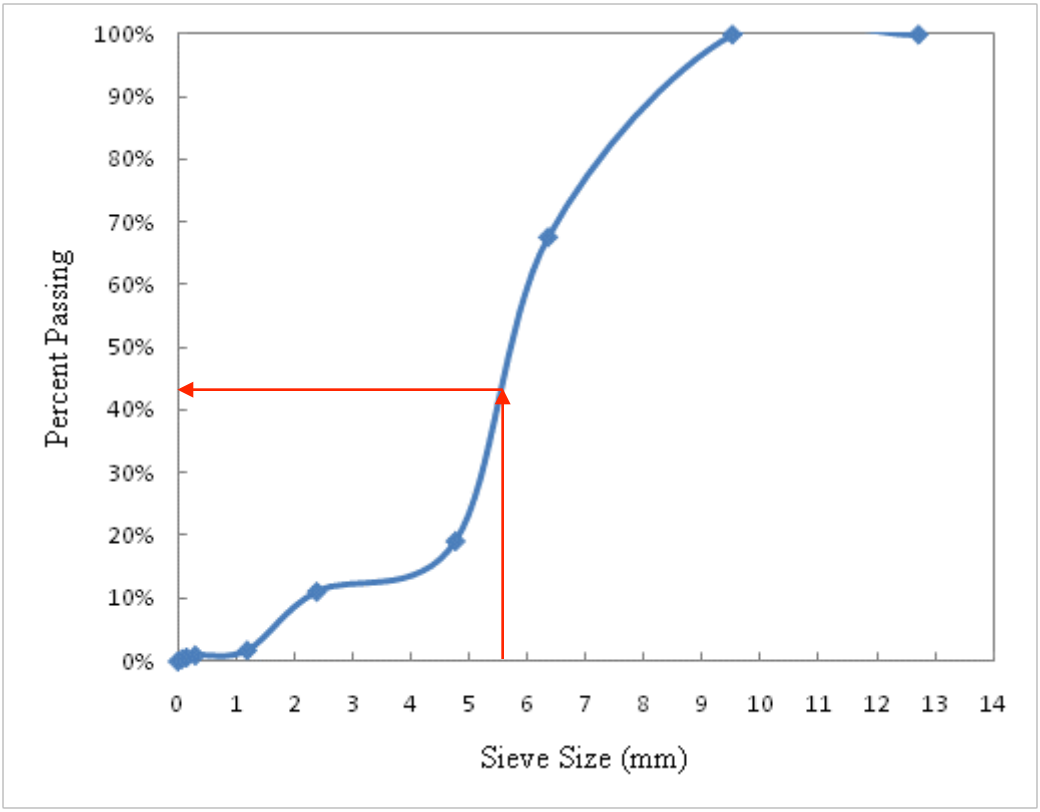

Figure 67 Percentage passing plot for Lightweight Gradation A

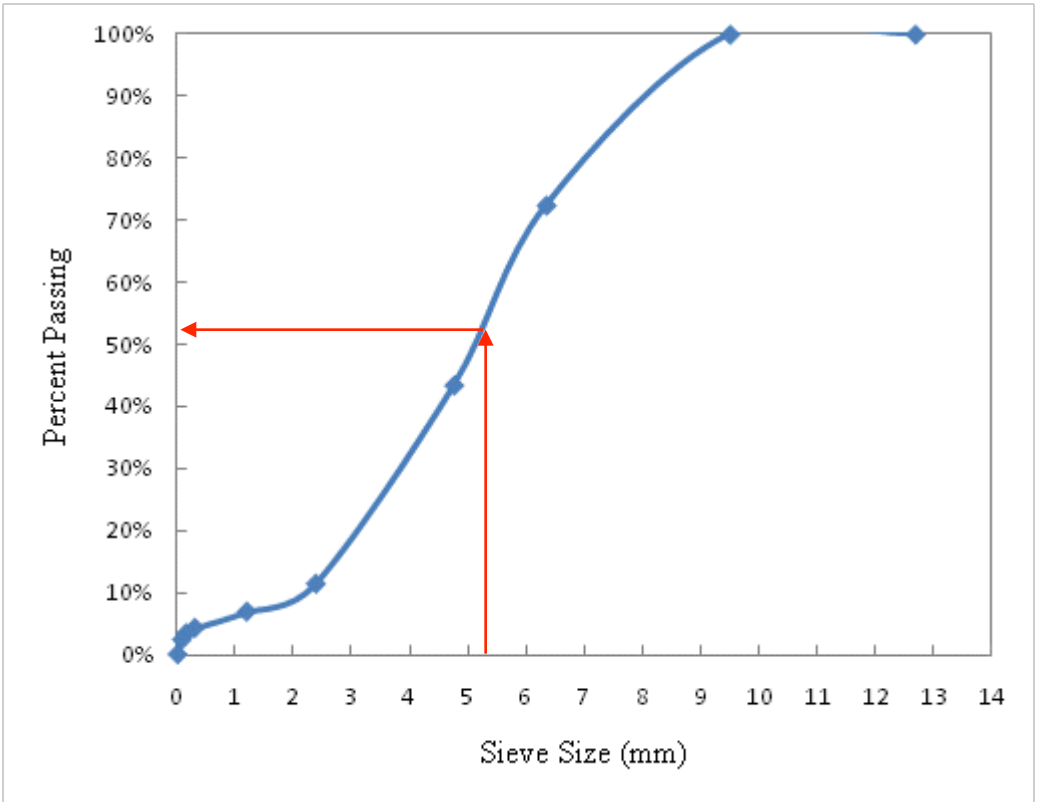

Figure 68 Percentage passing plot for Lightweight Gradation B

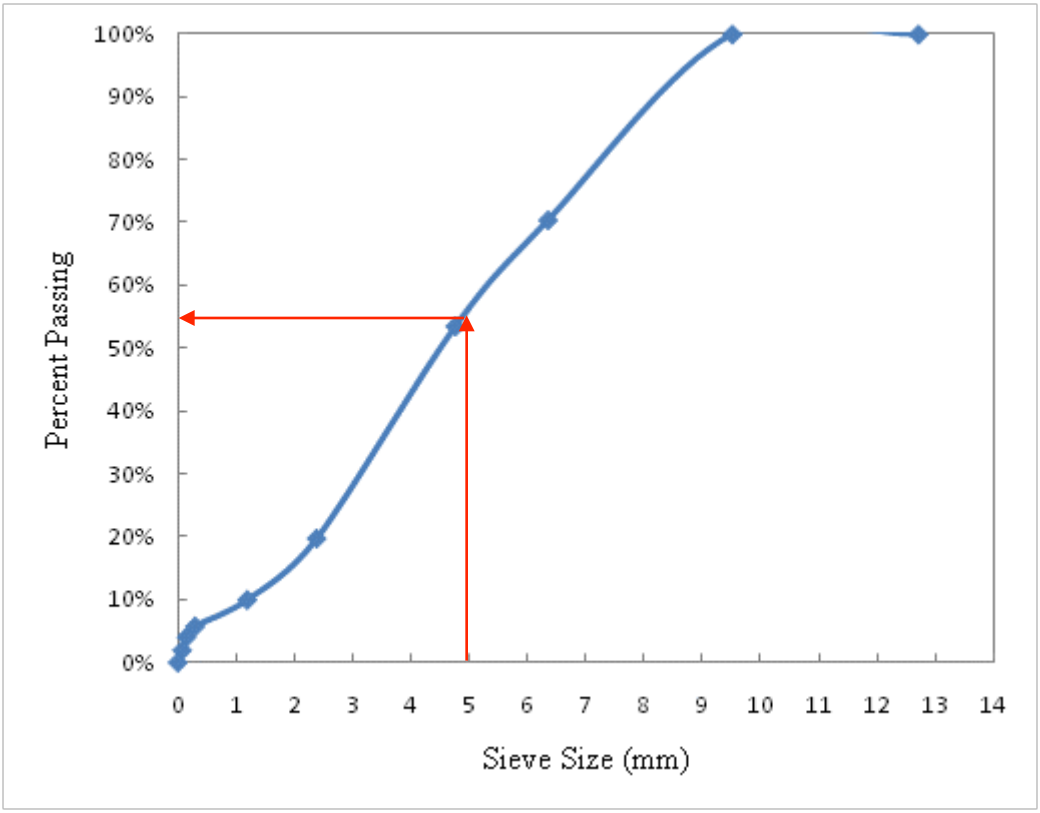

Figure 69 Percentage passing plot for Lightweight Gradation C

Although the finding that the 100% valley average value is close to the 50% passing sieve size is encouraging, it needs further investigation because, intuitively, twice the 50% embedment depth (i.e., 100% valley average) should be close to the largest aggregate size. The research team realizes that the percentage passing gradation plots in Figure 64 to Figure 69 are based on 3-D data, whereas the aggregate surface profiles in Figure 58 to Figure 63 are 2-D. Therefore, it is necessary to compare these two types of plot in the same dimension. An inverse stereology method is adopted for this comparison.

Stereology is the process of constructing a 3-D geometrical structure from 2-D information, namely the geometry of cross-sections on several parallel planes. Inverse stereology essentially involves *statistically* approximating the apparent area distribution in a randomly cut section from the actual specimen based on its volumetric aggregate gradation (Zhang 2003). In this study, the 3-D gradation is converted to a 2-D gradation using this inverse stereology method. The results are shown in Figure 70.

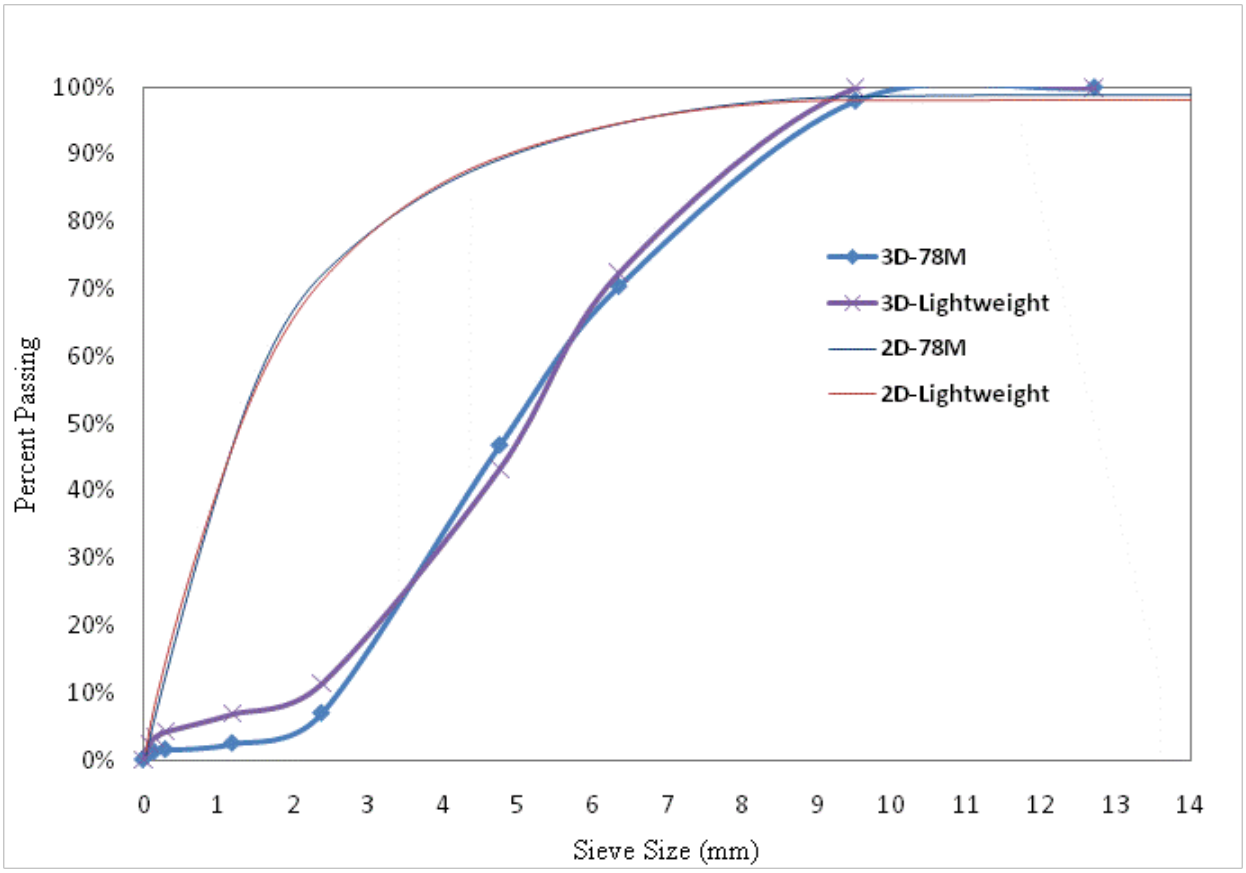

Figure 70 3-D aggregate gradation chart converted to 2-D aggregate gradation chart, for both 78M granite and lightweight aggregate, using inverse stereology

According to the 2-D gradation plots, the 100% valley averages of the granite 78M and lightweight aggregate particles (ranging from 5 to 6 mm) are closer to the 90% passing sieve size. The fact that several aggregate particles are above the 100% valley averages in Figure 58 to Figure 63 supports this finding from the 2-D gradation plot.

The ability to detect the bottom of the surface treatment is crucial when determining the aggregate texture depth. Without the ability to measure the *full* texture depth, the researchers could not, with full confidence, come to any conclusions regarding the depth at which the aggregate is embedded within the emulsion. Even if the field construction team proposed to lay a single-seal layer of aggregate, it could not be verified that the constructed layer was *actually* a single seal based solely on the exposed texture view. This problem can be seen in Figure 71, where the surface profile of each diagram is the same, but the embedment depth of the aggregate is much greater in diagram B.

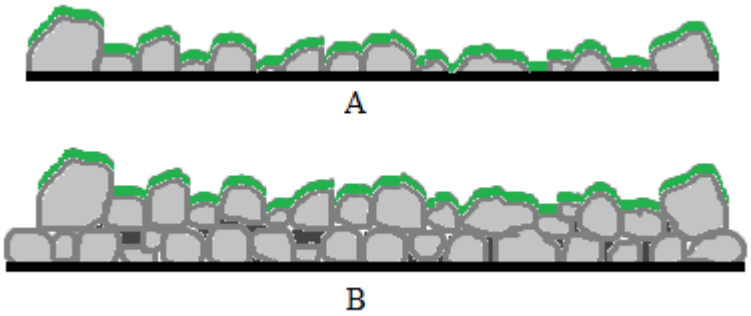

Figure 71 (A) Diagram showing the exposed surface profile; (B) diagram showing the same surface profile, but with more aggregate submerged

In the field, it is impossible to know the baseline at which the aggregate comes in contact with the existing surface. Unlike the surface of the board test performed in the lab, the existing asphalt surface profile is not completely uniform or flat, and it has a texture profile of its own. So, when measuring the exact depth of the chip seal layer, it is necessary to know not only the profile of the exposed surface (i.e., the top of the chip seal layer), but also the profile of the existing asphalt surface (i.e., the bottom of the chip seal layer). Another factor to consider when calculating the exact embedment depth of the surface treatment is that, depending on the AAR, the construction speed, or a number of other factors, the single layer of aggregate that was proposed prior to construction could be double-stacked or even triple-stacked in some cases. That is to say, the consistency with which the aggregate spreader drops the aggregate is not as reliable as it is when the research team places the aggregate by hand. Establishing the bottom surface profile of a constructed chip seal is a difficult task, but is one that governs the successful determination of the aggregate embedment depth from the 3-D laser profiler scan.

7. CONCLUSIONS AND FURTHER RESEARCH

The research detailed here presents an effort to identify, refine, and develop chip seal test methods that can be used together to predict chip seal performance. The BBS test method is identified as a promising means of determining the adhesion and cohesion properties of emulsion. This test method uses PATTI, which is relatively inexpensive (less than $5,000) and simple to use. It is found that the BBS test differentiates the adhesion performance of different emulsions.

Two new test methods are developed from this study. They are the modified sweep test and the 3-D laser profiler. The modified sweep test is based on the sweep test method specified in ASTM D7000; however, the modified sweep tester replaces the stiff-bristled brush in the original sweep tester with a free-rolling, free-spinning rubber wheel to simulate the horizontal and vertical forces induced by the front wheels of a vehicle. Also, a height adjustment mechanism and load cell are incorporated in the modified sweep test machine to ensure and maintain a constant vertical pressure of the wheel on the chip seal specimen. The 3-D laser profiler is equipped with a point laser and photoelectric sensor to measure the surface profile and to take digital images of the chip seal pavement surface in order to evaluate aggregate embedment and bleeding. A preliminary investigation is undertaken to determine aggregate embedment depth from the chip seal surface profile, and the results indicate that the 100% valley average is close to the 50% passing sieve size. This finding may be used to establish the surface profile of chip seal pavements with different percentages of embedment depth from the aggregate gradation with additional research.

The following research topics are identified to take full advantage of and implement the recommended test methods from this project:

- An algorithm to estimate the aggregate embedment depth from constructed chip seal pavements needs to be developed. The preliminary findings from this study look promising for accomplishing this task.
- The test methods developed in this study need to be applied to chip seals with a wide range of material types and application rates to determine their sensitivity to mix design factors and to establish acceptance criteria.
- Developed acceptance criteria need to be validated by field testing.

8. REFERENCES

ASTM. 2005. *Standard Practice for Calculating Pavement Macrotexture Mean Profile Depth*. American Society for Testing and Materials, ASTM Designation E1845, Volume 04.03 Road and Paving Materials; Vehicle-Pavement Systems.

ASTM. 2004. *Standard Test Method for Measuring Pavement Macrotexture Properties Using the Circular Track Meter.* American Society for Testing and Materials, ASTM Designation E2147, Volume 04.03 Road and Paving Materials; Vehicle-Pavement Systems.

ASTM. 2004. *Standard Test Method for Measuring Pavement Macrotexture Depth Using a Volumetric Technique*. American Society for Testing and Materials, ASTM Designation E965, Volume 04.03 Road and Paving Materials; Vehicle-Pavement Systems.

ASTM. 2008. *Standard Test Method for Sweep Test of Bituminous Emulsion Surface Treatment Samples*. American Society for Testing and Materials, ASTM Designation D7000, Volume 04.03 Road and Paving Materials; Vehicle-Pavement Systems.

Benson, F. J. and B. M. Gallaway. 1954. Study of Some Variables Affecting Retention of Aggregate by Asphalt Surface Treatments. *Roads and Streets*: 113-1954.

Cackler, E.T., T. Ferragut, D. S. Harrington, R. O. Rasmussen, and P. Wiegand. 2006. *Evaluation of U. S. and European Concrete Pavement Noise Reduction Methods: Part 1*, Task 2 Report, Cooperative Agreement DTFH61-01-X-00042. National Concrete Pavement Technology Center. Ames, Iowa.

Davis, D., M. Stroup-Gardiner, J. A. Epps, and K. Davis. 1990. Correlation of Laboratory Tests of Field Performance for Chip Seals. *Transportation Research Record* 1300, TRB, National Research Council, Washington, D.C.: 98~107.

Epps, J.A. and Gallaway, B.M. , "Conventional Chip Seals as Corrective Measure for Improved Skid Resistance", TRR 523, 1974.

Gransberg, D. D. and D. M. B. James. 2005. *Chip Seal Best Practices*. NCHRP Synthesis 342, Transportation Research Board, Washington, D.C.

Hanson, I. D. and B. D. Prowell. 2004. *Evaluation of Circular Texture Meter for Measuring Surface Texture of Pavements*. Report 04-05. National Center for Asphalt Technology (NCAT).

Hegarty, E. 2008. *I.A.T. Guidelines for Surface Dressing in Ireland*. 1st Sprayed Sealing Conference – Cost-Effective High Performance Surfacings, Adelaide, Australia.

Herrin, M., C. R. Marek, and K. Majidzadeh. 1968. *Surface Treatments: State-of-the-Art*. Highway Research Board. Special Report 96.

Hunter, R. N. 2000. *Asphalts in Road Construction* (first edition). London: Thomas Telford Publishing.

Jayawickrama, P. W. and B. Thomas. 1997. Correction of Field Skid Measurements for Seasonal Variations in Texas. *Transportation Research Record: Journal of the Transportation Research Board* 1639, TRB, National Research Council, Washington, D.C.

Kandhal, P. S. and J. B. Motter. 1987. *Criteria for Accepting Precoated Aggregates for Seal Coats and Surface Treatments*. Research Project 83-19, Final Report. Pennsylvania Department of Transportation.

Kearby, J. P. 1953. Tests and Theories on Penetration Surfaces. *Transportation Research Record: Journal of the Transportation Research Board* 271, TRB, National Research Council, Washington, D.C.: 232-237.

Kim, Y.R. and J.S. Lee. 2005. Optimizing Gradation for Asphalt Surface Treatments. Report No. FHWA/NC/2005-15, North Carolina Department of Transportation.

McGhee, K. K. and G. W. Flintsch. 2003. *High-Speed Texture Measurement of Pavement*. Final Report, Virginia Transportation Research Council, VTRC 03-R9.

McHattie, R. L. 2001. *Asphalt Surface Treatment Guide*. Publication FHWA-AK-RD-01-03, Alaska Department of Transportation and Public Facilities.

McLeod, N. W. 1969. A General Method of Design for Seal Coats and Surface Treatments. *Proceedings of the Association of Asphalt Paving Technologists* 38: 537-630.

Meegoda, J. N., Rowe, G, M., Dr. Geoffrey M. Rowe, Hettiarachchi, C. H., Bandara, N. and Sharrock, M. J., “Project 2000-34, Correlation of Surface Texture, Segregation, and Measurement of Air Voids," New Jersey Department of Transportation, 2002.

North Carolina Department of Transportation. 2002. *Standard Specifications for Roads and Structures*. N.C. Department of Transportation Design Services Unit.

Pidwerbesky, B., J. Waters, D. Gransberg, and R. Stemprok. 2006. *Road Surface Texture Measurement using Digital Image Processing and Information Theory*. Report 290, Land Transport New Zealand Research, Land Transport New Zealand.

Page, S. J., J. E. Patrick, and D. M. S. Dongol. 1998. *Alternative to Sand Circle Test for Measuring Texture Depth*. Report No. 110, Transfund New Zealand Research, Transfund New Zealand.

Shuler, S. 1990. Chip Seal for High Traffic Pavements. *Transportation Research Record: Journal of the Transportation Research Board* 1259, TRB, National Research Council, Washington, D.C.: 24-33.

Stroup-Gardiner, M., D. E. Newcomb, J. A. Epps, and G. L. Paulsen. 1990. Laboratory Test Methods and Field Correlation for Predicting the Performance of Chip Seals. *Asphalt Emulsion*, ASTM STP 1079: 2~19.

Texas DOT. Tex-216-F Aggregate Retention Test. ftp://ftp.dot.tx.us/pub/txdot-info/cst/TMS/200-F_series/pdfs/bit216.pdf

The Asphalt Institute. 1964. *Asphalt Surface Treatment and Asphalt Penetration Macadam*. Manual Series No. 13 (MS-13) (First edition).

Transit New Zealand. 2005. *Chipsealing in New Zealand*. Controlling Authorities and Roading, New Zealand.

Tredrea, P. 2008. *Development of Laboratory Measures to Assess Surfacings used in High Stress Applications*. Austroads Publication No. AP T105/08, Austroad, Inc.

Yazgan, B. and S. Senadheera. 2004. *A New Testing Protocol for Seal Coat (Chip Seal) Material Selection*. Transportation Research Board, TRB, 2004 Annual Meeting CD-ROM.

Zhang, Pu. 2003. *Microstructure Generation of Asphalt Concrete and Lattice Modeling of its Cracking Behavior under Low Temperature*. North Carolina State University Department of Civil, Construction, and Environmental Engineering, Doctor of Philosophy Dissertation.